ACTIVE PLANT CONSTITUENTS ENRICHED NANOSTRUCTURED LIPID CARRIERS EMBEDDED INTO 3D PRINTED WAFER FOR ORAL CANCER MITIGATION IN NORTH-EASTERN REGION OF INDIA

Research work

Submitted by

Chaudhari Vishal Sharad

Department of Pharmaceutics

Under the Guidance of

Subham Banerjee, *Ph.D., MNASc., MRSC.*

Assistant Professor

Department of Pharmaceutics

National Institute of Pharmaceutical Education and Research, Guwahati

Department of Pharmaceuticals

Ministry of Chemical and Fertilizers, Government of India

Guwahati, Assam-781101

ABSTRACT

The need for localised drug delivery of plant-based active constituents as particulate systems against oral cancer is desired to ensure not only the delivery of particulates but also the release of the drug at the diseased site. Hence, active constituent enriched nanoformulations embedded in 3D printed wafers could be a holistic approach to address the unmet localised drug delivery needs. Co-encapsulation of both piperine and quercetin in nanostructured lipid carriers (PQ-NLCs) through a solvent evaporation technique and characterised for several physicochemical properties and in vitro cellular evaluations, followed by *in vivo* pharmacokinetic profiling in rats and ultimately integrated with 3D printed mouth dissolving wafers for the translational aspect. Characterisation of NLCs showed that particle size distribution was sufficiently below 200 nm; polydispersity index (PDI) less than 0.3 with a negative charge on the surface of the nanoparticles. More than 90% of the drug was encapsulated in the case of quercetin and piperine, with an enhanced drug dissolution profile following Higuchi release kinetics. The pharmacokinetic profile showed an enhancement in the relative bioavailability of quercetin and piperine (20.72-and 4.67-fold, respectively). This can be attributed to the increased solubility, absorption, and residence time of the drug delivered at the nanometer scale. Lyophilized PQ-NLCs in the powdered form were loaded inside fused deposition modelling (FDM) mediated 3D printed polymeric wafers. Complete nanoparticle release from the designed 3D wafers occurred within 120 min and quantified the concentration of nanoparticles released through Derived KCPS from dynamic light scattering. Improved *in vitro* drug release profile along with enhancement in the relative bioavailability and pharmacokinetic profile was achieved through NLCs as compared to pristine drugs. NLC delivery through fabricated 3D printed wafers system at the desired site of action can be considered as the latest additive manufacturing-driven treatment approach against oral cancer mitigation.

Keywords: NLCs, Piperine, Quercetin, OSCC, 3D printing, wafer.

1. Introduction

Cancer is one of the most life-threatening diseases worldwide. Being a multifactorial disease, oral cancer is ranked 6th in the list of cancers. It is classified as head and neck cancer (HNC). It has been observed that continuous and chronic use of tobacco, areca nut, and betel quid leads to precancerous lesions in the oral cavity. The most affected areas were the oral squamous epithelial cells, tongue, gingiva, jaw bone, and lips. Oral squamous cell carcinoma (OSCC) is a cancer of the epithelial tissue of the oral mucosal lining of the oral cavity. It accounts for 90% of all head and neck cancer cases. Early stage symptoms could not be detected as the main prognostic factor in this case.

Oral squamous cell carcinoma (OSCC) is a type of head and neck cancer. It accounts for approximately 90% of all head and neck cancer cases. According to a 2014 report from the World Health Organization (WHO), 53842 cases in males and 23161 cases in women were found in India (**Figure 1.1**). This also showed mortality rates of 18.3% in men and 6.8% in women with oral and oropharyngeal cancer (**Figure 1.2**). According to a recent survey of the Indian Council of Medical Research (ICMR), Bengaluru, a greater number of cases of oral cancer were observed in the northeastern states of India compared with the rest of the states. This comparison showed that the year cumulative survival rates in the early stages of HNC were 73.6 % and 40.5%, respectively, and in locally advanced stages, it dropped to 44.5% and 16.9% in the rest of India and northeast India, respectively (**Figure 1.3**). The detection of oral cancer in later stages III or IV is a significant reason for the very low survival rate in patients with OSCC. Many districts in northeast India showed large numbers of population-based cancer registries (PBCRs), such as Kamrup urban district, Cacchar district, East Khasi Hills district, Dibrugarh district (Assam state), Meghalaya state, Papumpare and Pasighat district (Arunachal Pradesh state), and Aizwal district (Mizoram state).

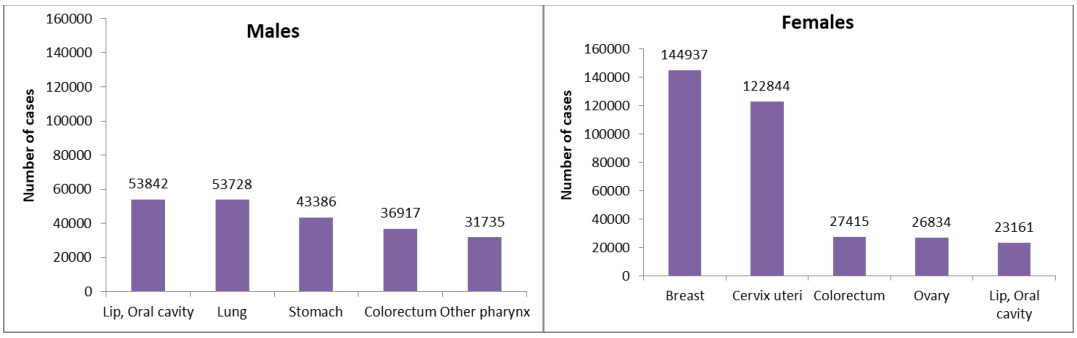

Figure 1. 1. Graph from WHO report 2014 showing the number of cases with respect to the site of cancer

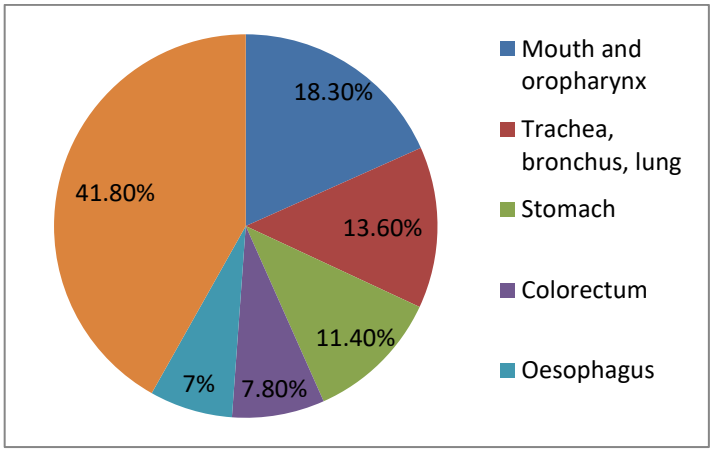

Figure 1. 2. Pie-charts showing mortality rates of cancer patients

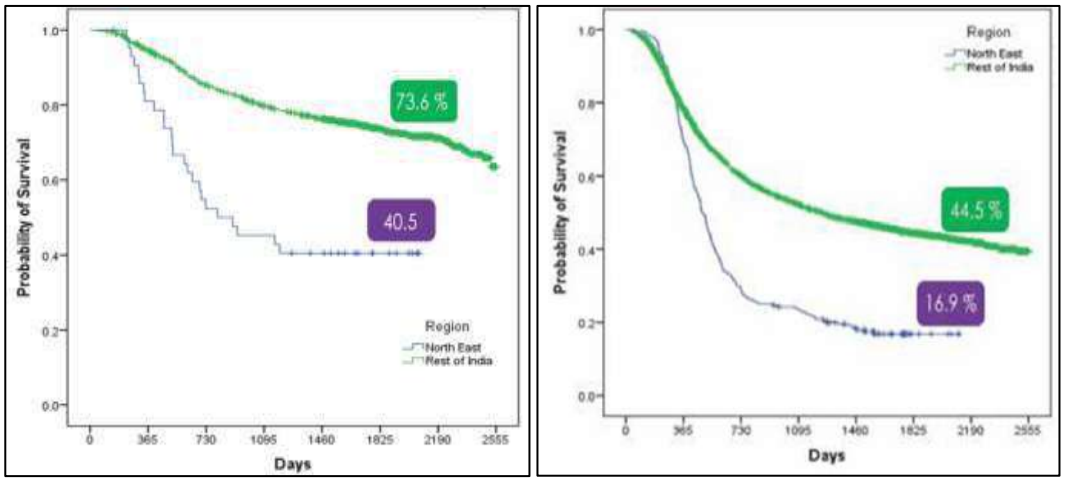

Early stages **Locally advanced stages**

Figure 1. 3. Five year cumulative survival of Head & Neck cancer

1.1. Possible risk factors of OSCC

Oral cancer is a cancer of the oral cavity and is caused by exposure to various carcinogens. There are various factors such as chewing of tobacco, betel quid, areca nut, gutkha, cigarette smoking, alcohol, dietary factors, Human papilloma virus (HPV), potentially malignant lesions, genetic factors etc., which causes oral squamous cell carcinoma

1.1.1. Tobacco

Tobacco consumption is a common habit in both India and Southeast Asia. Tobacco is consumed by both males and females as a stimulant. People use it in the form of smokeless tobacco for chewing purposes. Tobacco is used in betel quid, gutkha, mawa, or slaked lime. Tobacco contains more than 300 carcinogens and pro-carcinogens, such as polyacrylic aromatic hydrocarbons, such as benzo α-pyrene and tobacco-specific nitrosamines, such as nitronor-nicotine (NNN) and 4-(methyl nitrosamino) 1-(3-pyridyl)1-butanone (NNK). These carcinogens form electron-deficient oxidised products with the help of oxidative enzymes and

covalently bind to DNA-generating adduct mutated regions. Benzo α-pyrene undergoes oxidation with CYP1A1 and CYP2E1 enzymes, leading to the formation of benzo α-pyrene diol epoxide which increases susceptibility to chromosomal damage by mutagens. Tobacco increases DNA and fibroblast damage.

1.1.2. Betel quid & Areca nut

Betel leaf is a betel quid, which is a mixture of tobacco, areca nut, slaked lime, spices, saffron, flavouring agents, and sweeteners which are packed in betel leaves. Betel leaves contain nitrosamines which undergo auto-oxidation in saliva due to the presence of alkaline pH due to slaked lime. This generates reactive oxygen species (ROS) which cause structural damage to the oral mucosa, initiate tumour generation, damage several salivary proteins of the oral mucosa, and gene mutations. Betel chewing has several effects, including palpitations, a warm sensation in the face and body, increased blood flow to the face, profuse sweating, and heightened alertness.

Hence, considering the seriousness of the prevalence of nanoparticles in the region of northeastern India and their root causes, further steps are required for its prevention. Depending on the availability of high-end facilities and their cost, treatment is required, which can be effective, cheap, and accessible to all. In this context, nanoformulations can be rescued, which provides several advantages and can effectively deliver herbal components. Hence, nanoformulations can be considered an important tool for treating such deadliest diseases.

1.2. Natural products

Nature's baskets have been providing all sources of energy derivatives to all forms of life since its inception [1]. Nature acquires an arsenal of therapeutically significant molecules against multiple ailments [2]. Age-old traditional practices [3] to the modern drug discovery arena are largely dependent or inspired by natural chemical moieties [4]. Natural products such as alkaloids, glycosides, saponins, terpenoids, and phenolics, carry out most of the therapeutic activities in our physiology [5].

Table 1. 1. Broad classification of anticancer drug

Sr.No.	Class	Subclass
1	Chemotherapy	Alkylators, antibiotics, antimetabolites, topoisomerase inhibitors, mitosis inhibitors
2	Hormonal therapy	steroids, anti-estrogens, anti-androgens, anti-aromatase agents
3	Immunotherapy	interferons, interleukins, vaccines

The global mortality load in the current scenario can be attributed to diseases such as metabolic disorders [6], microbial infections [7], and genetic inadequacies [8], and few others. Among them, cancer is one of the predominant global killers, with an estimated 9.6 million deaths worldwide, with 18.1 million new cases. Broadly, anticancer therapeutics [9] can be classified as listed in **Table 1.1**. Many of these molecules are synthetic, semi-synthetic, or in terms of their origin.

In general, naturally occurring anticancer molecules are obtained from microbial, plant, or marine sources [10] (**Table 1.2**). The vast array of secondary metabolites through inherent combinatorial chemistry by nature has propelled the possibility of therapeutic molecules with significant activity.

Table 1. 2. Naturally occurring anticancer drugs

Microbial source	**Plant source**	**Marine source**
Daunorubicin, doxorubicin (adriamycin), epirubicin, pirirubicin, idarubicin, valrubicin, amrubicin Bleomycin, phleomycin Actinomycin D, actinomycin Mithramycin, streptozotecin, Pentostatin, Mitosanes mitomycin C, Enediynes calicheamycin, Glycosides rebeccamycin, Macrolide lactones epotihilones, Ixebepilone 2″-deoxycoformycin/pentostatin Salinosporamide A	Vinblastine, Vincristine, Etoposide, Teniposide, Taxol, Navelbine, Taxotere, Camptothecin, Topotecan, Irinotecan, Arglabin, Homoharringtonine, Ingenolmebutate, Masoprocol/Nordihydroguaiaretic acid, Peplomycin, Solamargines, Alitretinoin, Elliptiniumacetate, Etoposide phosphate	Cytarabine, Pederin Theopederins, Annamides Trabectedin, Aplidine Ecteinascidin, Eribulin Plinabulin

Natural molecules have shown promising anticancer properties at the laboratory scale. Despite such considerable results, properties such as poor solubility, narrow therapeutic window, inferior absorption rate, and lower bioavailability, as well as stability issues, have halted the use of bare molecules or common formulations. According to many studies, these formulations also appeared to possess an inappropriate pharmacokinetic profile and reduced elimination half-life, resulting in compromised activity as a consequence [11]. Therefore, nanoparticles have been introduced to counter the shortcomings of existing preparations and formulations. Nano-formulations were found to possess an amicable construct, surface properties, lower side effects, and improved pharmacokinetic properties when compared with the preceding formulations.

1.3. Nanoformulations

Nanoparticles are defined as particles ranging from 1 to 100 nm in dimensions [12]. Tailor-made approaches, such as nano-formulation constructs, result in an improved pharmacokinetic profile, reduced side effects, and superior surface area to volume ratio. Broadly, these formulations can be classified as organic or inorganic nanoparticles [13].

1.3.1. Lipid Nanoconstructs

According to the Biopharmaceutics Classification System (BCS), most drugs fall into classes II and III, where drugs are either less soluble or less permeable. In the case of synthetic drugs, modification of their physicochemical properties or formulation strategies can easily solve these issues. However, in the case of natural products, most of the drugs fall into BCS class IV and are hydrophobic in nature, with very low solubility in water [14]. This decreases the oral bioavailability of the natural products. Hence, nanotechnology has been developed to overcome these issues by formulating nano-dimensional formulations such as polymeric nanoparticles, nanoemulsions, and micelles [15]. Along with polymers, surfactants, co-surfactants, and block copolymers need to be used to formulate nanoconstructs. The use of synthetic excipients as a major component in formulation development may raise concerns about safety and toxicity. Therefore, there is a need for safe and non-toxic excipients for nanoconstruct development. The use of lipid excipients has solved the problem associated with other excipients, and many advantageous drug delivery systems can be developed.

Lipid nanoconstructs are a wide term covering many types of lipid-based nanoparticles as well as vesicular drug delivery systems such as liposomes, lipid micelles, lipid emulsions, solid lipid nanoparticles, and nanostructured lipid carriers **(Figure 1.4)** [16]. These systems can easily dissolve lipophilic drugs in their lipid domains in a dispersion medium which increases their drug-loading capacity and entrapment efficiency.

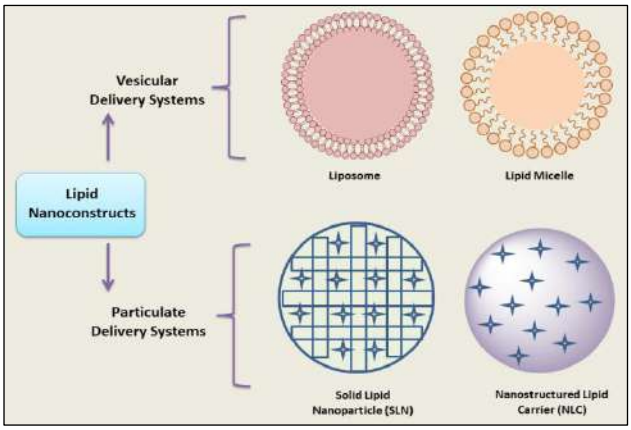

Figure 1. 4. Different illustration of lipid nanoconstructs

The ultimate aim is to increase the bioavailability and cellular uptake of drugs through lipid-based nanoconstructs **(Figure 1.5)**, and ligand-based specific targeting is possible [17]. These lipid nanoconstructs are explained well below under vesicular delivery systems and particulate delivery systems with a thorough literature review along with examples of different drugs delivered through them.

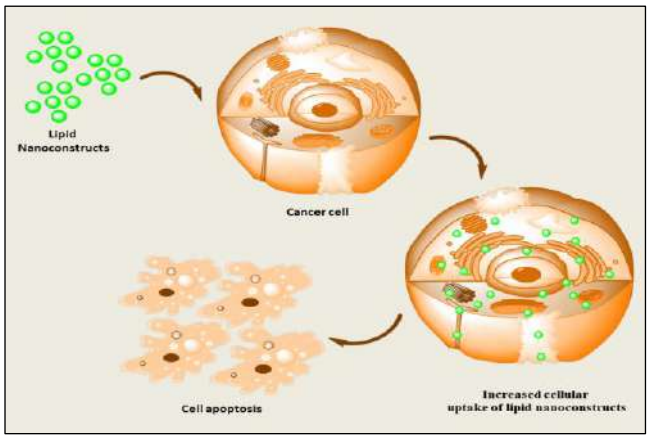

Figure 1. 5. Improved cellular uptake of lipid nanoconstructs in cells causing death

2. Aim and Objectives

2.1. Aim

Active Plant Constituents Enriched Nanostructured Lipid Carriers Embedded into 3D Printed Wafer for Oral Cancer Mitigation in North-Eastern Region of India

2.2. Objectives

- To develop and validate RP-HPLC method for the simultaneous detection and estimation of quercetin and piperine.
- To formulate the individual and combinations of piperine and quercetin-loaded nanostructured lipid carriers (NLCs).
- To perform detailed in vitro physicochemical characterisation, an in vitro release study and its kinetics mechanism were performed.
- To perform *in vitro* cellular investigations of NLCs in oral squamous cell carcinoma (FaDu cells).
- To develop and validate a bio-analytical method for the simultaneous detection and estimation of quercetin and piperine by LC-MS/MS analysis and its application to *in vivo* pharmacokinetic studies in rats.
- To prototype & validate 3D printed mouth dissolving wafers loaded with NLCs for an *in vitro* release study.

Analytical Method Development and Validation of Reverse-Phase High-Performance Liquid Chromatography (RP-HPLC) Method for Simultaneous Quantifications of Quercetin and Piperine

1. Introduction

Combinations of natural plant active constituents as potential drugs and their nanostructured formulations have been used to treat many diseases for synergistic effects [18]. Proper detection and quantification of such drug combinations with good sensitivity can be achieved using validated analytical methods [19].

Quercetin is a natural flavonoid obtained from various edible sources, such as red onions, apples, tomatoes, red grapes, green tea, black tea, and fresh green leafy vegetables [20]. Quercetin has therapeutic potential for diseases such as cardiovascular, cancer, and neurodegenerative diseases by exerting antioxidant and anti-inflammatory activities [21]. Another naturally occurring alkaloid, piperine, is obtained from the fruits of black pepper and long pepper. Piperine has been reported to have anti-inflammatory, antihypertensive, hepatoprotective, and antitumor properties [22]. Unfortunately, these two drugs have poor aqueous solubility [23] and photosensitivity-related severe issues [24]. In addition, quercetin undergoes rapid chemical degradation in gastric pH media [25]. Therefore, incorporation of these two drugs into a suitable single lipid-mediated nanostructured formulation, especially NLCs, is helpful in overcoming critical pharmaceutical challenges [26]. Hence, a rapid, sensitive, precise, and accurate RP-HPLC validated method is essential for the simultaneous analysis of quercetin and piperine from a single NLC matrix. Furthermore, to validate the lipid-mediated nanoparticulate performances concerning their *in vitro* % drug entrapment efficiency (DEE), % drug loading (DL), and cumulative % drug release, a simple RP-HPLC method is indispensable.

Interestingly, few validated analytical reports have been reported on estimation of quercetin by RP-HPLC method [27], piperine by various means [24b] and UV-visible spectrophotometric validated method for simultaneous estimation of piperine, quercetin, and curcumin in a mixture [28]. However, to the best of our knowledge, no suitable validated analytical method has been reported for the simultaneous detection and quantification of quercetin and piperine in their co-loaded lipid-mediated nanoformulations. Hence, the objective of the present study was to develop and validate an RP-HPLC method for the simultaneous analysis of quercetin and piperine in NLC formulations. NLC formulations improve drug solubility, chemical stability, and photosensitivity.

2. Materials and Methods

2.1. Materials

Quercetin, piperine, squalene (liquid-lipid), and dialysis sac (12 kDa molecular weight cut-off) were purchased from Sigma-Aldrich Chemicals (St. Louis, MO, USA). Compritol ATO-888 (solid lipid) was obtained as a gift from Gattefosse (France). HPLC-grade

acetonitrile (ACN), methanol, and glacial acetic acid were procured from Merck Specialities Pvt. Ltd. (Mumbai, India). Hydrogen peroxide was purchased from Hi-Media Laboratories Pvt. Ltd. (Mumbai, India). HPLC-grade Milli-Q water was used as previously filtered through a Milli-Q filtration system (Millipore GmBH, Germany). HPLC or analytical grade solvents, chemicals, and reagents were utilised throughout the analytical method validation and *in vitro* applications.

2.2. Selection of wavelength

Primary standard stock solutions (1000 µg/mL each) were prepared for both the drugs dissolved in methanol and diluted further to make secondary stock solutions at a concentration of 10µg/mL each to obtain ultraviolet-visible (UV-Vis) spectra. Aliquots of that concentration were taken in a quartz cell cuvette and scanned to detect wavelength with maximum absorption (λ_{max}) in the range190-800 nm using methanol as a blank in a double beam UV-vis spectrophotometer (UV-2600, Shimadzu, Japan). Finally, the merged overlay of the UV absorption spectrum for both drugs was obtained to determine the isobestic wavelength with maximum absorption of both drugs.

2.3. Instrumentation

An auto sampler mediated (WPS 3000 TSL Analytical) high-performance RP-HPLC (UltiMate 3000, Thermo Fisher Scientific, US) equipped with quaternary pump (LPG-3400 RS, Smartflow™) and PDA detection system (DAD 3000) was used. This system was operated using Chromeleon® software (version 7.2.8) to control the instrument parameters. The column temperature was controlled in an oven (TCC 3000 SD) to accommodate the columns inside the chamber. All standards were accurately weighed using a calibrated weighing balance (ME204/AD4, Mettler Toledo, Switzerland).

2.4. Chromatographic conditions

Effective chromatographic separation of quercetin and piperine was achieved on a Hypersil Gold C-18 column (5µm particle size ODS, 150 mm×4.6 mm) and a mobile phase consisting of a mixture of ACN and HPLC grade water (pH 2.6, adjusted with 2%w/v glacial acetic acid) in an isocratic elution mode. The mobile phase was filtered through a 0.45µm membrane filter with vacuum filtration assembly followed by bath sonication (Model: 08895-83, Cole-Parmer, Mexico) for 20 min before analysis. The flow rate of the mobile phase was 1 mL/min, the column temperature was 35±0.2°C and the injection volume was 20 µL.

2.5. Standard and sample solutions preparation

Primary standard solutions (1000 µg/mL each) for both quercetin and piperine were prepared in methanol. These solutions were covered with aluminium foil and stored in a refrigerator at 4 (±0.5°C) until analysis. Secondary stock solutions were prepared by diluting the primary standard solutions with a mobile phase.

Sample solutions were prepared to investigate *in vitro* % DEE, % DL [29] and cumulative % drug release using the developed and validated RP-HPLC method.

2.6. Assay validation

The RP-HPLC method developed for the simultaneous detection and quantification of quercetin and piperine was validated according to the International Council for Harmonisation (ICH) of Technical Requirements for Pharmaceuticals for Human Use Guidelines [30]. The method was validated with respect to specificity, linearity, range, precision, accuracy, sensitivity, and robustness. The system suitability study was performed according to the United States Pharmacopoeia (USP) guidelines [31].

2.6.1. Specificity

To determine the specificity of the developed method, quercetin and piperine, such as squalene and Compritol, were determined in the NLC matrix. Chromatograms were assessed for the presence of interfering peaks at analyte retention times. Furthermore, the specificity of the developed method was also determined after stress degradation of quercetin and piperine under hydrolysis and oxidative stress conditions and evaluating the interference of degradation products at the retention time of quercetin and piperine.

2.6.2. Linearity and range

Quercetin and piperine were accurately weighed and dissolved in 10 mL methanol separately to prepare a primary stock solution of 1.0 mg/mL. After diluting the above solutions, working standard solutions were prepared at 2, 4, 8, 16, 32, 64, and 128 µg/mL for quercetin and 1, 2, 4, 8, 16, 32, and 64 µg/mL for piperine. To determine the linearity and range, working standard solutions of different concentrations of quercetin and piperine were injected three times per concentration. The peak areas of each concentration were recorded, and the concentration versus peak area response of quercetin and piperine were constructed.

The range of the developed method for the determination of quercetin and piperine was determined based on the plot obtained for peak area against each concentration and response factor against concentration for every calibration standard. % RSD of response factor was determined to establish the range of analytes.

2.6.3. Accuracy

Accuracy was determined by estimating the % recovery of quercetin and piperine at low (LQC), middle (MQC), and high (HQC) quality control samples. Samples of known concentrations of LQC, MQC, and HQC levels for quercetin were 2µg/mL, 16µg/mL and 128µg/mL, respectively, while for piperine 1µg/mL, 8µg/mL and 64µg/mL, respectively, were prepared in triplicate for each concentration, and % recovery, % bias, and % RSD were calculated.

2.6.4. Precision

The precision of an analytical method is considered in terms of repeatability (intra-day precision) and intermediate precision (inter-day precision). The precision of the developed method was determined using relative standard deviation (%RSD). The intra - and inter-batch precision of the developed method was investigated by analysing QC samples at three different concentrations in three replicates. LQC levels of 2 µg/mL, MQC levels of 16 µg/mL,

and HQC levels of 128 µg/mL for quercetin and LQC of 1 µg/mL, MQC of 8 µg/mL, and HQC of 64 µg/mL for piperine were prepared and analysed on the same day for intra-day precision, and three different QC samples were prepared and analysed on three consecutive days for inter-day precision under similar analytical experimental conditions.

2.6.5. Sensitivity

The limit of detection (LOD) was used to determine the sensitivity of the analytical method based on the visual determination method. The limit of quantification (LOQ) was determined as 3.0 LOD.

2.6.6. Robustness

The robustness of the method was evaluated by deliberate variation in chromatographic conditions such as flow rate and mobile phase composition at LQC, MQC, and HQC samples of quercetin and piperine. The mobile phase composition was varied as ±2%, and the flow rate was ±0.20 mL/min. The effects of such changes on the resolution of drugs along with the tailing factor and theoretical plates were evaluated for robustness.

2.6.7. System suitability

Following USP [19], a system suitability test was performed to verify the suitability of the chromatographic system for the intended analysis. The test was performed by three replicate injections of standard solution of 50µg/mL of quercetin and piperine, and system suitability parameters were determined for their retention time, peak resolution, theoretical plate, height equivalent theoretical plate, separation factor, and tailing factor.

2.6.8. Stress studies

To determine the degradation behaviour, quercetin and piperine were exposed to different stress conditions. Quercetin and piperine were subjected to 0.1N HCl for acid hydrolysis, 0.1N NaOH for basic hydrolysis and water for neutral hydrolysis at 80°C for two hrs. Oxidative studies were performed in 15% H_2O_2 at 80°C for two hrs. The samples were neutralised to ensure that the pH of the sample was neutral before the HPLC injection. Further dilutions of samples were performed with the mobile phase, and the samples were analysed by HPLC.

3. Results and discussion

3.1. Method development

As both drugs are photosensitive in nature, special precautions were taken while preparing and handling the samples. The samples were prepared in amber coloured tubes and mostly wrapped in aluminium foil to avoid exposure to light. In the case of drug-loaded nanoformulations, encapsulation of drugs inside the lipid matrix prevents photodegradation but is still covered with aluminium foil to enhance the stability of formulations and is generally recommended. The absorbance measurements for both drugs were performed at a maximum wavelength of 346 nm, as depicted in **Figure 2.1**.

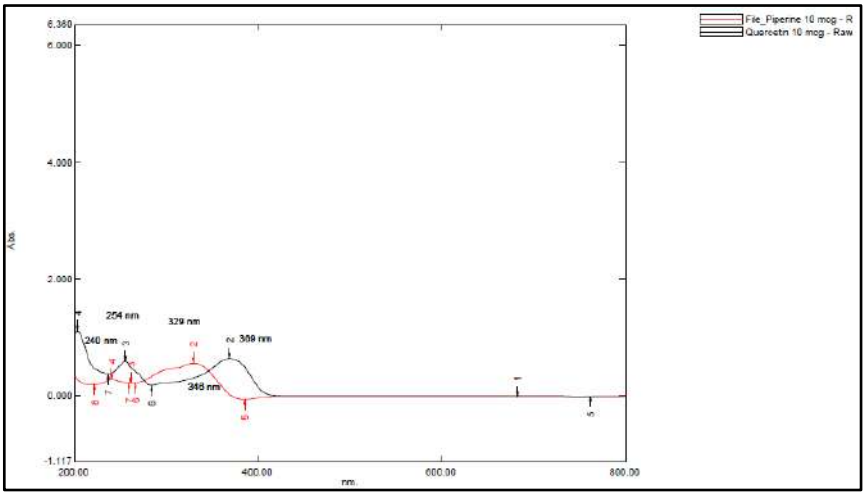

Figure 2. 1. UV-vis absorption overlay spectrum at 346 nm of Quercetin (black line) and Piperine (red line)

RP-HPLC method development for simultaneous quantification of quercetin and piperine was initiated with different ratios of mobile phase constituting water acidified with glacial acetic acid (2.0 % v/v, pH 2.6) as the aqueous phase and ACN as the organic phase. Finally, effective chromatographic separation of quercetin and piperine was achieved on a Hypersil Gold C-18 column (5µm particle size ODS, 150 mm×4.6 mm) and a mobile phase consisting of a mixture of ACN and HPLC grade water (pH 2.6, adjusted with 2.0%v/v glacial acetic acid) in an isocratic elution mode at a flow rate of 1mL/min. Quercetin and piperine eluted at retention time of 2.8 min and 10.3 min, respectively (**Figure 2.2**). System suitability parameters such as retention time, peak resolution, theoretical plate, height equivalent theoretical plate, separation factor, and tailing factor were found to be within acceptable limits.

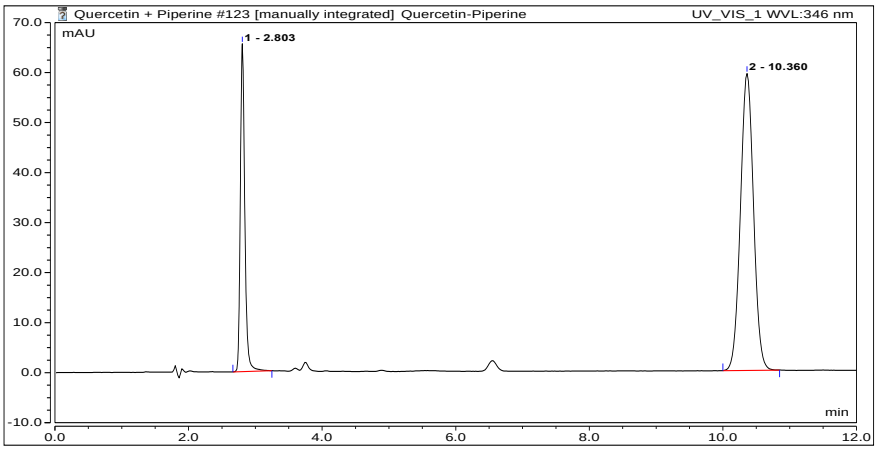

Figure 2. 2. Simultaneous RP-HPLC chromatogram of (1) Quercetin (retention time =2.80 min) and (2) Piperine (retention time =10.36 min) in standard drug solution mixtures composed of 16 µg/mL and 8 µg/mL, respectively.

3.2. Method Validation

3.2.1. Linearity and range

The standard calibration curve was linear over the concentration range of 2-128µg/mL and 1-64µg/mL for quercetin and piperine, respectively. The determination coefficients (R^2) obtained from the linear regression analysis were 0.9994 for quercetin and 0.999 for piperine. The equation of the calibration curve based on the mean peak and concentration (µg/mL) for quercetin and piperine were y = 0.8339x - 0.1984 and y = 2.3371x -1.1288, respectively.

3.2.2. Specificity

The chromatogram of blank matrix demonstrated absence of interference of any another peak corresponding to the matrix of NLCs at the retention time of 2.8 min and 10.3 min for quercetin and piperine, respectively (**Figure 2.3**). Furthermore, no degradation interference was observed after the stress degradation studies of quercetin and piperine under hydrolysis and oxidation conditions. Hence, the developed and validated HPLC method was specific for the simultaneous quantification of quercetin and piperine (**Figure 2.4**).

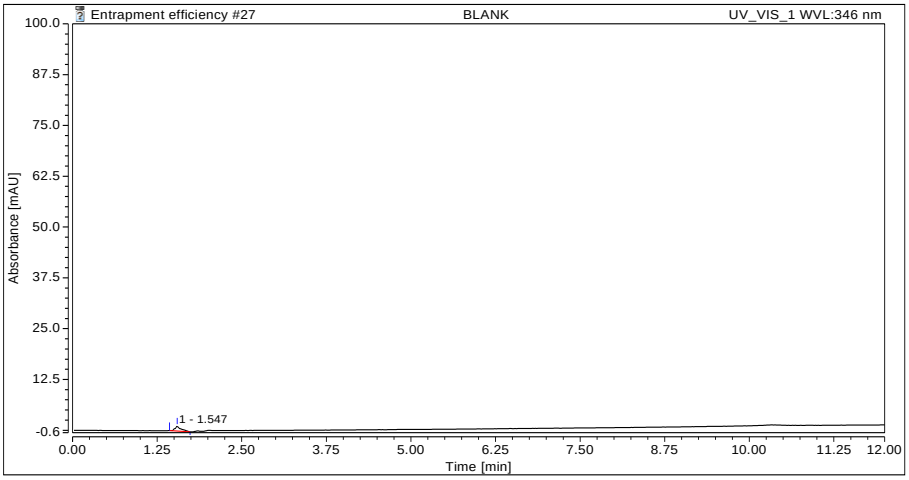

Figure 2. 3. Chromatogram of placebo NLCs extracted dispersion

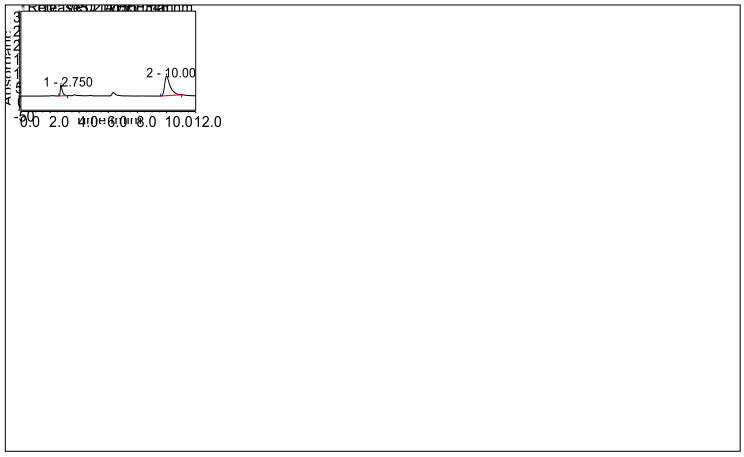

Figure 2. 4. Simultaneous chromatogram of (1) quercetin (t_R =2.75 min) with a concentration of 5.38 µg/mL and (2) piperine (t_R =10.00 min) with a concentration of 13.24 µg/mL from release study of dual-drug loaded NLCs dispersion.

3.2.3. Precision

Precision determines the effect of random errors on the repeatability of the method which is expressed as % RSD and % RSD less than 2%, is considered to be acceptable. Precision studies for the developed analytical methods include intra-and inter-day precision and are expressed as their corresponding % accuracy along with their % RSD for low-, medium-, and high-quality control samples (**Figure 2.5**). The overall % RSD for intra-day and inter-day precision for the proposed method was found to be less than 2% (**Tables 2.1** and **2.2**), respectively.

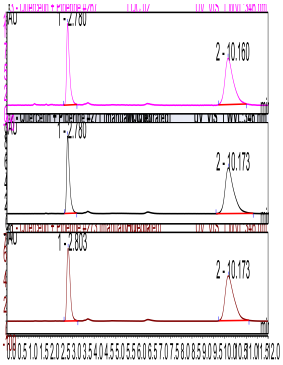

Figure 2. 5. Simultaneous chromatogram of (1) Quercetin (average retention time =2.78 min) and (2) Piperine (average retention time =10.17 min) for all quality control samples including LQC, MQC and HQC, respectively.

Table 2. 1. Intra-day precision values at different levels of the validated analytical method

Analytes	Nominal concentration level (µg/mL)	Found conc. (µg/mL)	% Accuracy	Intra-day precision (Repeatability) %R.S.D.
Quercetin	2.0	1.97 (±0.02)	98.06 (±1.24)	1.26
	16	15.12 (±0.09)	94.51 (±0.94)	0.60
	128	124.52(±0.85)	97.28 (±0.66)	0.68
Piperine	1.0	0.94 (±0.01)	94.68 (±1.19)	1.96
	8.0	7.44 (±0.06)	93.12 (±0.77)	0.83
	64	58.26 (±0.39)	91.04 (±0.61)	0.67

*Data expressed as mean (±SD), n=3.

Table 2. 2. Inter-day precision values at different levels of the validated analytical method

Analytes	Nominal concentration level (µg/mL)	% R.S.D. of Inter-day precision (Intermediate)		
		Day 1	Day 2	Day3
Quercetin	2.0	1.12	0.78	0.46
	16	0.52	0.99	0.93
	128	1.33	0.62	1.42
Piperine	1.0	0.58	0.37	0.67
	8.0	1.95	1.79	0.98
	64	1.04	0.28	0.82

*Data expressed as mean (±SD), n=3.

3.2.4. Accuracy/recovery

The accuracy of the analytical method determines the degree of closeness between the obtained values and the true values, and is expressed as a percentage recovery. The overall % recoveries for the LQC, MQC, and HQC samples were in the range of 92 %–98% for both quercetin and piperine. The percent recoveries for quercetin and piperine were well within the acceptance criteria. The results of the accuracy of the proposed method are listed in **Table**

2.3. This shows that the proposed method is accurate for the simultaneous estimation of both drugs.

Table 2. 3. Accuracy values at different levels of the validated analytical method

Analytes	Nominal concentration (µg/mL)*	Found conc. (µg/mL)±SD	% Accuracy*	% RSD
Quercetin	2	1.89 (±0.01)	94.66 (±0.72)	0.76
	16	15.27 (±0.09)	95.46 (±0.56)	0.59
	128	121.55 (±0.83)	94.96 (±0.65)	0.70
Piperine	1	0.92 (±0.01)	92.30 (±1.17)	0.53
	8	7.81 (±0.03)	97.66 (±0.40)	0.40
	64	59.84 (±0.20)	93.50 (±0.32)	0.76

***Data expressed as mean (±SD), n=3

3.2.5. Sensitivity

With reference to ICH guideline Q2R1, LOD was determined by the visual determination method, where LOQ was determined to be 3.0 times the LOD. Therefore, LOD was found to be 0.66µg/mL and 0.33µg/mL for quercetin and piperine, respectively, as shown in **Figure 2.6**. LOQ values were obtained as 2.0µg/mL and 1.0µg/mL for quercetin and piperine, respectively. These values are adequate for the accurate and precise detection and quantitation of quercetin and piperine.

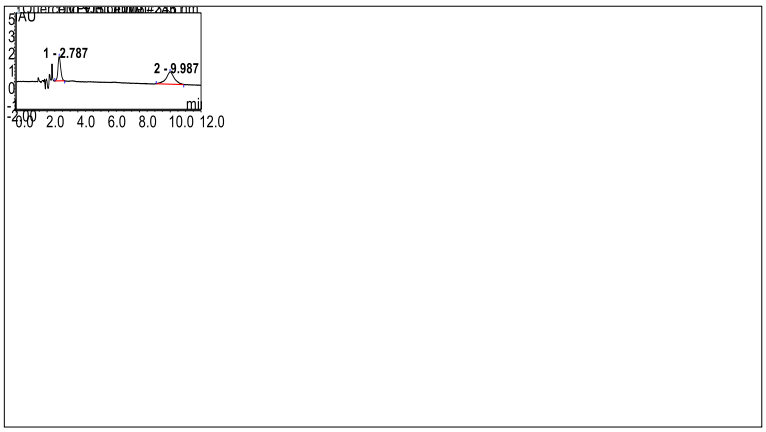

Figure 2. 6. Simultaneous chromatogram of Quercetin and Piperine for the determination of LOD values for both the drugs i.e. 0.66 µg/ml and 0.33 µg/ml for quercetin and piperine, respectively.

3.2.6. Robustness

To determine the robustness of the developed analytical method, the effects of deliberately changing the composition and flow rate of the mobile phase on the resolution, tailing factor, and theoretical plates were studied for the LQC, MQC, and HQC samples. The slight variation in composition or flow rate did not cause any significant variation in resolution, theoretical plate, or tailing factor, as mentioned in **Table 2.4**. This indicates that the developed method is robust and self-sufficient to analyse the two drugs simultaneously.

Table 2. 4. Robustness of the validated analytical method

S. No.	Parameters	Analytes	Sample conc. (µg/mL)*	Resolution R (±SD)	Tailing Factor T (±SD)	Theoretical Plates N (±SD)
A. *Change in composition of mobile phase*						
1.	Acidified Water : ACN (58:42)	Quercetin	2	-	1.83(±0.01)	2897(19)
			16	-	1.78(±0.04)	2809(05)
			128	-	1.55(±0.01)	2321(10)
		Piperine	1	16.41(±0.081)	1.41(±0.04)	4003(49)
			8	15.82(±0.006)	1.48(±0.01)	3833(10)
			64	15.08(±0.026)	1.21(±0.01)	3602(14)
2.	Acidified Water : ACN (60:40)	Quercetin	2	-	1.71(±0.02)	2992(07)
			16	-	1.64(±0.02)	3114(46)
			128	-	1.45(±0.01)	2974(26)
		Piperine	1	17.71(±0.006)	1.32(±0.03)	4120(60)
			8	17.79(±0.006)	1.30(±0.02)	4106(22)
			64	16.93(±0.01)	1.21(±0.01)	3678(05)
3.	Acidified Water : ACN (62:38)	Quercetin	2	-	1.66(±0.02)	2851(45)
			16	-	1.61(±0.02)	2912(52)
			128	-	1.49(±0.02)	2524(06)
		Piperine	1	18.85(±0.460)	1.17(±0.02)	4139(110)

			8	18.58(±0.035)	1.32(±0.02)	3883(26)
			64	17.50(±0.131)	1.19(±0.02)	3482(53)
B. *Change in flow rate of mobile phase*						
1.	0.8 mL/min	Quercetin	2	-	1.80(±0.02)	2986(26)
			16	-	1.69(±0.02)	3195(05)
			128	-	1.48(±0.03)	3073(16)
		Piperine	1	17.63(±0.026)	1.35(±0.04)	4076(28)
			8	17.80(±0.026)	1.33(±0.01)	4096(14)
			64	16.96(±0.055)	1.23(±0.01)	3670(38)
2.	1 mL/min	Quercetin	2	-	1.71(±0.02)	2992(07)
			16	-	1.64(±0.02)	3114(46)
			128	-	1.45(±0.01)	2974(26)
		Piperine	1	17.71(±0.006)	1.32(±0.03)	4120(60)
			8	17.79(±0.006)	1.30(±0.02)	4106(22)
			64	16.93(±0.01)	1.21(±0.01)	3678(05)
3.	1.2 mL/min	Quercetin	2	-	1.65(±0.02)	2886(12)
			16	-	1.62(±0.02)	2928(18)
			128	-	1.45(±0.02)	2787(10)
		Piperine	1	17.20(±0.05)	1.23(±0.01)	3878(22)
			8	17.20(±0.06)	1.30(±0.02)	3854(40)
			64	16.58(±0.04)	1.17(±0.01)	3562(11)

*****Data expressed as mean (±SD), n=3

3.2.7. System suitability

To determine the system suitability, retention time, resolution, theoretical plate, height equivalent theoretical plate, separation factor, and tailing factor were studied for both drugs.

Each drug was injected at a concentration of 50 µg/mL to determine the suitability of the system. The resolution for both drugs was found to be 16.93 (±0.07, which indicated well-resolved peaks. The peak resolution, theoretical plate, tailing factor, and height equivalent theoretical plate were found to be within acceptable limits, as shown in **Table 2.5**. The proposed validated analytical method fulfilled the requirements for system suitability.

Table 2. 5. System suitability parameters of the validated analytical method

Analytes	**Conc. (µg/mL)**	**Retention time (t_R-min)***	**Peak resolution (R)***	**Theoretical plate (N)***	**Tailing factor (T)***	**HETP* (mm)**
Quercetin	50	2.81 (±0.004)	-	2757 (±08)	1.54 (±0.036)	0.0544 (±0.0001)
Piperine	50	10.277 (±0.006)	16.93 (±0.07)	3751 (±37)	1.26 (±0.047)	0.0400 (±0.0004)

***Data expressed as mean (±SD), n=3.

3.2.8. Stress studies

Stress studies were performed to determine the stability of quercetin and piperine under oxidative and hydrolytic stress conditions, as shown in Table 6. Quercetin was found to undergo degradation under acidic and basic hydrolytic stress conditions at 80°C for 2 h, whereas piperine underwent partial degradation under hydrolytic stress conditions. Complete degradation was observed for quercetin when exposed to 0.1 N NaOH stress conditions. Both drugs were stable under oxidative stress conditions. Piperine showed less than 10% degradation under acidic and basic hydrolytic stress conditions, as shown in **Table 2.6**, as displayed in **Figure 2.7**. In addition, individual drugs were subjected to acid and base hydrolysis to confirm the degradation of drugs under similar conditions (Figure 2.8). The degradation product of quercetin was eluted at the retention time of 2.0 min and 3.8 min. Whereas, the degradation product of piperine eluted at 4.93 min and 6.61 min at a fixed wavelength of 346 nm. The degradation of quercetin and piperine under extreme pH conditions provides evidence for the rationality of choosing the NLC formulations where dual drugs were loaded into it; NLCs can protect quercetin against gastric acid degradation.

Table 2. 6. % Recovery of quercetin and piperine after stress conditions

Stress condition	**Sample treatment**	**Quercetin**	**Piperine**
		% Recovery (±SD)*	**% Recovery (±SD)***
Hydrolysis	0.1(N) HCl, 2hr.	67.60 (±10.15)	92.84 (±3.07)

	0.1(N) NaOH, 2hr.	-	94.19 (±0.58)
	Water, 2hr.	100.16 (±2.14)	97.09 (±0.48)
Oxidation	15% H_2O_2, 2hr.	107.64 (±1.78)	99.58 (±1.66)

*****Data expressed as mean (±SD), n=3.

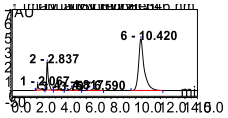

(A) 0.1N HCl, 2 hr.

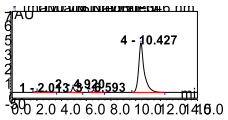

(B) 0.1N NaOH, 2 hr.

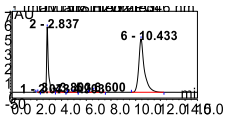

(C) 15% H_2O_2, 2 hr.

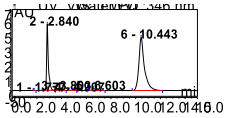

(D) Water, 2 hr.

Figure 2. 7. Simultaneous RP-HPLC chromatogram generated under various stress study conditions for quercetin and piperine in combination, respectively

4. Summary

The proposed analytical method for the simultaneous detection and quantification of quercetin and piperine by RP-HPLC was developed and validated according to ICH. The developed method was further validated in terms of specificity, linearity, range, accuracy, precision, sensitivity, and system suitability. The present method was found to be simple, rapid, precise, and accurate for the simultaneous quantification of quercetin and piperine in dual-drug-loaded NLCs for the estimation of % DEE, % DL, and cumulative % drug release in co-loaded NLCs. This method includes a single-step sample preparation to extract both drugs from the complex matrix, and the absence of an interference peak at the retention times demonstrates the specificity of the method. An in vitro drug release study revealed that the formulation of NLCs improved the solubility and stability of quercetin and piperine. The developed method can easily be applied for the simultaneous detection and quantification of both these drugs in other lipid-based nanoformulations such as solid-lipid nanoparticles, polymer-lipid hybrid nanoparticles, and lipid drug conjugates for *in vitro* and *in vivo* studies.

This work was published in the ***Journal of Pharmaceutical and Biomedical Analysis*** (**Impact Factor: 3.983**), and this validated method can be further used to estimate the concentration of quercetin and piperine in terms of entrapment efficiency and drug loading in the developed NLC formulation and *in vitro* drug release study.

Nanostructured lipid carriers as a strategy for encapsulation of active plant constituents: Formulation, in-vitro physicochemical characterizations and cellular evaluations to improve apoptosis in Oral Squamous Cellular Carcinoma (FaDu Cells)

1. Introduction

Quercetin showed dose-dependent cell cycle arrest with inhibition at the G1 and S phases along with mitochondria-mediated apoptosis in the SCC 25 cell line [32]. In the SAS cell line of oral cancer, quercetin inhibited the PIK3 and MAPK pathways and reduced the expression of metalloproteinases [33]. Studies on the anti-cancer activity of piperine in oral cancer KB cell lines have shown that it modulates cellular DNA content with cell cycle arrest at G2/M phase along with the generation of reactive oxygen species (ROS) [34]. Piperine has a high permeation rate because of its lipophilic and unionised nature and non-saturable absorption kinetics [35]. Phytoconstituents such as quercetin and piperine have been widely explored in cancer cell lines, especially in oral cancer. Piperine has been found to inhibit p-glycoprotein efflux [36]; hence, it acts as a penetration-enhancing agent for other drugs. Both phytoconstituents act on different pathways in the prognosis of oral squamous cell carcinoma, which may give rise to new combination drugs from natural origin as a treatment. This provides a rationale for this combination treatment for oral squamous cell carcinoma (OSCC).

Quercetin is a BCS Class IV drug [14], which is photosensitive in nature and exhibits low gastrointestinal absorption and extensive first-pass metabolic effects [24a]. This leads to a severe decrease in the bioavailability of quercetin after oral administration [37]. Interestingly, similar properties have been found in the case of piperine, that is, low aqueous solubility [23b], photosensitivity [24b] but high permeability (log P: 2.25) [38], thereby it is categorised under the BCS II category. To utilise their potential in pharmaceuticals, there is an unmet need for advanced drug delivery systems preferably lipid-mediated to overcome all these challenges and deliver these drugs through an imperfect lipid matrix system with high loading capacity [39] [18].

Concerning formulation aspects for active plant constituents, lipid nanoformulations (LNFs) can be considered as a well-recognized option for the delivery of these hydrophobic constituents [40], [41]. Solid lipid nanoparticles (SLNs) and NLCs are lipid-based particulate systems (not vesicular systems) which have been rated as high as per delivery perspective among LNFs [42], [43]. Solid lipid nanoparticles constitute a single solid lipid which enables low drug loading and low stability due to oozing out of the drug during crystallisation of solid lipids [44], whereas NLCs comprise both solid and liquid lipid mixtures which provide anomalous matrix structures and are categorised into three types: imperfect crystal, amorphous, and multiple [45]. Hence, maximum drug loading can be achieved with high stability [46]. Hence, NLCs can be a better option than SLNs for achieving the desired physicochemical properties of the formulated delivery systems [47]. Therefore, we preferred NLCs as a suitable lipid-based nanoformulation platform for the sequential delivery of quercetin and piperine to obtain the desired physicochemical properties. In addition, we aimed

to incorporate both drugs into NLCs and their characterisation using several techniques, followed by *in vitro* cellular evaluation and bio-distribution in rats.

2. Materials and methods

2.1. Materials

Glyceryl behenate, commercially known as Compritol® 888 ATO, was obtained as a gift from Gattefosse, France. Quercetin, piperine, squalene (SQL), green fluorescent Coumarin-6 dye, and dialysis sac with a molecular cut-off (MWCO) of 12 kDa were purchased from Sigma-Aldrich Chemical (St. Louis, MO). HPLC-grade acetonitrile, methanol, and glacial acetic acid were obtained from Merck Pvt. Ltd., Mumbai, India. Emulsifiers such as Tween 80, Span 80, and acetone were purchased from HIMEDIA Laboratories Pvt. Ltd., Mumbai, India. Ethanol was purchased from EMSURE® Grade (Merck KGaA, Darmstadt, Germany). Water was purified with a Milli-Q & ELIX water purification system (Merck Millipore, USA) and used throughout the experiments. Modified Eagle's medium (MEM), foetal bovine serum (FBS), penicillin, streptomycin, and trypsin/EDTA were purchased from Invitrogen Life Technologies, USA.

2.2. Formulation development of NLCs

The low aqueous solubility of quercetin and piperine plays an important role in formulation development. Solvent evaporation through the high-shear homogenisation method was used for NLCs preparation [48]. Compritol® 888 ATO, as a solid lipid and squalene as a liquid lipid, was selected [49]. Compritol® 888 ATO, squalene, and piperine were solubilized in chloroform, while quercetin required acetone for solubilisation. Span 80 was added to the lipid mixture as an emulsifier to improve the solubility of the drug and lipids after mixing both solutions by vortexing with a digital infrared vortex mixer. An aqueous surfactant solution of Tween 80 was prepared as a dispersion medium. Slow addition of the drug-lipid solution into the aqueous surfactant solution was performed under a high shear homogeniser (T25 digital ULTRA TURRAX®, IKA® Germany) at 15000 rpm under cold conditions. Homogenisation was continued until complete evaporation of the organic solvent was used. Sonication was then performed for the prepared dispersion using a probe sonicator (VCX500, SONICS Vibra cell, USA) with an amplitude or sonication power of 20% with on-off cycles of 8 and 12 s, respectively, under cold conditions. The resultant nanoparticles were recovered from the dispersion by centrifugation at 4°C (Eppendorf Centrifuge 5810R, Germany) using a Macrosep® 0.2 µm filter (Pall Corporation, Washington, USA) for 90 min at 3800 rpm to restrict submicron or larger particles [29].

Blank NLCs were prepared using similar procedures, except without the addition of piperine and quercetin. Drug loaded NLCs formulations like Quercetin loaded NLCs (Q-NLCs), Piperine loaded NLCs (P-NLCs) and Piperine-Quercetin co-loaded NLCs (PQ-NLCs) were prepared with the above-mentioned procedure. The composition of the formulations and their percentages (% w/w) for the design of NLCs are listed in **Table 3.1**. These formulations were freeze-dried using sucrose as a cryoprotectant using a lyophilizer (L-300, BUCHI, Switzerland) for further analysis, including thermal and XRD characteristics.

Table 3. 1. Optimized components for various NLC formulations

Components	**Blank NLCs (% w/w)**	**P-NLCs (% w/w)**	**Q-NLCs (% w/w)**	**PQ-NLCs (% w/w)**
Compritol 888 ATO (Solid lipid)	70	50	60	40
Squalene (Liquid lipid)	25	25	25	25
Piperine	-	20	-	20
Quercetin	-	-	10	10
Span 80	2.5	2.5	2.5	2.5
Tween 80	2.5	2.5	2.5	2.5

2.3. Characterization of NLCs

2.3.1. Particle size, Polydispersity index (PDI) and Zeta potential

The mean hydrodynamic diameter of the prepared NLCs was measured using a particle size analyser (Nano-ZS, Malvern Instruments Ltd.). The PDI for NLCs reflects homogeneity among the particle populations. The zeta potential was determined using the same equipment at the ambient temperature.

2.3.2. Drug entrapment efficiency and drug loading

The total amount of drug entrapped within the nanoparticles is always represented by the entrapment efficiency of nanoparticles [50]. This is one of the most important parameters for the characterisation of drug-loaded nanoparticles. In the case of drug-loaded nanostructured lipid carriers (NLCs), the inside core provides space for drug entrapment. The prepared NLCs were passed through a 3KDa filter (Macrosep® Advance Centrifugal Device, Pall Corporation, Port Washington, NY) with the help of a cooling centrifuge at 4°C and 2422 g for 15 min to remove the free drug from the NLC dispersion [29 51]. Particles retained over the 3KDa filter represent true nano-dispersion. To extract drugs entrapped within the NLCs, the true nanodispersion was treated with a solvent mixture of chloroform and acetone in a ratio of 1:1. Then, the dispersion with the solvent mixture was vortexed for 30 min, which allowed chloroform to disrupt the lipid matrix and allowed both drugs to be solubilized in a solvent mixture. Both aqueous and organic layers were separated and filtered through a 0.22 µm syringe filter. RP-HPLC analysis of the samples was carried out to determine the drug entrapped within the nanoparticles along with the free drug. Quercetin and piperine were estimated using a previously validated RP-HPLC method [52].

2.3.3. Transmission electron microscopy (TEM)

The surface morphological features of the prepared NLCs were estimated using transmission electron microscopy. NLC samples were examined at different magnifications using lanthanum hexaboride (LaB_6) cathodes as a source with high resolution using transmission electron microscopy (TEM) (FEI Tecnai T20, Osaka, Japan) [26].

2.3.4. Differential scanning calorimetry (DSC)

To determine the presence of any crystal form of pristine API in the lipid matrix, differential scanning calorimetric analysis was performed (DSC-3, Mettler Toledo, Switzerland). Aluminium pans were used to record thermograms. An empty pan was used as the reference. Approximately 5 mg of sample was placed in a sample pan and crimped with a crimping machine for tight sealing of the pan. The heating rate was kept at at10°C.min^{-1} within the range of room temperature (25°C) to 500°C. Nitrogen purging was performed at a 20mL.min^{-1} flow rate to maintain a stable inert atmosphere [29].

2.3.5. X-ray powder diffraction (XRD)

to determine the nature of the lyophilized nanostructured lipid as crystalline or amorphous, x-ray crystallography was performed with the help of X-ray diffractometry (BRUKER D8 ADVANCE). The X-ray source was Cu Kα (λ=1.5406Å), and the operation current and voltage applied were kept at 40mA and 40KeV respectively. The angular range for data collection was 5°-60° along with a step size of 0.05° and step time 0.3 secs. XRD analysis was performed for quercetin (API), piperine (API), Q-NLCs, P-NLCs, and PQ-NLCs, along with a blank formulation using the above-mentioned protocol [29].

2.3.6. *In vitro* drug release study

To determine the amount of drugs released from the developed NLCs, *an in vitro* drug release study was conducted using the dialysis bag method [53]. The dialysis sac was activated by soaking it overnight in 35% v/v ethanol in water, which was selected as a dissolution medium for *in vitro* drug release studies [54]. An accurately measured volume of the NLC dispersion was kept in a previously soaked dialysis membrane tied to both ends to prevent leakage of the NLC dispersion into 4mL of dissolution medium. An incubator shaker (CIS-18 PLUS, REMI Electrotechnik, Ltd., Japan) was used to maintain stirring at 125 rpm and 37°C. Aliquots of 200 µL were withdrawn and replaced with an equal volume of fresh dissolution medium to maintain sink conditions. Sampling was performed at predetermined time intervals from 0.08, 0.5, 1.0, 1.5, 2, 4, 6, 8, and 12 h. All samples were filtered through 0.2 µm syringe filters and analysed using a previously validated RP-HPLC method. The *in vitro* drug release profile was plotted from the% cumulative drug release as a function of time (h).

The above-mentioned protocol was used to perform *an in vitr*o drug release study for Q-NLCs, P-NLCs, and PQ-NLCs in triplicate. In addition, the pristine drug was suspended in water as 1 mg.mL^{-1} and performed the *in vitro* drug release study was performed for pure drug as pristine quercetin and pristine piperine in triplicate. To determine the best fitting equations for release data, mathematical modelling of drug release kinetics was applied using relevant

kinetic models, including zero-order [29, 55], first-order [29], and Higuchi [29, 56] and the Korsmeyer-Peppas model [57].

2.3.7. Haemolysis assay

To determine the hemolytic properties, the nanoparticles were exposed to blood components for a certain incubation period. In this study, particles were exposed to a 1% RBC solution in PBS pH 7.4 for a half-hour at 37±0.5°C in an incubator. Spectrophotometric evaluation for haemoglobin quantification was performed at 540 nm using a multi-detection plate reader (Spectramax i3X, Molecular Devices, USA) after centrifugation for 5 min at 2000 rpm at room temperature. Water was used as a positive control, while PBS pH 7.4 was used as a negative control [58].

2.4. Cell culture conditions

FaDu (ATCC HTB-43; squamous cell carcinoma) was procured from the American Type Culture Collection (Manassas, VA, USA) and cultured in MEM medium supplemented with 10% foetal bovine serum (FBS) and penicillin-streptomycin. The cells were maintained in a humidified incubator at 37 °C with 5% CO_2 (HERACELL VIOS 150, Thermo Scientific). Cell lines were subcultured through enzymatic digestion with 0.25% trypsin/1mM EDTA solution after reaching approximately 70 %–80% confluency.

2.4.1. Cytotoxicity assay

To determine the cytotoxic potential, an MTT assay was performed for optimised drug-loaded NLC formulations and then compared with the combination of both drugs in their pristine solution form. FaDu cells (8×10^3) were seeded in 96 well sterile plates and treated with different concentrations of drugs for 24 h. NLCs were also compared to pure drugs in their individual forms. Media from the upper layer were replaced with 100µL of fresh media containing 20µL MTT (5 mg/ml). The cells were then incubated for 4 h to form the MTT formazan crystals. Then 200µl DMSO was added with gentle shaking, which dissolves formazans released from cells. After incubation for 15 min, the absorbance of the coloured solution was measured at a wavelength of 570 nm using a microplate reader (SPECTRA MAX I3X, Molecular Devices LLC, USA). IC_{50} values for NLC formulations were determined against oral cancer cell lines after 24 h and used for further molecular analysis.

2.4.2. Internalization of NLCs

Coumarin-6 loaded NLCs were prepared as previously described. Coumarin-6 was solubilized in the organic phase and then transferred to an aqueous surfactant solution under HSH. True Coumarin-6 loaded NLCs were obtained after filtering through a Macrosep® 0.2 µm filter under centrifugation at 4°C [59].

To perform cellular internalisation of NLCs along with their characterisation, FaDu cells were seeded on coated coverslips kept in 6-well plates and allowed to attach to the surface of the coverslip during an overnight incubation period. Then the treatment was given with fluorescent (coumarin-6) labeled NLCs for different time points of incubation 15 min, 30 min & 1 hr. Cells were washed in triplicate using phosphate-buffered saline (PBS) before and

after fixation with 4% paraformaldehyde (PFA) for 15 min in the dark. Cells were washed in triplicate with PBS followed by actin filaments stained with rhodamine phalloidin, which was previously diluted 1:100 in 1% BSA in PBS and incubated for 15 min. Cells were washed three times with PBS, and the coverslips were dried and mounted with ProLong Gold^{TM} anti-fade reagent (Thermo Scientific Co., MA) with DAPI (4, 6-diamidino-2-phenylindole), a mounting medium (Invitrogen) on the frosted glass slides. Images were acquired using a confocal microscope (CLSM) (TCS SP8, Leica Microsystems, Germany) in the blue, green, and red channels, respectively. All images were analysed using the Leica LAS-X software. All samples were freshly prepared and imaged in triplicate to ensure the reproducibility of the experiment [29].

2.4.3. Detection of apoptosis through AO/EtBr staining

The acridine orange (AO)/ethidium bromide (EtBr) staining technique was used to observe characteristic apoptotic morphological changes using confocal laser scanning microscopy. FaDu cells (1×10^5) were treated with the IC_{50} dose of NLC formulations and for pure drugs (equivalent concentrations of IC_{50} dose NLCs) for 24 h. Morphological changes were observed by confocal laser scanning microscopy. After 24 h, untreated cells and treated cells were washed with PBS before staining with AO (1 µg/ml) and EtBr (1µg/ml) in a ratio 1:1 incubated for 20 min. The cells were washed with PBS before mounting on glass slides with Prolong gold anti-fade reagent and visualised under a confocal microscope to observe changes in the morphological features of apoptosis [60].

2.4.4. Identification of mitochondrial morphology through JC-1 dye

The alteration in mitochondrial membrane potential ($\Delta\Psi m$) can be analysed with the help of JC-1 dye using a confocal laser scanning microscope. JC-1 dye forms J-aggregates in cells with intact mitochondrial membrane potential and forms monomers in case of impaired mitochondrial membrane potential. Cells were treated at doses with IC_{50} NLC formulations and for pure drugs (equivalent concentrations to IC_{50} dose NLCs) and incubated for 24 h. Cells were then washed with PBS pH-7.4 followed by the addition of JC-1 dye (2 µM) to each sample well. After incubation for 20 min, the cells were washed in triplicate using PBS and imaged using a confocal microscope. Red and green denote J-aggregates and J-monomers, respectively [61].

2.4.5. Annexin-V FITC dot plot assay

Annexin-V FITC is a calcium-dependent phospholipid-binding protein with a high affinity for phosphatidylserine. It binds to apoptotic cells on the surface of exposed cells. FaDu cells (2×10^5) were treated with the IC_{50} dose of NLCs and pristine drug (equivalent concentrations of the IC_{50} dose of NLCs) for 24 h. Cells were trypsinized and centrifuged at 3000 rpm for 5 min, followed by washing of the cell pellet with PBS (pH 7.4), and resuspended in 100 µL of binding buffer. Cells were incubated with annexin V-FITC and propidium iodide (PI) for 20 min. Samples were diluted with 400 µL binding buffer and analysed using a flow cytometer (Attune NXT software, Thermo Fisher Scientific, Singapore). The different quadrants in the Annexin V/PI analysis represent the different cell populations; FITC-negative and PI-negative cells are indicated as viable cells; FITC positive

and PI negative represent early apoptotic cells; FITC positive and PI-positive cells are late apoptotic cells; FITC negative and PI-positive cells are necrotic cells [61].

2.5. Bio-distribution of Coumarin-6 loaded NLCs

Healthy Sprague Dawley (SD) rats (5-7 weeks of age, weighed between 220-250 gram, either sex) were obtained from the Animal House Facility, National Institute of Pharmaceutical Education and Research (NIPER), Guwahati, Assam, India (IAEC Approval No.: NIPER/PE/19/24). Animals were acclimatised to the conditions and then kept deprived of food for 6 h before dosing Coumarin-6 loaded NLCs. At a dose volume of 5 mg/kg, Coumarin-6 loaded NLCs were administered through a per-oral route using oral gavage. After 6 h of dosing, animals were perfused with PBS (pH 7.4) to remove the blood contaminant before organ collection, including the oral mucosa, tongue, and salivary gland. The organs were removed and washed with Phosphate-buffered saline (PBS; pH-7.4). For qualitative estimation, a portion of the tissue was sectioned using a cryotome (CMI1950UV, Leica) using tissue freezing media with a thickness of 5µm. Sections were mounted on a glass slide with an anti-fade reagent and then observed under a fluorescence microscope (EVOS FL Auto, Thermo Scientific). For quantification, approximately 100-150 mg of tissue was weighed from each organ, homogenised with methanol, and centrifuged at 13000 rpm for 10 min. The supernatant was used for dye quantification using Spectramax (i3X, Molecular Devices, USA) by measuring the fluorescence intensity (excitation at 457 nm and emission at 501 nm). The concentration of the dye is expressed as ng/g of tissue.

$$\text{Concentration of dye (ng/gm)} = \frac{\text{Concentration of dye(ng/ml)}}{\text{Weight of tissue(gm)}}$$

3. Results

3.1. Formulation development of NLCs

Drugs selected for the development of NLCs have been reported to have anticancer potential. It was very challenging to encapsulate both hydrophobic drugs in a single matrix. Hence, nanostructured lipid carriers (NLCs) were selected and designed to co-encapsulate these drugs in combination to be effective against oral cancer. Solvent evaporation through a high-shear homogenisation method was implemented for the synthesis of NLCs. Compritol® 888 ATO, a solid lipid, makes nanoparticles rigid while squalene, a liquid lipid, prevents the crystallisation of solid lipids through an anomalous structure of the lipid matrix. Compritol® 888 ATO, which is soluble in chloroform and quercetin, is insoluble in chloroform, complicating the procedure. Polysorbate 80 and Tween 80 are non-ionic surfactants were used in higher concentrations, comprising 5%, which are having HLB values of 4.3 and 15, respectively. A lower lipid concentration allows proper distribution of sonication energy throughout the nanodispersion and yields a lower particle size [47]. In addition, homogenisation followed by sonication with the use of higher surfactant concentrations drastically reduced the particle size and helped stabilise the formulation [62]. An optimised nanoformulation with co-encapsulation of both quercetin and piperine was possible because of all these factors and provided the necessary flexibility for variations among these excipients.

3.2. Characterization of optimized NLCs

3.2.1. Particle size, PDI and Zeta potential

Optimised NLC formulations were analysed for particle size, PDI, and zeta potential using a Zetasizer, and the results are listed in **Table 3.2**. The hydrodynamic diameters of the prepared NLCs were analysed immediately after the synthesis. It showed that particles synthesized with an optimized formulation method were well below 0.2 µm, which selectively represents the true nano population containing a dispersion of NLCs. The zeta potential represents the charge on the surface of the nanoparticles. The prepared NLCs were negatively charged.

Table 3. 2. Particle size, PDI and ZP values of different optimized NLCs samples

Sr. No.	Formulation	Particle size(nm)	PDI	Zeta Potential (mV)
1.	Blank NLCs	91.26 ±9.57	0.257 ±0.001	-17.33 ±6.33
2.	Piperine NLCs	115.7 ±6.26	0.258 ±0.083	-8.67 ±2.72
3.	Quercetin NLCs	116.6 ±30.9	0.171 ±0.019	-25.9 ±3.84
4.	Piperine-Quercetin NLCs	120.1 ±44.3	0.159 ±0.059	-19.6 ±10.1

*Data expressed as mean (±SD), n=3

3.2.2. Percent DEE and DL

According to the previously mentioned procedure, the % drug loading and % drug entrapment efficiency of the optimised NLC formulations were determined and are presented in **Table 3.3**. NLCs are known to encapsulate more drugs than solid lipid nanoparticles because they have an amorphous structure inside the matrix. Both quercetin and piperine are lipophilic, allowing lipid molecules to entrap these drugs in a lipid-based matrix system. This provides clear evidence for the greater drug encapsulation ability of the NLCs.

Table 3. 3. DEE and DL values of different optimized NLCs samples

Sr. No.	**NLCs formulation**	**DEE (%)**	**DL (%)**
1.	Piperine NLCs	91.80 ± 2.51	2.14 ± 0.79
2.	Quercetin NLCs	93.18 ± 5.5	1.05 ± 0.76

3.	Piperine-Quercetin NLCs	Piperine: 92.4±2.86 Quercetin: 87.17±6.06	Piperine: 4.26 ± 2.08 Quercetin: 1.41 ± 1.01

*Each value represents the mean ± SD (n=6)

3.2.3. Transmission electron microscopy (TEM)

The surfaces of the prepared NLCs were spherical, mimicking the DLS results below 200 nm. The core part is light in colour, covered with a dark border showing the exact structure of NLCs, as shown in **Figure 3.1**. NLCs were found to be intact particles, as the drugs were accommodated inside the lipid matrix. As NLCs are second-generation lipid nanoformulations, having the capacity to encapsulate more drugs is visible in the TEM image of drug-loaded NLCs which were found to be loaded with drugs with more than 90% entrapment efficiency, as mentioned in **Table 3.3**.

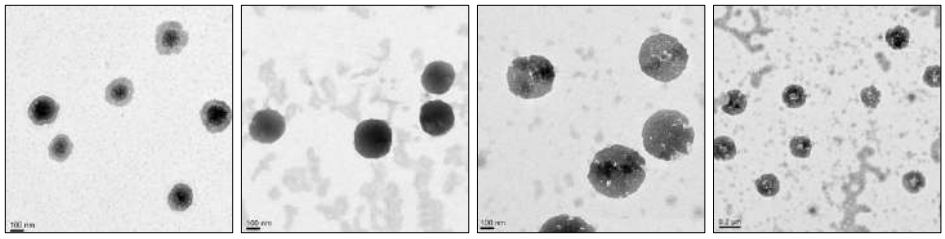

(a) (b) (c) (d)

Figure 3. 1. TEM images of formulations (a) Blank-NLCs, (b) Q-NLCs, (c) P-NLCs, and (d) PQ-NLCs, respectively.

3.2.4. Differential scanning calorimetry (DSC)

The DSC thermograms obtained for all samples are shown in **Figure 3.2**. DSC thermograms of pristine piperine and quercetin showed sharp endothermic peaks at 131°C and 316 °C due to the melting of the drugs, respectively. Drug-loaded NLCs in lyophilized form showed that the sharp endotherm at the melting temperature of drugs was absent, indicating that the drug was completely encapsulated inside the matrix in an amorphous form and no drug was present on the surface of the particles. An almost similar profile was observed with blank NLCs showing melting at 186°C followed by degradation of sucrose at 220-225°C. Overall, these observations confirmed the formation of NLCs with drugs entrapped in their amorphous form.

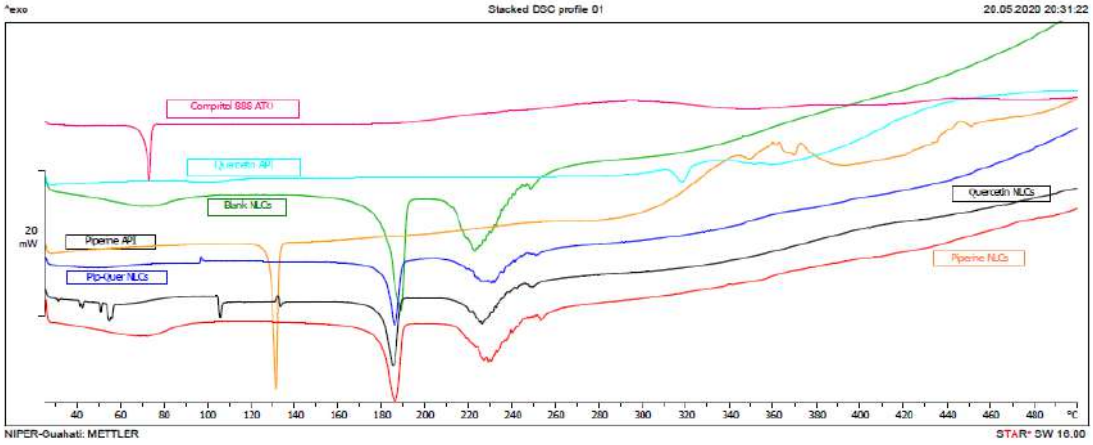

Figure 3. 2. Thermogram obtained from DSC including Quercetin API, Piperine API, Blank NLCs, P-NLCs, Q-NLCs and PQ-NLCs.

3.2.5. X-ray powder diffraction (XRD)

The prediction of the nature of the drug and solid lipid to crystalline and amorphous forms was performed using XRD analysis. The X-ray diffractogram obtained after XRD analysis of the pristine and prepared NLC formulations is shown in **Figure 3.3**. Generally, the structure of NLCs consists of an outer shell of solid lipid and an inner core of a mixture of both solid and liquid lipids, which provides maximum space for a drug to get entrapped into it. The intensity of the peaks was found to be reduced after drug loading into the NLCs as compared to pure APIs. The percent degree of crystallinity was also found to be reduced after incorporation into NLCs as compared to pure APIs. In the case of P-NLCs, the % degree of crystallinity was reduced by 62.89% compared with piperine API. Similarly, a 49.72% reduction in the% degree of crystallinity was observed for Q-NLCs against quercetin API. This explains the amorphous conversion of drugs after their incorporation into NLCs. The absence of sharp peaks in drug-loaded NLCs showed that the drug was converted into an amorphous form when entrapped into NLCs. Sharp intense peaks in blank NLCs can be due to the crystallisation of sucrose, which was used as a cryoprotectant during the lyophilisation of the NLC dispersion.

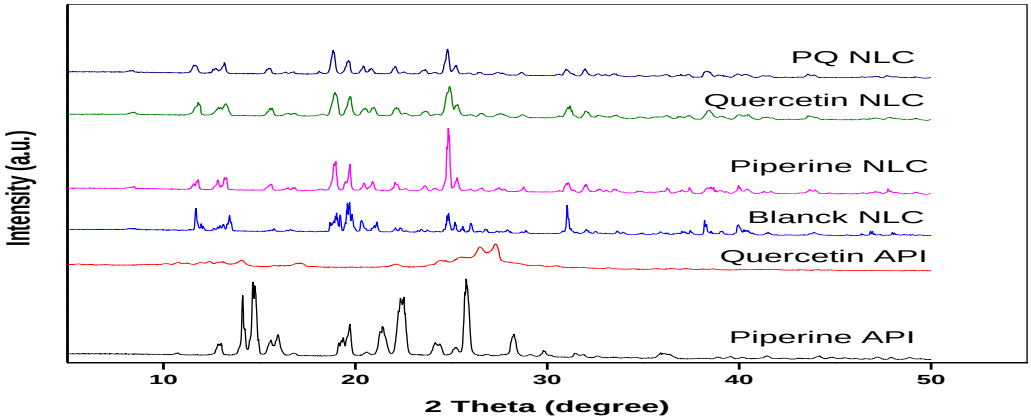

Figure 3. 3. X-ray diffractogram of various compounds including Quercetin API, Piperine API, Blank NLCs, P-NLCs, Q-NLCs and PQ-NLCs.

3.2.6. *In vitro* drug release study

The release study for optimised drug-loaded NLCs along with a pure drug solution was performed using the dialysis sac method. The graph of % cumulative drug release vs. time (h) is plotted in **Figure 3.4** and **Figure 3.5** for the pristine drug and drug-loaded NLCs, respectively. According to the drug release profile, pristine quercetin solution showed a 20.42±2.7% drug release within 12 h, while the piperine drug solution showed 21.11±1.7% drug release. Q-NLCs showed a maximum of 45.0±1.3% of quercetin released within 12 h, while P-NLCs released 38.40±5.2% of piperine at the same time. PQ-NLCs followed the Higuchi equation with a diffusion-mediated drug release pattern, while sequential NLCs followed the Korsemeyer-Peppas model with n<0.45, representing quasi-diffusion kinetics, as shown in **Table 3.4**. Compritol® 888 ATO, a solid lipid, tends to form rigid particles, which restricts the burst release of drugs from a solid matrix. This could be the reason for the slow diffusion of drugs from the lipid matrix into the diffusion medium. The rigidity of NLCs can be considered an important factor in drug release. It can be predicted to have a more sustained release pattern when administered *in vivo*.

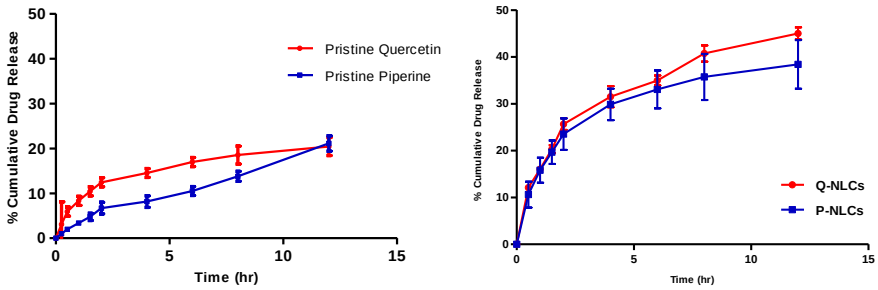

Figure 3. 4. Drug release profile from prepared sequential drug loaded NLCs and individual pristine API dispersions.

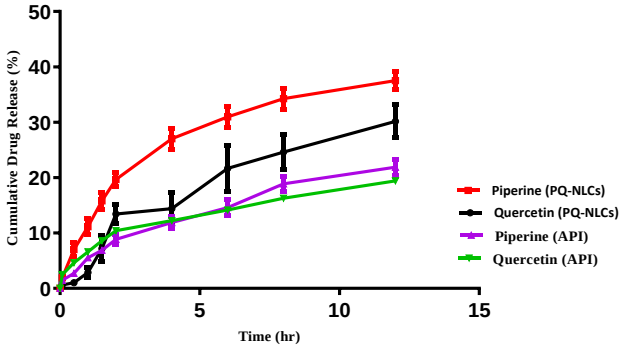

Figure 3. 5. Drug release profile for PQ-NLCs formulations and PQ-Pristine API in combination.

Table 3. 4. Various mathematical models, regression coefficient (R^2) values of different optimized NLCs formulations

Formulation	Zero order	First order	Higuchi	Korsemeyer-Peppas

		R^2 *	R^2 *	R^2 *	R^2 *	n*
PQ-NLC	**P**	0.826 (±0.013)	0.9277 (±0.031)	0.9641 (±0.004)	0.960 (±0.008)	0.535 (±0.048)
	Q	0.8923 (±0.031)	0.8799 (±0.006)	0.9296 (±0.013)	0.887 (±0.009)	1.04 (±0.031)
P-NLC		0.803 (±0.059)	0.9266 (±0.019)	0.9245 (±0.039)	0.951 (±0.036)	0.418 (±0.076)
Q-NLC		0.865 (±0.025)	0.8552 (±0.063)	0.9717 (±0.014)	0.972 (±0.01)	0.419 (±0.016)

*Data expressed as mean (±SD), n=6.

3.2.7. Haemolysis assay

The safety evaluation of nanoparticles is one of the most important characteristics determined through a hemolysis assay. No hemolysis was observed with the lyophilized NLCs, as shown in **Figure 3.6** and **3.7**. Blank and drug-loaded NLCs were found to be stable and compatible, without any interaction with blood cells.

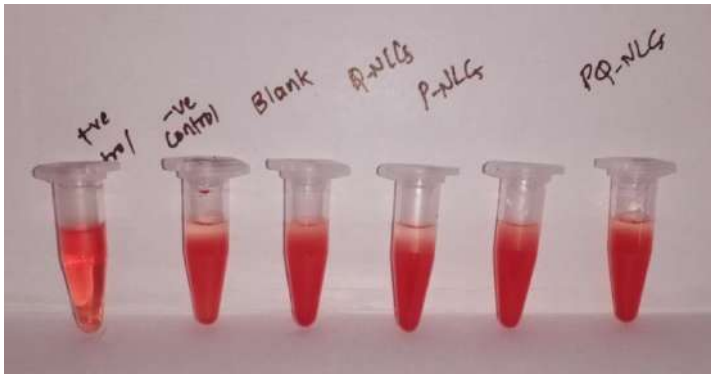

Figure 3. 6. Images for samples from haemolysis assay

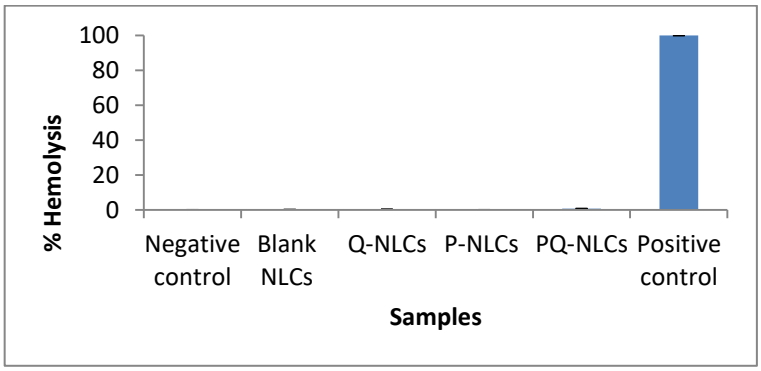

Figure 3. 7. Haemolysis assay performed with NLCs and control samples

3.3. *In-vitro* cellular evaluation

3.3.1. Cytotoxicity assay

To determine the anti-tumor activity of drug-loaded NLCs on the growth of FaDu cells, IC_{50} values were measured using the MTT assay, as shown in **Figure 3.8** and it was found to be 2.391 µM for P-NLCs, 0.799 µM for Q-NLCs and 0.934 µM for the prepared PQ-NLCs, respectively. The IC_{50} values were estimated at 24 h of exposure in comparison with the pristine drug, blank NLCs, and control, as shown in **Figure 3.9**. The IC_{50} of drug-loaded NLCs was found to be significantly lower than that of the free drug at a time interval of 24 h. Therefore, the IC_{50} concentration of PQ-NLCs in 24 h was considered more toxic than that of the free drug combination in FaDu cells. The combination of API at the IC50 dose did not significantly reduce the viability percentage as compared to the control cells. The percentage of cell viability was significantly decreased in the case of PQ-NLCs exposed to FaDu cells, compared to control as well as with the free combination drug-treated cells ($p < 0.001$). However, there were no significant changes in cell viability after treatment with Blank-NLCs compared to untreated cells. It has been reported that the IC_{50} value for quercetin is approximately 50µM when treated against the SSC-9 cell line [63], while piperine showed an IC_{50} value of 124 µM against the KB cell line [34]. In the case of curcumin and genistein co-loaded NLCs, where more cytotoxicity was observed, might be due to the efficient internalisation of NLCs [64]. Hence, it is self-explanatory that formulations such as NLCs improve the cytotoxic potential of drugs as compared to pure drug solutions. Overall, the results showed that the formulation showed a higher cytotoxic potential at a lower concentration than the pristine drug solutions.

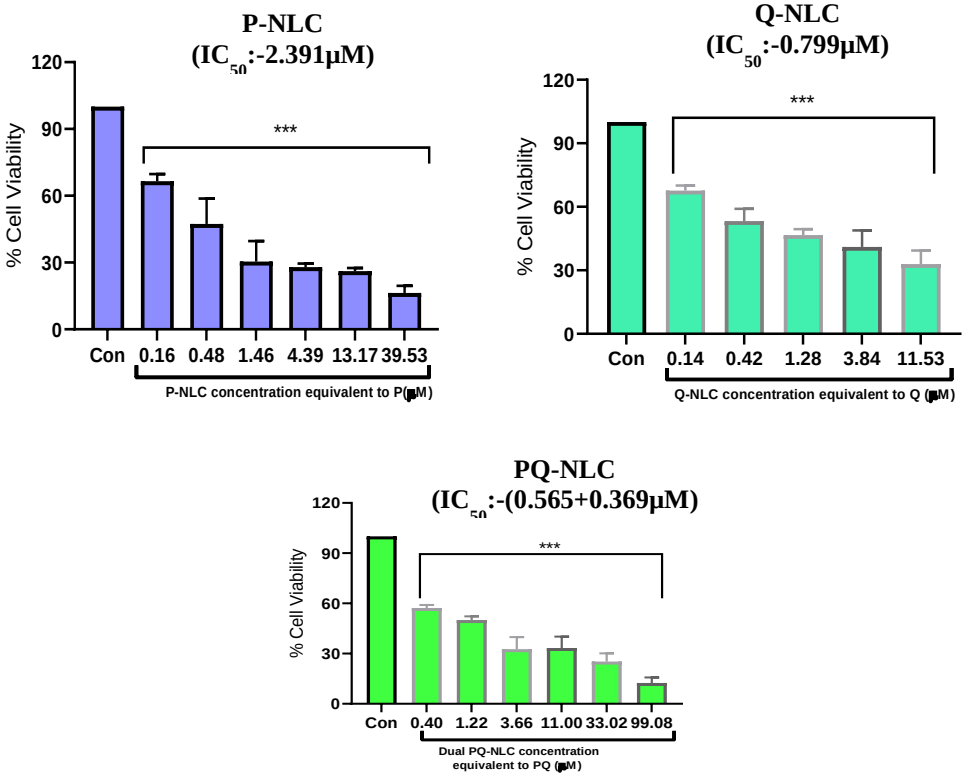

Figure 3. 8. Effect of P-NLC,Q-NLC & PQ-NLC on the viability of Oral cancer cell line (FaDu). Cells were treated with different concentration of P-NLCs; Q-NLCs & PQ-NLCs for 24 hr. Cell viability was determined by using MTT assay. Data were represented as Mean ± SEM triplicate independent experiments. Statistical analysis were performed one way ANOVA followed by Dunnett's Test ***p<0.001 Vs Control.

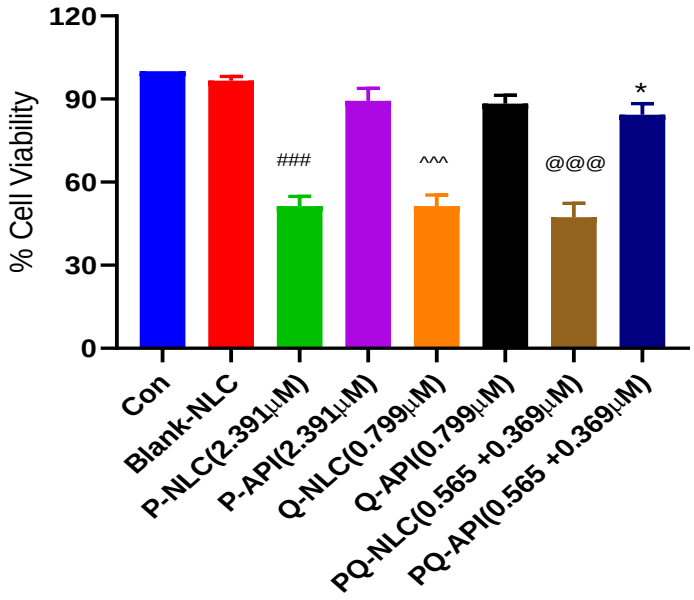

Figure 3. 9. Effect of P-NLC,Q-NLC & PQ-NLC on the viability of Oral cancer cell line (FaDu). Cells were treated with IC_{50} concentration of P-NLCs; Q-NLCs & PQ-NLCs for 24 hr along with the equivalent concentration of individual pristine drug and blank. Values are presented as Mean ± SEM (n=3) and the comparisons are made on the basis of one-way ANOVA followed by Bonferroni multiple test, *P< 0.05 vs Blank; ###P< 0.001 P-API vs P-NLCs, ^^^P< 0.001, Q-API vs Q-NLCs, &@@@P< 0.001 PQ-API vs PQ-NLCs.

3.3.2. Internalization and Characterization of NLCs by fluorescence microscopy

Cellular uptake of nanoparticles is a key parameter to be determined after formulation development. The rate and extent of particle uptake generally depend on the physicochemical characteristics of the particles, including their size, zeta potential, and shape. Stable uptake of nanoparticles, followed by degradation by lysosomal enzymes, causes the release of drugs encapsulated within the lipid matrix. Therefore, to understand the rate-dependent mechanism of cellular uptake of NLCs, coumarin-6 labeled NLCs were incubated with FaDu cells *in vitro*, as shown in **Figure 3.10A**. The images showed that particles were internalised within 15 min, with more than 95% co-localization, with a correlation coefficient of approximately 0.9524. Further, incubation of coumarin-6 labelled NLCs with cells showed saturation of nanoparticles with almost similar percent co-localization, as shown in **Figure 3.10B**. This suggests that particles are easily engulfed by cells within a very short period. Images were taken with DAPI (blue dye), fluorescent (Coumarin-6) labelled NLCs (green dye), rhodamine phalloidin, actin staining (red dye), and merged. Colour intensity reflects higher colocalization with no background. An overall study proved that particles are extremely

suitable for the treatment of cancer as they show maximum co-localization in a very short time.

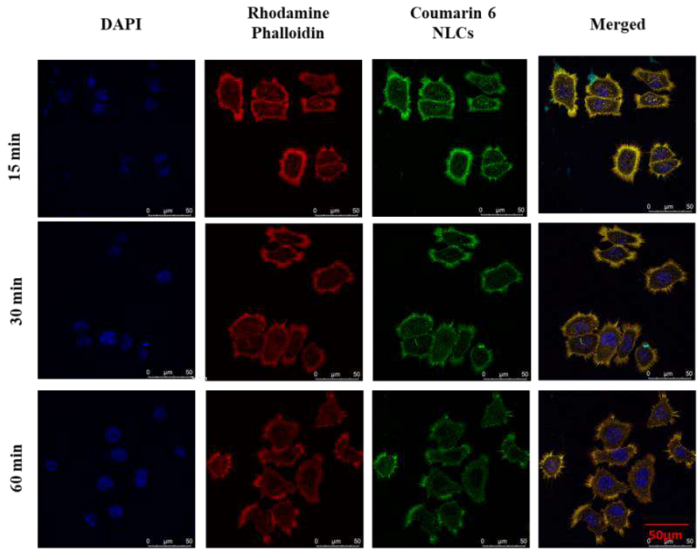

(A)

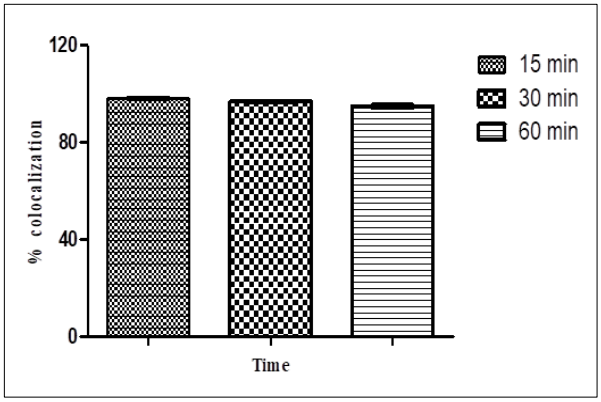

(B)

Figure 3. 10. Cellular uptake of Couarin-6 dye loaded NLCs, (A) Confocal microscopic images for cellular internalization of Coumarin-6 NLCs in FaDu cells (B) Plot of % co-localization at a time interval of 15, 30, and 60 min, respectively.

3.3.3. Detection of apoptosis through AO/EtBr staining

A confocal microscopic observation after 24 h of treatment with the IC_{50} dose of PQ-NLC on FaDu cells stained with AO/EtBr depicts both early and late apoptotic features such as chromatin condensation, membrane blebbing, the formation of apoptotic bodies, and fragmented nuclei. Staining with AO/EtBr confirmed both late and early apoptotic changes in FaDu cells induced after treatment with PQ-NLCs. For comparison purposes, P-NLCs and Q-NLCs were also performed for this assay along with their pure drug solutions. The treatment was given at IC_{50} concentrations of the formulation along with pure drug solution, and images are shown in **Figure 3.11**. The formulations showed more apoptotic changes than the pure drug solutions. Dual drug-loaded NLCs showed more early and late apoptotic changes in all treatments.

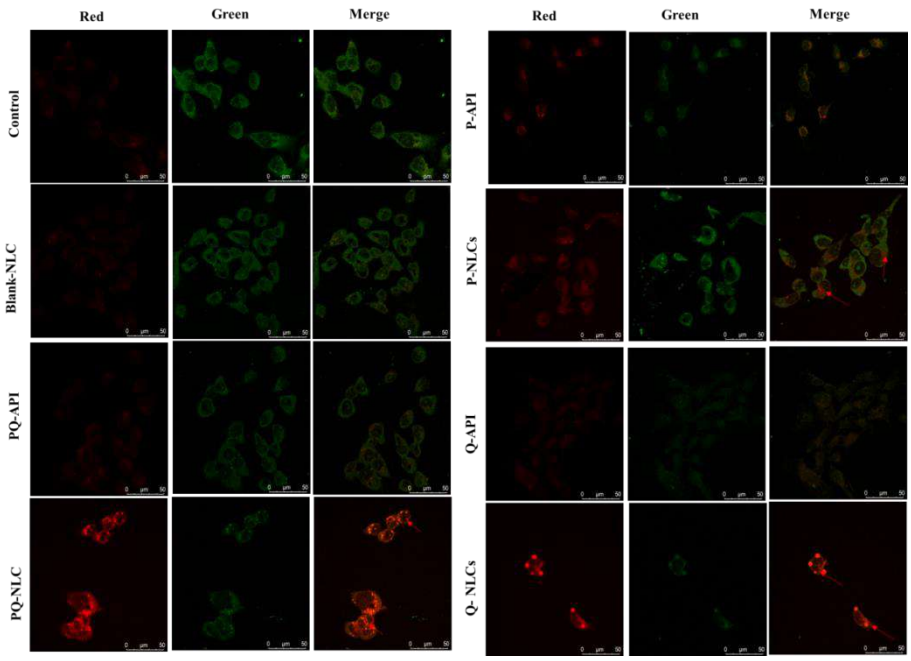

Figure 3. 11. Effect of drug encapsulated NLCs on early apoptotic changes studied through dual AO/EtBr staining.Representative images of FaDu cells treated with Blank NLCs and drug encapsulated NLCs along with pristine drugs for 24h and subsequently stained with dual staining [AO (1 µg/ml): EtBr (1 µg/ml) in 1:1 ratio] for 30 min. The cells were visualized under the confocal microscope in three respective channels (green, red, and merged) with 63X magnification, which indicates the apoptotic morphological changes after 24h drug treatment.

3.3.4. Identification of mitochondrial morphology through JC-1 dye

JC-1 is a cationic dye used to determine mitochondrial depolarisation and mitochondrial membrane potential. The decrease in red fluorescence intensity and increase in green fluorescence intensity indicates mitochondrial depolarisation due to the opening of the mitochondrial permeability transition pore (MPTP) as a result of the loss of intracellular accumulation of J-aggregates and increase in their monomeric form (green). This leads to mitochondrial membrane disruption and loss of function. Treatment with IC_{50} dose P-NLCs, Q-NLCs, and PQ-NLCs increased JC-1 monomer in cells, which was observed in confocal microscopic images, resulting in increased green fluorescence intensity, suggesting early apoptotic mitochondrial depolarisation ($\Delta\psi$) (**Figure 3.12A** and **3.12B**). The treatment was also given at IC_{50} concentrations of the sequential formulation along with their pure drug solution, and images are also represented. The formulations caused more mitochondrial depolarisation than the pure drug solutions. Dual drug-loaded NLCs showed a lower fluorescence intensity ratio than the other NLCs, indicating maximum depolarisation of the mitochondrial membrane, leading to cell death.

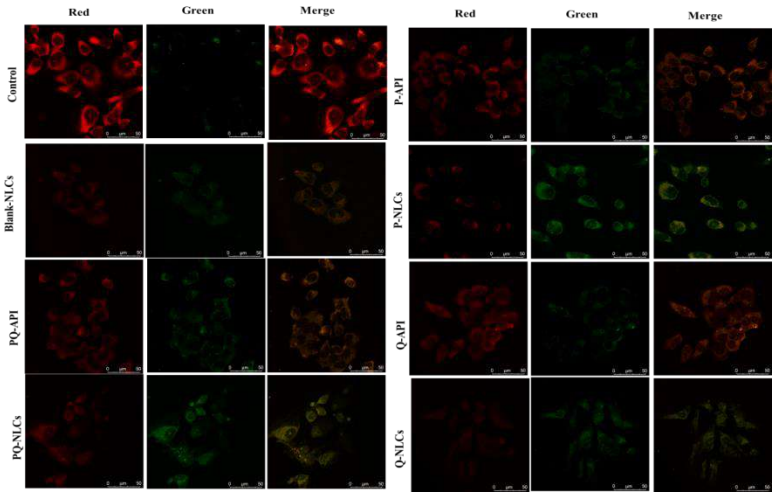

(A)

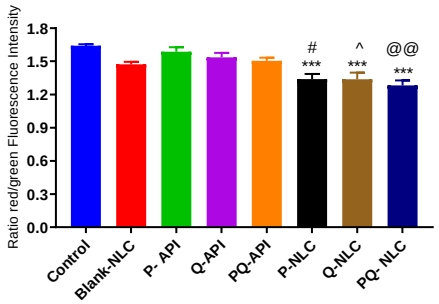

(B)

Figure 3. 12. Effect of drug encapsulated NLCs on mitochondrial membrane potential (Δψ).(A) Representative images of Fadu cells treated with Blank-NLCs and drug encapsulated NLCs along with pristine drugs for 24h and subsequently stained with JC-1 dye (2µM) for 30 min. The cells were visualized under confocal microscope in three respective channels (green, red and merged) with 63X magnification. (B) Results were expressed in the terms of ratio of red/green fluorescence intensity. Values are presented as Mean ± SEM and the comparisons are made on the basis of one-way ANOVA followed by Bonferroni multiple test, ***P< 0.001 vs Control; #P< 0.05 P-API vs P-NLCs, ^P< 0.05, Q-API vs Q-NLCs, &@@P< 0.01 PQ-API vs PQ-NLCs.

3.3.5. Annexin-V FITC dot plot assay

Flow cytometric analysis was used to determine apoptosis using annexin V FITC and PI dual staining. The lower left quadrant (Q1) represents the live cell population, the lower right quadrant (Q2) is regarded as the early apoptotic cell population, whereas the upper right quadrant (Q3) is considered as the late apoptotic cell population, and the upper left quadrant (Q4) is represented as the necrotic population. Flow cytometric analysis indicated that after 24 h of treatment with IC_{50} PQ-NLC on FaDu cells significantly increased the percentage of late apoptosis and early apoptosis compared to untreated cells, as well as treatment with respective free drug concentrations (**Figure 3.13A** and **3.13B**). However, no significant changes were observed in the percentage of total apoptotic cells exposed to blank-NLCs. Necrotic indices of

FaDu cells were not significantly altered in response to the IC_{50} doses of P-NLC, Q-NLC, and PQ-NLC, along with an equivalent concentration of the free drug.

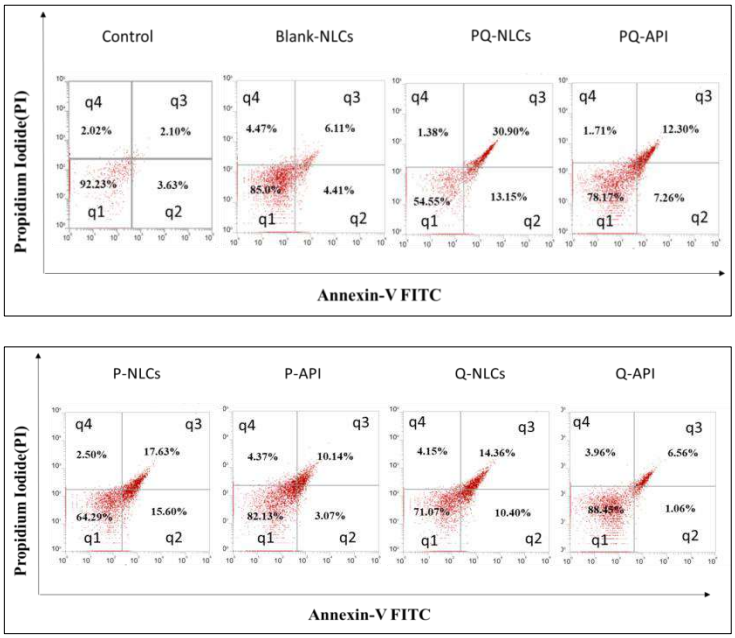

(A)

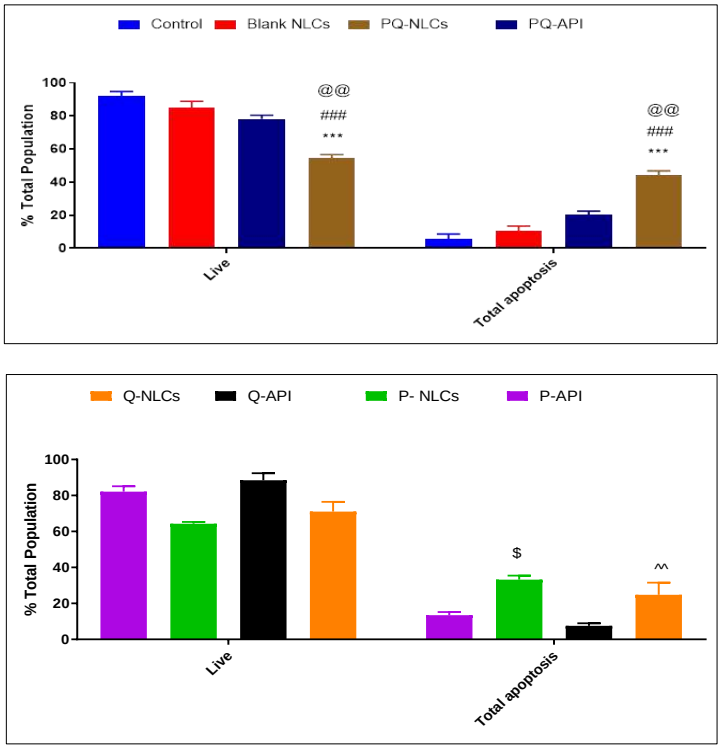

(B)

Figure 3. 13. Effect of drug encapsulated NLCs on induction of apoptosis assessed by using Annexin-V FITC/PI.(A) Representative images of flow cytometry upon FaDu cells treated with Blank NLCs and drug encapsulated NLCs along with pristine drugs for 24h and subsequently stained Annexin-V FITC/PI for 20 min by flow cytometry. Lower left Quadrant (q1): live cells; lower right quadrant (q2): early apoptosis; upper right quadrant (q3): late

apoptosis; upper left quadrant (q4): necrotic cells. (B) Results were expressed in the terms of % Total Population. Values are presented as Mean ± SEM and the comparisons are made on the basis of Two-way ANOVA followed by Bonferroni multiple test, *P< 0.05, **P< 0.01, ***P< 0.001 vs Control; #P< 0.05 P-API vs P-NLCs, ^P< 0.05 Q-API vs Q-NLCs & @@P< 0.01 PQ-API vs PQ-NLCs.

3.4. *In-vivo* bio-distribution of NLCs

Determination of *the in vivo* distribution of nanoparticles is an important aspect that needs to be studied. The utilisation of dye-loaded nanoparticles for determining the *in vivo* fate of nanoparticles in terms of bio-distribution has been studied earlier. Quantitative estimation has been studied in tissues through the determination of dye concentration, while qualitative evaluation through fluorescence imaging using fluorescence microscopy [65]. Coumarin-6, a green fluorescent dye, was loaded into the NLCs. Coumarin-6 loaded NLCs were prepared using a procedure similar to that mentioned earlier and were used for biodistribution studies in rats. After 6h of per-oral administration at a dose volume of 5 ml/kg of Coumarin-6 loaded NLCs, various organs were removed for histological evaluation.

Coumarin-6 loaded NLCs were found to reach almost all organs, including the tongue, salivary gland, and oral mucosa, as shown in **Figure 3.14A**. Sufficient concentration can be achieved through NLCs in oral tissues such as the oral mucosa, salivary gland, and tongue, as shown in **Figure 3.14B** and is considered to reach the regions of the buccal cavity and can be used as an effective treatment for oral cancer.

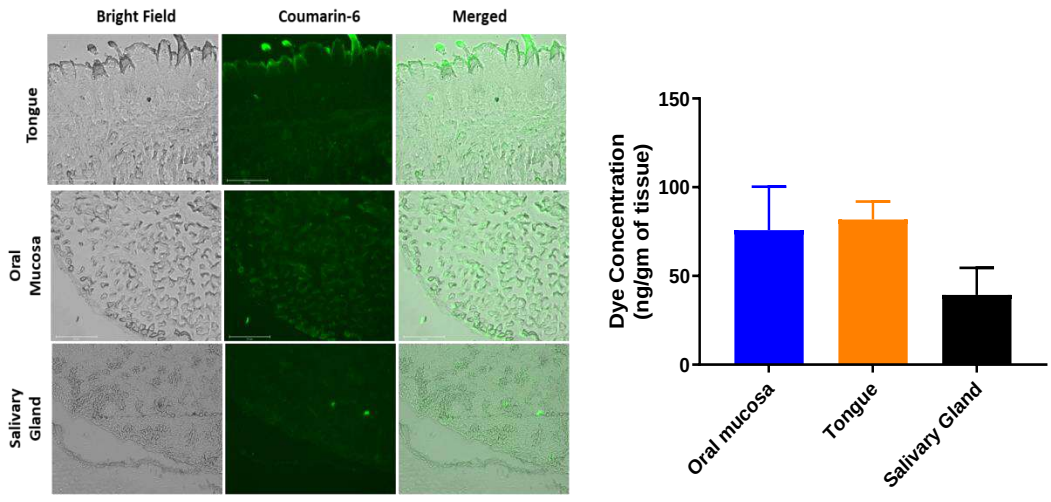

(A) **(B)**

Figure 3. 14. Bio-distribution of prepared NLCs. (A) Fluorescence microscopic images of thin sections of various tissues obtained from rats for bio-distribution of orally administered Coumarin-6 loaded NLCs visualized under the fluorescence microscope, (B) Quantification of dye in respective tissues by measuring the fluorescence intensity.

4. Discussion

Compritol® 888 ATO was selected as a solid lipid because it provides good rigidity to nanoparticles, while squalene was selected as the liquid lipid which forms the inner core of

the NLCs along with the outer layer of the solid lipid. This reflects the good compatibility between Compritol® 888 ATO and squalene, as similar results have been reported previously [49]. Both lipids and piperine were solubilized in chloroform, while quercetin required acetone for solubilisation. Span 80 was added as an emulsifier to aid in the proper mixing of drugs and lipids in solutions. Tween 80, a water-soluble surfactant with a hydrophilic-lipophilic balance (HLB) value of 15, plays an important role as a co-emulsifier and stabilises the formulation system. In addition, the addition of more than one surfactant helps to reduce the particle size of NLCs [66], [67]. Overall, the choice of all components for formulation development was heavily driven with the aim of developing an optimised stable nanoformulation encapsulating hydrophobic drugs.

Characterisation of the NLCs showed that the particle size distribution was sufficiently below 200 nm. The reduced size of particles facilitates easy passage through the gastrointestinal membrane, which increases the permeability of drugs after encapsulation in a nano-sized lipid matrix [68]. Such smaller particles can show enhanced penetration and retention effects with slower clearance through the reticuloendothelial system [69]. The polydispersity index (PDI) of the prepared NLCs was found to be less than 0.3. This showed that the particles were highly monodispersed and represented a homogenous population. The uniform distribution of small-sized nanoparticles is suitable for the development of nanomedicines [42]. A negative charge on the surface of nanoparticles is required to achieve nanodispersion stability (Das and Chaudhury, 2011). Surfactants used in formulation development, such as Tween 80 and Span 80, are non-ionic (Banerjee et al., 2018) hence, the variability of negative surface charges can be considered either due to the presence of different drugs or different lipid matrices. The DLS results were well supported by image-based microscopic techniques, such as AFM and TEM. NLCs are known to encapsulate more drugs owing to the presence of an amorphous structure in the lipid matrix (Das and Chaudhury, 2011). Hence, more than 90% of the drug was encapsulated in quercetin and piperine. And it has been well supported through TEM images as the spherical-shaped nanoparticles showed the anomalous structure inside the matrix as the same kind of reports was reported earlier [42]. Thermal degradation of pristine drugs was observed at a higher temperature, whereas in the case of NLCs, a major weight loss was observed around 200-220°C. The loss of integrity of the sucrose particles can be attributed to melting followed by degradation in the form of caramelisation of sucrose, leading to a significant loss of weight in the lyophilized formulation [70]. In the case of pure drugs, the majority of thermal oxidation occurred at a temperature of approximately 325-345°C for quercetin, as observed previously [71] and 310-340°C for piperine, and the steeper curve shows complete degradation up to 500°C. Steps in the degradation of piperine and quercetin are absent in the case of NLCs, indicating their interaction with lipids [71]. The reduction in the crystallinity of drugs after encapsulation in the lipid matrix leads to amorphous conversion, as can be observed from the DSC and XRD plots. Thermograms obtained from DSC showed a sharp melting of sucrose at approximately 186°C with its degradation near 220°C, as previously observed in the case of freeze-dried sucrose [72]. The depression of the melting point can be due to size reduction to the nano level and increases the effective surface area, which significantly increases the heat transfer capacity. The addition of liquid lipids with homogenous homogenisation caused the lipid matrix to be anomalous.

Using surfactants and fast quenching into nano-sized particles through homogenisation, NLCs restrict *the in situ* crystallisation of drugs in formulation systems [73]. Both drugs, piperine and quercetin, entered the molecular level and then became entrapped inside the NLCs, as similar evidence was obtained from our DSC study. It also helps to confirm the absence of drugs on the surfaces of the nanoparticles. The intensity of the peaks decreased, which indicates the conversion of a drug into an amorphous form during entry into NLCs [74]. The decrease in the degree of crystallinity also confirmed the amorphous conversion of the drugs into NLCs.

The *in vitro* drug release study of pure drug solution and drug-loaded NLCs showed an extension of drug release with an almost biphasic release pattern. The pure drug solution was found to release 20.42±2.7% and 21.11±1.7% in the case of quercetin and piperine, respectively. NLCs sustained the initial burst release which leads to almost 38.40±5.2% and 45.0±1.3% drug release from P-NLCs and Q-NLCs, respectively. In the case of NLCs, initially, a linear release was observed, followed by a steady state until 12 h. The linear release is due to drugs encapsulated in the peripheral part of particles, while the steady state in the release pattern can be correlated with deeper encapsulation of drugs in the lipid matrix. The slow release was mainly due to the slow erosion of the lipid matrix, by which the remaining drugs entrapped inside the core of the NLCs were released in a prolonged manner [54b]. In the case of PQ-NLCs, quercetin was found to be released at 30% and piperine to 37.5% which is higher than that of the pristine drug dispersion, which is less than that of PQ-NLCs. According to the mechanism of drug release kinetics, drug-loaded NLCs were found to follow Higuchi release kinetics for quercetin (R^2 = 0.9296) and piperine (R^2 =0.9641). This explains why the drug released from the NLCs followed the diffusion process. The presence of liquid lipid prevents the *in situ* crystallisation of solid lipids and causes the matrix to be anomalous; hence, higher drug encapsulation can be expected in the case of NLCs [75]. Piperine (log P: 3.38) was more lipophilic than quercetin (log P = 1.81). This allowed piperine to encapsulate within the lipid matrix in a larger proportion than quercetin when administered in combination. In addition, Compritol® 888 ATO, a solid lipid solubilized in chloroform only, and piperine also showed solubility in the same solvent, while quercetin was not soluble in it. Due to its higher lipophilicity and solubility, piperine showed more release compared to quercetin from dual drug-loaded PQ-NLCs. In addition, the rigidity obtained in the case of NLCs due to Compritol® 888 ATO leads to slower diffusion of drugs from the lipid matrix [76]. Higher drug encapsulation in NLCs followed slow diffusion of the drug from tiny liquid nano-compartments of deeper parts of the solid-liquid lipid matrix with longer diffusion distance [75]. This explains why the drug released from the NLCs followed the diffusion process. Safety evaluation performed for lyophilized NLCs showed no hemolysis as compared to the positive control, considering the negative (PBS) and positive (water) control values of 0% and 100%, respectively. The slight increase in particle size and minor reduction in the zeta potential of the prepared NLCs can be attributed to the cohesion or aggregation of particles. The insignificant changes confirmed the physical colloidal stability when stored at 4°C. This confirmed that the prepared NLCs are safe and can be used for further evaluation of *in vitro* cell lines and animal applications.

It has been reported that the IC_{50} value for quercetin is approximately 50µM when treated against the SSC-9 cell line [63], while piperine showed an IC_{50} value of 124 µM against

the KB cell line [34]. The combination of both drugs in a single NLC matrix showed a synergistic effect with improved cytotoxic potential. Overall, the results showed that the formulation showed a higher cytotoxic potential at a lower concentration than the pristine drug solutions. The rate and extent of particle uptake generally depend on the physicochemical characteristics of the particles, including their size, zeta potential, and shape. Stable uptake of nanoparticles, followed by degradation by lysosomal enzymes, causes the release of drugs encapsulated within the lipid matrix. Colour intensity reflects higher colocalization with no background. The formulations showed more apoptotic changes than the pure drug solutions. Dual drug-loaded NLCs showed more early and late apoptotic changes in all treatments. The decrease in red fluorescence intensity and increase in green fluorescence intensity indicates mitochondrial depolarisation due to the opening of the mitochondrial permeability transition pore (MPTP) as a result of the loss of intracellular accumulation of J-aggregates and increase in their monomeric form (green). This leads to mitochondrial membrane disruption and loss of function. Annexin V FITC and PI dual staining were used to quantify the necrotic indices in FaDu cells using flow cytometry. Quantitative estimation has been studied in tissues through the determination of dye concentration, while qualitative evaluation through fluorescence imaging using fluorescence microscopy [65].

5. Summary

In this study, we successfully incorporated active plant constituents inside the lipid-mediated matrix using solvent evaporation through a high shear homogenisation technique using Compritol® 888 ATO, a solid lipid that provides rigidity to nanoparticles and squalene, which forms an anomalous structure inside the lipid matrix. Dual drug-loaded NLCs prepared by encapsulation of quercetin and piperine were characterised for their particle properties, including size, PDI, and ZP. In addition, microscopic evaluation revealed greater drug encapsulation within the lipid matrix. The improved drug release profile was obtained using NLCs, as compared to the pristine drugs. The overall characterisation confirmed nano-sized monodispersed negatively charged spherical particles with an anomalous structure inside the matrix, which allowed the amorphous conversion of drugs during encapsulation. A biphasic release pattern was observed with drug-loaded NLCs as an initial linear pattern followed by a stationary phase. The safety of NLCs was evidenced by the absence of hemolysis in the blood samples. Both drug-encapsulated NLCs proved to be more cytotoxic than pristine drug solutions, with faster cell internalisation. Cellular apoptosis assays showed an increase in apoptosis in the oral cancer cell lines. *The in vivo* bio-distribution of Coumarin-6 labelled NLCs in rats confirmed the efficient distribution in oral cavity parts, which is essential for the treatment of oral cancer. The overall scenario predicts an improvement in the activity of both drugs after encapsulation in NLCs. There is scope for *in vivo* assessment of these NLCs in terms of pharmacokinetics and pharmacodynamics.

The present work has been published in two parts in two different journals: ***Chemistry and Physics of Lipids*** (IF: 3.329), where physicochemical characterisations of sequentially loaded NLCs were studied and the ***European Journal of Pharmacology*** (IF: 4.439), where dual drug-loaded NLCs were characterised for *in vitro* cellular evaluations in OSCC cell lines such as FaDu cells. Further, there is scope for *in vivo* evaluation of NLCs.

LC-MS/MS Method for Simultaneous Estimation of Quercetin and Piperine: Development, Validation, and Application to a Pharmacokinetic Study of NLCs

1. Introduction

The combination of dietary and medicinal phytoantioxidants enhances their effectiveness and reduces the associated side effects [77]. Quercetin, 2-(3, 4-dihydroxyphenyl)-3, 5, 7-trihydroxychromen-4-one, is a natural flavonoid found in various edible compounds with potent antioxidant and anti-cancer potential. Structurally, the presence of two pharmacophores in the chain of quercetin allows the scavenging of reactive oxygen species [78]. Quercetin acts as an antineoplastic agent through various pathways, including cell cycle arrest at the G1 and S phases, mitochondria-mediated apoptosis [32], and reduction in the expression of metalloproteinases, leading to the inhibition of PIK3 and MAPK pathways [33]. Piperine, (2E, 4E)-5-(1, 3-benzodioxol-5-yl)-1-piperidin-1-ylpenta-2, 4-dien-1-one, is a natural bioenhancer that has been well explored for the enhancement of bioavailability of several active components [79]. Unfortunately, these two drugs have poor aqueous solubility and photosensitivity-related severe issues. In addition, quercetin tends to undergo rapid chemical degradation in gastric pH media as well [52]. Therefore, incorporation of these two drugs into suitable single lipid-mediated nanostructured formulations, especially NLCs, is helpful in overcoming critical pharmaceutical challenges [80]. These NLCs have been well characterised in terms of *in vitro* characterisation and cellular evaluations in the oral cancer cell line EJP Reference. The *in vivo* pharmacokinetic profiles of the prepared NLCs were determined.

Several analytical methods have been reported for the bioanalytical estimation of quercetin in plasma, including HPLC with UV detection [81], electrochemical detection [82] and fluorescence detection [83]. Because of the poor solubility and permeability of quercetin, detection at very low concentrations is a major obstacle for analysts. Several attempts have been made to develop and validate the LCMS/MS method for the estimation of quercetin [84]. In addition, enhancement of the bioavailability of quercetin estimated through various nanoformulations followed by LCMS/MS analysis includes quercetin-loaded solid lipid nanoparticles [85], quercetin biodegradable nanoparticles [86]. In addition, bioenhancers such as piperine can also improve the bioavailability of quercetin. The simultaneous estimation of both drugs in biological samples, such as plasma, has not yet been studied. Hence, the rapid, sensitive, precise, and accurate LC-MS/MS method is essential for the simultaneous analysis of quercetin and piperine in rat plasma. Furthermore, the application of the developed method must be evaluated in terms of the pharmacokinetic profile of optimised nanostructured lipid carriers containing quercetin and piperine.

2. Experimental

2.1. Chemicals and reagents

Quercetin, piperine, and squalene (liquid lipid) were purchased from Sigma-Aldrich Chemicals (St. Louis, MO, USA). Compritol ATO-888 (solid lipid) was obtained as a gift from Gattefosse (France). LCMS grade acetonitrile (ACN), methanol, and formic acid were procured from Merck Specialities Pvt. Ltd. (Mumbai, India). HPLC-grade Milli-Q water was used as previously filtered through a Milli-Q filtration system (Millipore GmBH, Germany).

2.2. Animals

Male Sprague–Dawley rats weighing 200–230 g were used in this study. The animals were provided with a standard laboratory diet and water throughout the experiment. The animals were acclimatised to laboratory conditions for 1week prior to the experiments. The experimental protocol was approved by the Animal Ethical Committee and conducted in accordance with the National Institutes of Health Guide for the Care and Use of Laboratory Animals (National Research Council, 2011).

2.3. Instrumentation

The analysis was carried out on a Waters Acquity H-Class UPLC system (Waters, Milford, MA, USA) equipped with a quaternary solvent manager, column compartment, and autosampler with an FTN injector. Mass spectrometric analysis was carried out on a Water Xevo-TQXS triple quadrupole mass analyser (Waters, Milford, MA, USA) equipped with an electrospray ionisation source. Data acquisition was performed using MassLynx v.4.2 software. The samples were evaporated using an Eppendorf concentrator plus (Eppendorf, Hamburg, Germany).

2.4. UPLC/ESI-MS/MS conditions

UHPLC-MS/MS analyses were performed using a Water Xevo-TQXS triple quadrupole mass analyser (Waters, Milford, MA, USA). The separation of quercetin, piperine, and IS (fisetin) in the plasma matrix was achieved using a Waters Acquity BEH C_{18} column (50 mm X 2.1 mm, 1.7 µm). The mobile phase was composed of 0.1% formic acid in water (A) and 0.1% formic acid in acetonitrile (B) in gradient mode. The gradient was set as follows: (Tmin/% proportion of solvent B): 0-0.2/2, 0.2-5/95, 5-8/95, 8-10/2, and 10-12/2 with a flow rate of 0.2 mL/min, the column temperature was maintained at 45°C, and the injection volume was 3 µL. The positive ion ESI mode was employed for the ionisation of quercetin, piperine, and fisetin (internal standard, IS). MS/MS data were acquired in the multiple reaction monitoring mode (MRM). The MRM transitions for quercetin, piperine and fisetin are 303.04 > 152.9, 286.12 > 201.04 and 287.01 > 136.93 respectively. The cone voltage and collision energy of 2V and 36 eV for quercetin, 2V and 20 eV for piperine and 2V and 37 eV for fisetin, respectively, and a dwell time of 0.097 s. The following electrospray ionisation inlet conditions were used: capillary 0.5 kV, cone 3 V, source temperature 150 °C, desolvation

temperature 500 °C, cone gas flow 150 L/h, and desolvation gas flow 1000 L/h. Instrument control and data acquisition were carried out using the MassLynx software (version 4.2). The TargetLynx application manager was used for the quantitative data analysis.

2.5. Preparation of stock, working solutions and IS

Stock solutions of quercetin and piperine were prepared by dissolving 1 mg in 1mL of LCMS grade methanol to obtain a final concentration of 1000 µg/mL. Further serial dilutions were performed using the previously prepared stock solutions to prepare primary aliquots of quercetin and piperine in methanol for calibration curve and quality control (QC) samples. Similarly, a primary stock solution of 1 mg/ml of internal standard (fisetin) was prepared in methanol and further diluted to prepare a working solution of 50ng/ml.

2.6. Preparation of calibration curve and quality control samples

Calibration curves were prepared by dissolving appropriate amounts of quercetin and piperine in rat blood plasma (90 µL) in the concentration range of 0.1–200 ng/mL. Three quality control samples for quercetin and piperine were prepared at low concentration (0.75 and 0.3 ng/mL, LQC), medium concentration (50 and 50 ng/mL, MQC), and high concentrations (100 and 100 ng/mL, HQC), respectively. Along with this, LLOQ for quercetin and piperine (0.25 and 0.1 ng/mL) samples were prepared, respectively. Blank plasma samples were prepared in a similar manner and analysed.

2.7. Sample pre-treatment and extraction

Protein precipitation was implemented to extract analytes from the rat plasma. Rat plasma (90 µL) was extracted with 1mL of ethyl acetate and n-heptane (50:50; liquid–liquid extraction), followed by vortexing for 10 min (Vibramax, Heidolph, India). The samples were then centrifuged at 8,000 rpm for 5 min at 4°C. The supernatant was collected and evaporated at 30°C under vacuum (TurboVap, Caliper Life Sciences, India). The residue was reconstituted with 100 µL of methanol containing fisetin as an internal standard (50ng/mL) and centrifuged for 5 min. Samples were then transferred to glass inserts containing vials and subjected to LC-MS/MS analysis.

2.8. Method validation

The bioanalytical method was validated in accordance with FDA guidelines (US Food and Drug Administration, 2001). Several validation parameters were assessed, including specificity, selectivity, linearity, sensitivity, precision, accuracy, recovery, and matrix effects.

2.8.1. Specificity and selectivity

Blank rat plasma and spiked plasma samples were screened in triplicate to investigate the specificity and selectivity of the developed method. These samples were analysed for the detection of endogenous interference at retention times of both analytes and IS.

2.8.2. Linearity and sensitivity

Linearity was evaluated with a total of eight calibration standards over a concentration range of 0.1–200 ng/mL. The calibration curves were constructed by plotting the peak ratio of the working analytes (quercetin and piperine) with the internal (fisetin) standard (y-axis) versus the concentration of analytes obtained (x-axis) and evaluated for correlation coefficient, slope, and intercept. The lowest concentration (LLOQ) of the calibration curve sample should detect a variation of <20%.

2.8.3. Precision and accuracy

The intraday and interday precision and accuracy of the developed method were investigated for QC samples at four different concentrations. The acceptable limit of CV was <20% for LLOQ and <15% for LQC, MQC, and HQC, according to FDA guidelines. The differences in the observed and nominal concentrations in terms of percentages represent the accuracy of the method.

2.8.4. Recovery and matrix effect

Recovery was determined by comparing the responses of QC samples (low, medium, and high concentrations) with the responses of analytes from post-extracted plasma samples with equivalent concentrations. Recovery studies for quercetin and piperine were performed at three concentration levels (QC) in rat plasma.

2.8.5. Stability study

To determine the stability of the analytes, samples were stored under different conditions and evaluated at the LQC, MQC, and HQC levels. The benchtop stability of plasma samples was evaluated at room temperature for 8 h. Auto-sampler stability was measured at 4 °C for 24 h. For freeze–thaw stability, samples were stored at -20 °C and thawed at room temperature every 24 h. The extracted samples were determined after three freeze–thaw cycles. The obtained results of the stability samples were compared with the nominal concentrations of the analytes at 0 h.

2.9. Pharmacokinetic study

Sprague‑Dawley rats were fasted overnight before the experiment. The rats were randomly divided into six groups, each consisting of three rats. Quercetin-piperine dispersion and PQ-NLCs were then administered to each group. To determine the pharmacokinetic (PK) parameters, blood samples were withdrawn from retro-orbital sinus at the following time points: 0.25, 0.5, 1, 2, 4, 6, 8, 12, 24 and 48 hours after dosing. Blood samples were collected in heparinized Microteiner®, followed by centrifugation (5000 rpm for 10 min), and the isolated plasma samples were stored at -80°C until analysis.

Plasma samples were thawed properly, and 90 µL of plasma was extracted with extraction solvent followed by vacuum concentration. Samples were reconstituted using

methanol containing 50ng/mL ng/mL IS and analysed using the developed LC-MS/MS method.

3. Results and discussion

3.1. Method development and validation

The chemical representations of quercetin, fisetin, and piperine are shown in **Figure 4.1**. Quantification of both analytes was performed using the negative ionisation mode of LC-ESI-MS/MS for high sensitivity and selectivity of the data. The MRM transitions for quercetin, piperine and fisetin are 303.04 > 152.9, 286.12 > 201.04 and 287.01 > 136.93 respectively. The retention times were 4.39, 5.49 and 4.10 min for quercetin, piperine and fisetin respectively, with a total run time of 12 min as can be seen from chromatograms in **Figure 4.2**.

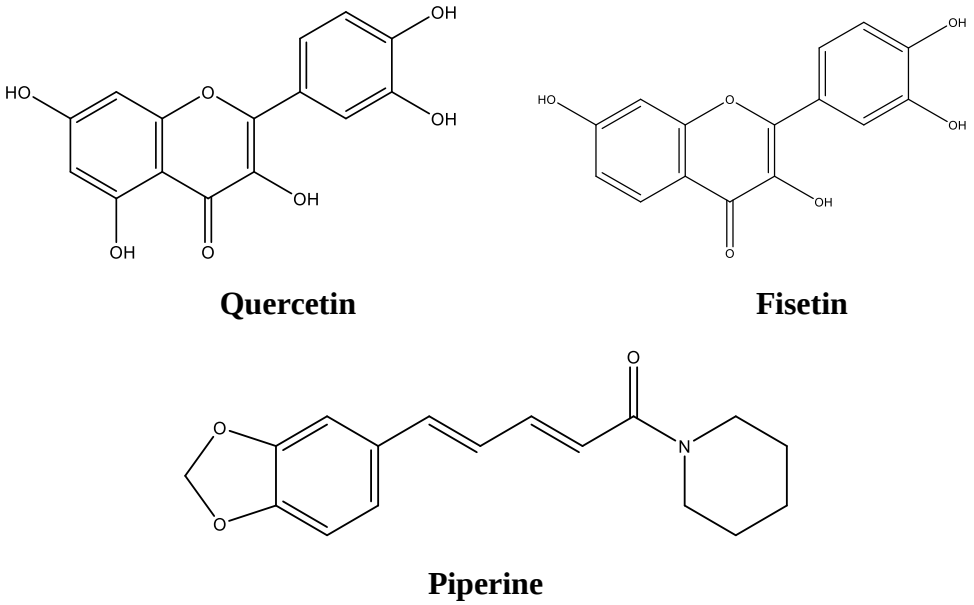

Quercetin **Fisetin**

Piperine

Figure 4. 1. Chemical structural representation of analytes, quercetin and piperine including internal standard as fisetin

3.2. Method validation

3.2.1. Specificity and selectivity

The absence of interference around the retention time of the analytes along with the IS was observed in the blank plasma samples. Retention times for quercetin, piperine, and fisetin (IS) were 4.36, 5.48, and 4.10 min, respectively. Representative chromatograms for blank plasma, blank spiked with ARE, blank plasma spiked with quercetin, and piperine at 4-hr post dose rat plasma samples are shown in **Figure 4.2**.

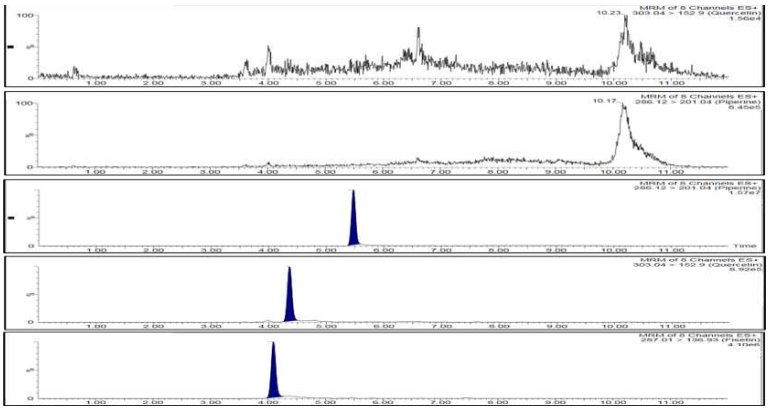

Figure 4. 2. UPLC-MS/MS Chromatogram representing blank plasma (A & B), and Piperine (C), Quercetin (D) and IS (E) in plasma samples, respectively.

3.2.2. Linearity and range

The calibration curve was linear in the range of 0.1–200 ng/mL for both piperine and quercetin, with a weighting factor of 1/x. The mean equation was y= 0.4211x + 0.04592 and y= 0.00681x + 0.00356, with correlation coefficients of r^2= 0.993 and r^2= 0.996 for piperine and quercetin, respectively.

3.2.3. Precision and accuracy

The intra- and inter-day precisions for quercetin and piperine were 0.15–3.07 % RSD and 0.15–4.45% RSD, respectively. The accuracy was 90.53–112.67% for quercetin and 90.28–112.67% for piperine. The values for precision (%RSD) and accuracy (% recovery) for both analytes were within acceptable limits (**Table 4.1**), and the chromatograms are shown in **Figure 4.3**.

Table 4. 1. Determination of intra- and inter-day precision and accuracy of quercetin and piperine

Analytes	**Sample**	**Intraday precision**		**Interday precision**	
		% Accuracy (mean ±SD)	**%RSD**	**% Accuracy (mean ±SD)**	**% RSD**
Quercetin	LLOQ	112 (±1.63)	1.46	112.67 (±2.49)	2.21
	LQC	94.07 (±2.89)	3.07	90.53 (±1.76)	1.95
	MQC	94.89 (±0.91)	0.96	94.27 (±1.06)	1.12
	HQC	101.97 (±0.15)	0.15	102.47 (±0.4)	0.39
Piperine	LLOQ	112 (±1.63)	1.46	112.67 (±2.49)	2.21

LQC	94.07 (±2.88)	3.07	95.71 (±2.43)	2.54
MQC	94.89 (±1.11)	1.17	91.08 (±4.05)	4.45
HQC	101.97 (±0.14)	0.15	90.28 (±1.35)	1.50

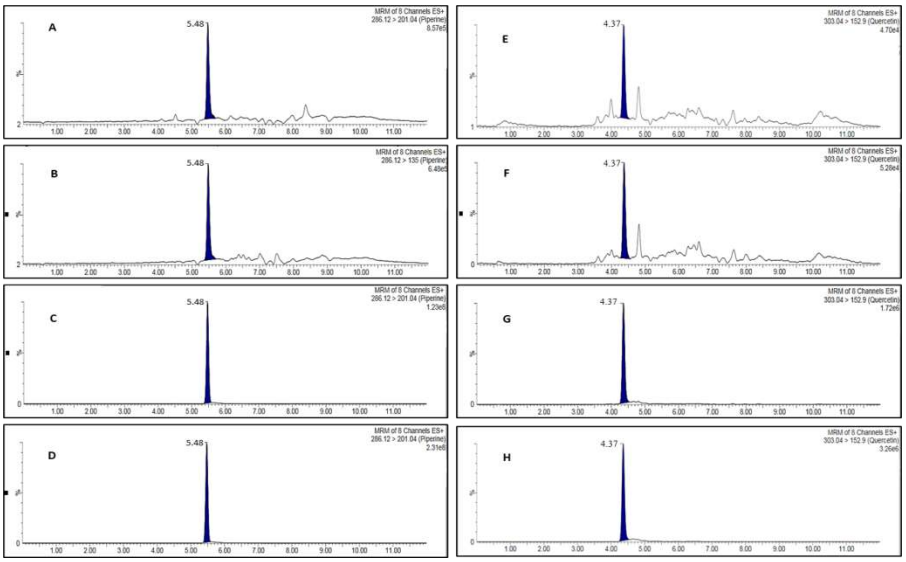

Figure 4. 3. UPLC-MS/MS chromatogram of Piperine (A to D) and Quercetin (E-G) at various concentration levels, A-LLOQ (0.1 ng/mL), B-LQC (0.3 ng/mL), C-MQC (50 ng/mL), D-HQC (100 ng/mL), E-LLOQ (0.1 ng/mL), F-LQC (0.3ng/mL), G-MQC (50 ng/mL),H-HQC (100 ng/mL)

3.2.4. Extraction recovery and matrix effect

The extraction recoveries of quercetin and piperine were >88% and >89%, respectively. The recovery of IS was >90%. The results from **Table 4.2** indicate that there was no endogenous interference in the quantification of the analytes.

Table 4. 2. Extraction recovery and matrix effect on developed method

Analytes	**Sample**	**% Recovery (mean ±SD)**	**Matrix effects (mean ±SD)**
Quercetin	0.3	88.79 (±1.99)	92.71 (±4.5)
	50	91.68 (±0.85)	89.05 (±3.2)
	100	92.82 (±0.57)	90.18 (±2.9)
Piperine	0.3	89.09 (±1.03)	91.08 (±5.6)

	50	91.00 (±0.46)	87.64 (±4.9)
	100	91.20 (±1.44)	90.98 (±23.1)

3.2.5. Stability study

The bench-top stability was determined by storing the samples at ambient temperature (25°C) for 8 h; the mean percentage change of analytes in plasma was less than ±10% from their nominal concentrations. The mean percentage changes of analytes in plasma during three freeze–thaw cycles were within the acceptance limits. The analytes were stable at 4 °C for 24 h in an autosampler (autosampler stability). The stability results are listed in **Table 4.3**.

Table 4. 3. Stability data of quercetin and piperine in rat plasma

Compound concentration (ng/mL)	**Bench-top stability**		**Auto sampler stability**		**Freeze-thaw stability**	
	% Accuracy	**%RSD**	**% Accuracy**	**%RSD**	**% Accuracy**	**%RSD**
Quercetin						
0.3	92.41 (±3.22)	3.48	97.97 (±9.79)	9.99	93.52 (±4.33)	4.63
50	92.34 (±3.14)	3.40	93.38 (±1.72)	1.84	105.69 (±6.23)	5.90
100	96.24 (±4.87)	5.06	96.00 (±5.54)	5.77	90.45 (±3.55)	3.93
Piperine						
0.3	89.72 (±1.4)	1.56	94.07 (±3.25)	3.45	96.23 (±4.79)	4.98
50	92.69 (±3.69)	3.99	100.9 (±10.64)	10.54	104.7 (±6.13)	5.86
100	91.20 (±3.31)	3.65	91.20 (±3.31)	3.63	91.20 (±3.54)	3.88

3.3. Pharmacokinetic profile

The developed and validated method was applied to estimate various PK parameters after oral administration of novel quercetin and piperine co-loaded NLCs in rats. The plasma

concentration-time profile after the oral administration of quercetin is shown in **Figure 4.4**. PK parameters were calculated using PK Analysis Add ins in MS Excel and are listed in **Table 4.4**. The mean area under the curve (AUC_{0-t}) of quercetin from PQ-NLCs was 824.36 ± 185.04 ng h /mL, and for piperine16877.66 ± 5589.65 h ng/mL, while the AUC0-t of orally administered quercetin and piperine API was 39.77 ±8.93 and 3612 ±1196.21 h ng/mL, construing a relative bioavailability enhancement of 20.72 and 4.67 folds, respectively. Maximum drug concentration (C_{max}) of APIs of quercetin and piperine was 13.66 ±4.88 and 393.0 ± 40.75 ng/mL (time to peak concentration, T_{max} of 0.33 and 3.33h), whereas NLCs showed the C_{max} of 283.07 ±101.11 and 1836.39 ±190.44ng/mL, with same T_{max}, respectively. Furthermore, results for mean residence time (MRT) also confirmed the sustained effect of quercetin (MRT: 11.46 h) as compared to piperine (MRT 4.59 h). The results demonstrate enhanced bioavailability after oral administration of PQ-NLCs as compared with API, probably owing to increased solubility, absorption, and residence time of the drug delivered at the nanometer scale.

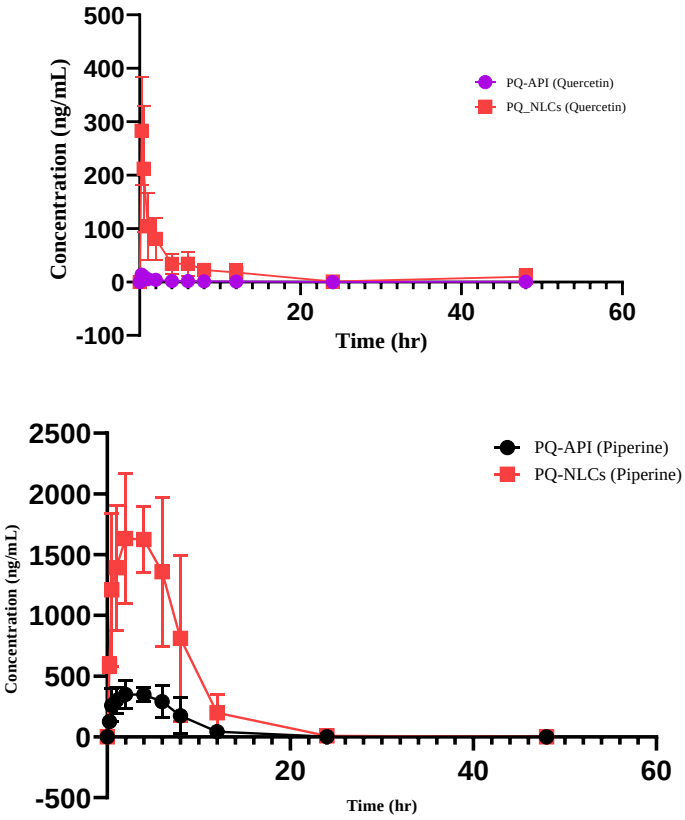

Figure 4. 4. Plasma concentration – time profiles of quercetin and piperine co-encapsulated NLCs and pristine API.

Table 4. 4. Stability data of quercetin and piperine in rat plasma

Parameter	Unit	Q-API	Q (PQ-NLCs)	P-API	P (PQ-NLCs)

C_{max}	ng mL^{-1}	13.66 ±4.88	283.07 ±101.11	393.0±40.75	1836.39±190.44
T_{max}	h	0.33 ±0.14	0.33 ±0.14	3.33 ±2.31	3.33 ±2.31
AUC_{0-t}	ng h mL^{-1}	39.77 ±8.93	824.36 ±185.04	3611.90 ±1196.21	16877.66 ±5589.65
$AUC_{t-\infty}$	ng h mL^{-1}	74.83 ±43.08	1551.07 ±892.84	3612.00 ±1196.04	16878.14 ±5588.89
$AUMC_{0-t}$	ng h mL^{-1}	455.93 ±307.29	9449.96 ±6369.12	16594.43 ±8714.78	77542.45 ±40722.43
$AUMC_{t-\infty}$	ng h mL^{-1}	1179.62 ±1458.98	24449.71 ±30239.88	16599.89 ±8707.61	77567.32 ±40689.77
$t_{1/2}$	h	9.73 ±5.50	9.73 ±5.50	2.87 ±0.57	2.84 ±0.53
K_e	h^{-1}	0.08 ±0.04	0.08 ±0.04	0.25 ±0.05	0.25 ±0.05
MRT	h	11.46	11.46	4.59	4.59
F	-	-	20.72	-	4.67

4. Summary

The bio-analytical method reported in the present study is the first LC-MS/MS quantitative assay to simultaneously determine quercetin and piperine in rat plasma. It was successfully implemented in estimating plasma concentrations of both drugs after a single dose of dual drug-loaded NLCs in a pharmacokinetic study in rats. The method was precise, accurate, specific, and satisfied with linearity and LLOQ. A simple, low-cost sample preparation with a shorter run time allowed for a much higher sample throughput analysis. The same validated method can be used to measure plasma concentrations of both drugs in humans, along with the bio-distribution of NLCs in various organs and tissues.

Fused Deposition Modelling (FDM) mediated 3D-Printed Mouth-Dissolving Wafers Loaded with Nanostructured Lipid Carriers (NLCs) for In-vitro Release

1. Introduction

The buccal cavity is an easy and frequently accessible part of the human body and has several opportunities for scientists with respect to drug delivery. The almost neutral environment of the oral cavity has a pH around 6.2 – 7.4 with a smaller surface area of 100 – 200 cm2 comprising stratified squamous epithelium [87]. It has been preferred because of faster absorption through the sublingual mucosa, bypasses the first-pass metabolism along with gastro-intestinal decomposition of drugs and localised delivery against buccal diseases. In addition, it shows better patient compliance due to easier administration and termination of treatment, if needed [88]. Major factors play an important role in buccal drug delivery, including residence time, drug absorption, pH, and saliva flow [87, 89]. Muco-adhesion and bio-adhesion reflect its residence, while the flow of saliva alters disintegration along with dissolution of the dosage form. In the case of nanoparticulate delivery systems for buccal application, improved permeability, modified release kinetics, enhanced solubility, and protection against degradation have been shown to increase drug efficacy. The major factors affecting the overall delivery system are particle size, charge, and mucus permeation [87]. To enhance the efficacy of the buccal delivery nanoparticles, a muco-adhesion-based slow-solubilizing matrix or dosage form is required to make nanoparticles available at localised sites of action.

3D printing technology has gained popularity in the era of drug delivery owing to its versatility and resourcefulness. The impact of additive manufacturing (AM) technology has spread enormously to explore various aspects among scientists. 3D printing is an innovative technology for the fabrication of three-dimensional objects using a computer-aided design (CAD) file. It follows layer-by-layer printing to provide a 3D structure to the designed object [90]. Various 3D printing techniques have been developed, such as fused deposition modelling (FDM), stereo lithography (SLA), and inkjet printing, have been developed, with a wider scope and diverse applications in several fields. In the pharmaceutical field, 3D printing has been developed in terms of personalised medicines, medical devices, tissue engineering, oral dosage forms, and other drug delivery prototypes [91]. Among these, FDM has made the basis for the development and evolution of 3D printing technology. FDM involves printing of objects using polymeric filaments through a nozzle with a small aperture for extrusion of the melted polymer. The FDM 3D printer works by melting the polymer filament and extruding the melt through a narrow hole from the extruder all occur within the print core part of the machine, and the extruded materials are 3D printed over a build platform by the movement of the print core in the X and Y axes and the build platform in the Z-axis. It is a type of successive melting and cooling of thermoplastic materials [92]. Based on the literature, polyvinyl alcohol (PVA) has been rated as one of the most important polymers in the field of 3D printing because of its ideal thermoplastic properties. It is soluble in water and has been

used as a support material in complex designs through dual-extrusion 3D printing. It is a colourless, odourless, non-toxic, biodegradable thermoplastic polymer with good thermal stability [93]. This polymer has been used as a drug carrier in pharmaceuticals [94]. Interestingly, the design of a 3D printed wafer is an innovative idea with the help of versatile polymers that can provide a new dimension to buccal delivery along with a localised drug delivery system. It is obvious that buccal delivery has been well explored with several delivery systems, such as semisolid formulations, buccal films, mouth-dissolving tablets, powders, and many more [95].

Nanostructured lipid carriers (NLCs) have been explored as delivery systems for natural actives with enhanced bioavailability and improved activity [40]. Active plant constituent-enriched NLCs have also been explored with enhanced efficacy against cancer treatment and are well summarised in our earlier article [18]. In our previous study, we successfully developed nanostructured lipid carriers enriched with active constituents, which require the cutting edge translational form of the dosage form to deliver it locally in the oral cavity [96]. In terms of localised drug delivery of NLCs, various formulations have been developed to provide local delivery in oral cancer, including buccal film [97], transdermal patches [98], and topical gels [99], and so on. However, the incorporation of 3D printed wafers prepared from biodegradable polymers to deliver nanoparticles in the buccal cavity provides a new dimension to the delivery perspective. It improves patient compliance, is easy to fabricate, and delivers cargo with a localised site of action.

Dynamic light scattering (DLS) is a sophisticated micromeritics technique for the determination of particle size in the nano range. In addition, an additive tool of derived KCPS (Kilo Counts per Second) for the estimation of several nanoparticles present in the nanodispersion, which corresponds to the concentration of nanoparticles [100]. Fluctuations in the measurement of light intensity in terms of photons, when measured per unit time, are known as the photon count rate. Based on this, the nanoparticle release from any dosage form can be determined. Hence, this opens a new dimension for the integration of nanoparticles with 3D printed prototypes in the field of pharmaceuticals and medicine.

Delivery of NLCs in their lyophilized format through biodegradable 3D printed wafers can be an excellent AM-driven dosage form against oral cancer through a localised drug delivery system. Therefore, we aimed to design a prototype using PVA-filament-derived 3D printed wafers using the FDM technique along with its physico-technological validations. Furthermore, these printed 3D wafers were characterised to determine their delivery potential to release particles from NLCs in terms of both qualitative and quantitative particle release rates.

2. Material and Methods

2.1. Materials

High-quality natural polyvinyl alcohol (PVA) filaments (2.85 mm in diameter) were procured from Ultimaker, Germany. Compritol® 888 ATO, as a solid lipid, was obtained as a

gift from Gattefosse, France. Active plant constituents, squalene (SQL) as a liquid lipid, and sucrose as a cryoprotectant, were purchased from Sigma-Aldrich Chemical (St. Louis, MO, USA). Sodium chloride, potassium hydrogen phosphate, potassium carbonate, calcium chloride dehydrate, magnesium chloride hexahydrate, sodium hydroxide, Tween 80, and Span 80 were purchased from HiMedia Laboratories Pvt. Ltd., Mumbai, India. Water was purified using a Milli-Q & ELIX water purification system (Merck Millipore, USA) and used throughout the experiments.

2.2. Methods

2.2.1. Design of 3D wafers

Solidworks software (SOLIDWORKS-2019, US) as a computer-aided design (CAD) software was used to design the 3D printed wafers and exported in the form of stereolithography (.stl) file into a 3D printer software (Ultimaker Cura Version 4.2.1, Singapore). The . The stl file format comprises all the given printing parameters and surface data of the 3D printed wafers needed for the 3D printer software to print the objects in the desired dimensions. The wafer was designed such that two parts would enclose a cavity fixed through screw-based projections using a lock-key system. The design of this 3D wafer was filed to an Indian Patent Office, and a favourable examination report was generated on 27 May 202116.

2.2.2. Printing of 3D wafers

The .stl was converted into a G-code file containing geometric information for printing the 3D wafer. To print wafers as a 3D object, an FDM technology-based 3D printer (Ultimaker 3, Ultimaker, Germany) was implemented. High-quality natural PVA, a water-soluble polymer in the form of a filament, was used for the 3D printing process. Printing parameters such as printing speed, print layer height, and printing temperature were varied in different batches, as shown in **Table 5.1**. The diameter of the nozzle of the 3D printer was around 0.4 mm, assuring the fine printing through it.

Table 5. 1. Process variations in 3D printing parameters

Wafer Code	**Printing parameters**		
	Printing temperature (°C)	**Printing speed (mm/s)**	**Layer height (mm)**
W1	215	70	0.1
W2	215	70	0.15
W3	215	80	0.1
W4	215	80	0.15

W5	225	70	0.1
W6	225	70	0.15
W7	225	80	0.1
W8	225	80	0.15

2.2.3. Loading of NLCs inside 3D wafers

Lyophilized NLCs were weighed accurately and loaded with utmost care into the 3D printed wafer. After proper loading of NLCs inside the 3D printed wafer matrix, it was enclosed by a cavity fixed through screw-based projections using a lock-key system with proper fixation. After fixation of the entire assembly, the embedded NLCs were subjected to *in vitro* NLC release studies.

2.3. Characterization of 3D wafers and NLCs

2.3.1. Physical appearance

To determine the shape, homogeneity, uniformity, and smoothness, all 3D printed wafers were investigated visually [81b].

2.3.2. Determination of physical dimensions

To characterise 3D wafers, physical dimensions such as length, width, and height were measured using a digital Vernier calliper (CD-6" ASX, Mitutoyo Corporation, Japan) [81b, 92a].

2.3.3. Determination of weight variation

Six randomly selected 3D wafers (with no NLC loading) from each batch were weighed individually on a digital single pan balance (Mettler Toledo, Switzerland), and the average weight of the 3D wafers was calculated, which provides a clear-cut idea related to the weight variation among 3D printed wafers.

2.3.4. Determination of loading capacity

The loading capacity of the 3D wafers was estimated by filling the lyophilized NLCs inside it, and then the wafers were fixed to each other with no leakage or spilling. NLCs were weighed in terms of their weight (mg) on a digital single-pan balance (Mettler Toledo, Switzerland).

2.3.5. Microscopy of 3D wafers

Surface microstructural analysis of the 3D printed wafer was performed using an inverted microscope (DMil, Leica, Germany). The upper and lower parts of the 3D wafer

were sequentially placed on the coverslip and then visualised under the 10x and 4x objectives of the inverted microscope.

2.3.6. Scanning electron microscopy (SEM)

SEM is a technique used to determine the surface morphology of NLCs and 3D printed wafers with the help of an electron beam under vacuum. Hence, surface morphological evaluation of lyophilized NLCs and 3D printed wafers was performed with field emission-SEM (FE-SEM, JSM-7610F, JEOL Japan).

2.3.7. Differential Scanning Calorimetry (DSC)

To determine the nature of the PVA filament and 3D wafer, DSC analysis was performed (DSC-3, Mettler Toledo, Switzerland). Approximately 5.0 mg of sample was placed in a sample pan and crimped with a crimping machine for tight sealing of the pan. The heating rate was maintained at 10°C/min within a temperature range of 25-350°C. Nitrogen purging was performed at 10mL/min flow rate to maintain a stable, inert atmosphere.

2.3.8. X-ray powder diffraction (XRD)

To determine the nature of the PVA filament and 3D wafer, XRD analysis was performed using a SmartLab diffractometer (Rigaku, Japan). Samples were sectioned as thin films and analysed by keeping the constant parameters as applied voltage and applied current of 45 kV and 120mA, respectively. The scan speed, omega, and step size were 4°/min, 1.0, and 0.02, respectively. The final data were plotted as 2θ values versus intensity.

2.3.9. Particle size analysis

The mean particle size and polydispersity index of the prepared NLCs were measured using a particle size analyser (Nano-ZS, Malvern Instruments Ltd.).

2.3.10. Preparation of artificial saliva

Artificial saliva was prepared using a previously reported method, with some modifications [101]. With the addition of concentrated hydrochloric acid (1.0 mL), approximately 500 mL of deionised water was adjusted to pH 2. Other components, such as sodium chloride (165 mg), potassium hydrogen phosphate anhydrous (340 mg), potassium carbonate (265 mg), calcium chloride dehydrate (75 mg), and magnesium chloride hexahydrate (85 mg), were weighed and solubilized in the previously prepared acidified water. The pH of the solution was adjusted to 6.8 ± 0.1, using 5 N sodium hydroxide solutions.

2.3.11. Determination of % Redispersibility of NLCs

Redispersibility is the dispersion of lyophilized powder using a specific solvent. To restrict irreversible aggregation during lyophilisation, a cryoprotectant must be added to the nanodispersion. Hence, the percent redispersibility of lyophilized NLCs was estimated in terms of the derived KCPS in artificial saliva. Approximately 1.0 ml of NLC dispersion

containing sucrose as a cryoprotectant was analysed through DLS and then lyophilized the same sample using a lyophilizer (L-300, Buchi, Germany). After complete drying, the lyophilized NLCs were mixed with a similar volume of artificial saliva by vortexing for 5 min. The samples were then analysed to determine the derived KCPS. Calculations were performed to estimate the % redispersibility of the lyophilized NLCs.

2.3.12. *In vitro* NLCs release study

The *in vitro* release profile pattern of the prepared lyophilized NLCs loaded into 3D printed wafers was determined using the photon count rate (in terms of KCPS measurement). Analysis of the photon count rate is desired as it represents a function of the size and concentration of scattering particles [100a]. Around 50.0 mg of Lyophilized NLCs were loaded inside the 3D printed wafers, and an in vitro NLC release study was performed in artificial saliva (pH-6.6) as a release medium at 37±0.5°C. At different time intervals, the medium containing the released NLC sample was removed and analysed using DLS (Zetasizer Nano ZS, Malvern Instruments Ltd., UK) [100b] with 4.0 mW He-Ne laser at 633 nm wavelength (red) as a plot of derived KCPS vs. time (min).

3. Results

3.1. Design and printing of 3D wafers

Computer-aided design (CAD) designs for 3D wafers are shown in **Figure 5.1**. To print wafers as a 3D object, an FDM-mediated 3D printer was implemented, and a natural, high-quality PVA filament was used as the polymer. Printing parameters such as printing temperature, printing speed, and layer height were varied in different batches, as shown in **Table 5.1**. The optimised wafers were characterised using various techniques.

Figure 5. 1. Computer-aided design (CAD) for the 3D printed wafer. It mainly consists of two parts, where (a) top part with 6 projections on its outer part, (b) bottom part with 6 holes on its outer part, and (c) Combined wafer assembly, respectively.

3.2. Characterization of 3D wafers

3.2.1. Physical appearance

The 3D wafer had a rectangular shape with a slightly rough surface at the edges and smooth flat surfaces. Both flat surfaces were slightly shiny, as shown in **Figure 5.3**.

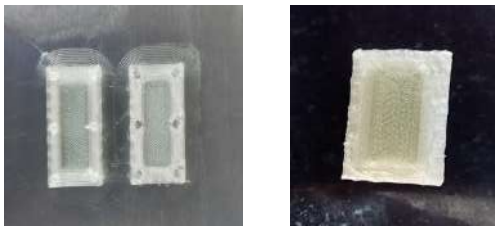

(a) (b)

Figure 5. 2. Various images of 3D printed wafers (a) two parts of the wafer (left: bottom part & right: top part), (b) complete wafer assembly (Side view), respectively.

Various images of 3D printed wafers (a) two parts of the wafer (left: bottom part & right: top part), (b) complete wafer assembly (Side view), respectively.

3.2.2. Physical dimensions

As per the aforementioned protocol, all batches of 3D printed wafers in the assembled form were measured for their thickness, length, and width in mm and their values are listed in **Table 5.2**. All values showed almost no significant differences in terms of their average values for the different printing process parameters.

3.2.3. Weight variation

The weight variation in different batches of 3D wafers was studied to determine the variations in the printability of 3D printers. Wafers from all batches were weighed in six replicates, and the average weights (± SD) for different batches are shown in **Table 5.2**.

3.2.4. Selection of 3D wafer

We found insignificant differences among them based on the properties evaluated for 3D wafers with variations in the printing parameters. These variations in terms of weight, thickness, length, and width, along with their physical appearance through visual inspection, were almost negligible, leading to the inability to segregate these different batches of wafers. This describes the uniformity in the printability of the FDM-based 3D printing of wafers. Hence, we selected only one of these for further evaluation.

Table 5. 2. Evaluation of different printing process parameters

Wafer Code	**Evaluation Parameters**			
	Weight (mg)*	**Thickness (mm)***	**Length (mm)***	**Width (mm)***
W1	565.90 (±10.85)	5.07 (±0.09)	21.84 (0.04)	11.86 (0.05)
W2	577.40 (±10.51)	5.23 (±0.08)	21.47 (±0.22)	11.75 (±0.08)

W3	525.98 (±29.57)	5.20 (±0.11)	21.70 (±0.08)	11.80 (±0.15)
W4	474.95 (±39.43)	5.40 (±0.24)	21.49 (±0.26)	11.65 (±0.32)
W5	534.52 (±17.38)	4.81 (±1.23)	21.81 (±0.05)	11.88 (±0.12)
W6	517.53 (±22.28)	5.26 (±0.13)	21.65 (±0.17)	11.68 (±0.3)
W7	553.63 (±7.18)	5.07 (±0.15)	21.84 (±0.04)	11.98 (±0.1)
W8	515.78 (±12.11)	4.97 (±0.19)	21.50 (±0.22)	11.83 (±0.07)

3.2.5. Loading capacity

The loading capacity of the 3D wafers was determined manually but accurately by filling the lyophilized NLCs inside the wafers. Approximately 50 ± 2.5 mg of lyophilized NLCs can quickly be loaded inside the 3D wafers. This is sufficient for the loading capacity for localised dosing and delivery of NLCs in a lyophilized format. This large amount of lyophilized active plant constituents enriched NLCs loading inside the 3D wafer can be ensured to be delivered without any leakage or spillage. Hence, the developed 3D wafers can be a good option for localised delivery of NLCs inside the oral cavity against oral cancer treatment.

3.2.6. Microscopy of 3D wafers

To determine the surface morphology and structure of the 3D wafer, a microscopic evaluation was performed under an inverted microscope, as shown in **Figure 5.3**. Images obtained from an optical microscope proved the layered structure of the printing, leading to a smooth surface of the 3D wafer. Layer-by-layer printing of natural PVA filaments using an FDM printer can be easily observed from microscopic images.

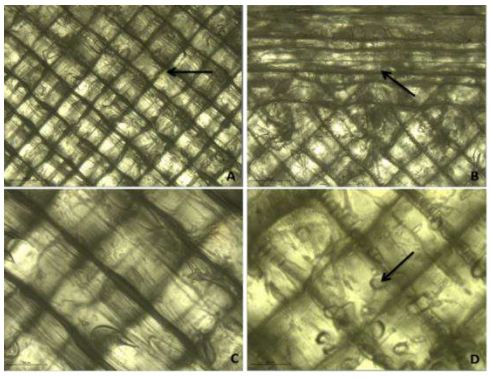

Figure 5. 3. Microscopic images of 3D printed wafers representing layer-by-layer printing structure from FDM 3D printer with the presence of mini pores over the surface highlighted by an arrow.

3.2.7. SEM

Field emission (FE-SEM) imaging was performed for NLCs, as in a lyophilized product format, as shown in **Figure 5.4A**. As the particle size was significantly smaller, the lyophilized particles required a high resolution for imaging. FESEM confirmed the nanostructured size of the NLCs. The surface morphology of the NLCs was found to be slightly rough and anomalous in nature. This does not reflect the complete spherical shape of the NLC particles. The addition of sucrose as a cryoprotectant induces the sticky nature of NLCs, which was observed due to the agglomeration of a few particle populations. The surface texture of the particles was relatively smooth, and no crystalline drug events were observed.

FESEM images of the 3D wafers are shown in **Figure 5.4B**. The surface of the wafer exhibited a gridline architecture with low roughness. This also indicates that the presence of mini-pores or mini-voids might be due to irregularities during the printing process.

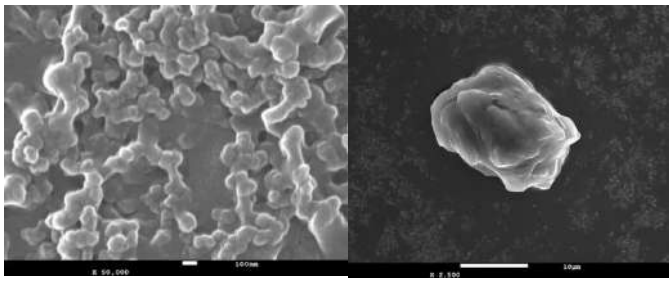

(A)

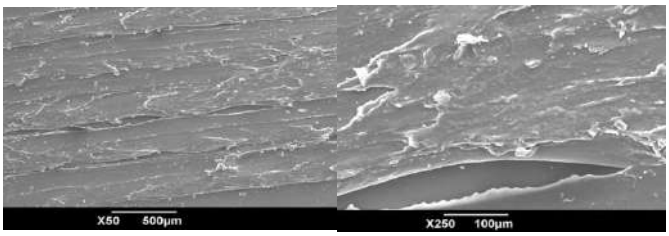

(B)

Figure 5. 4. SEM micrographs for NLCs and 3D printed wafer. (A) Lyophilized NLCs, and (B) 3D wafer.

3.2.8. DSC

DSC analysis was performed to determine the nature of the PVA filament in the pre-printing form and the 3D wafer after post-printing the PVA filament. The DSC thermograms obtained for all samples are shown in **Figure 5.5**. The PVA filament showed an endothermic peak around 185-190°C with decomposition at 320°C. A similar pattern of thermal signature

was also observed for the 3D wafer. This suggests that no significant changes occurred before and after printing the native natural PVA filaments. Therefore, no drastic effect occurred through the extrusion of the PVA polymer at approximately 215-225°C during printing. Similar observations were also reported by our research group [102].

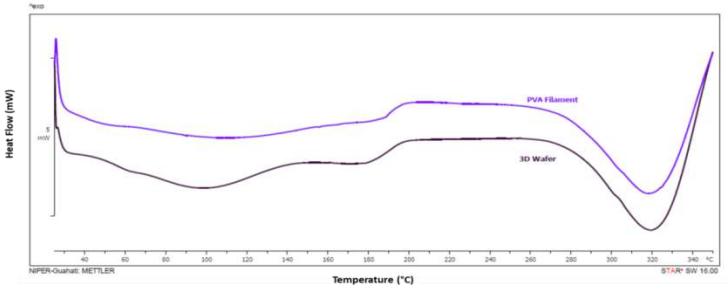

Figure 5. 5. DSC thermograms for 3D wafer and PVA filament, predicting the thermal stability behavior of PVA filament both in native form and post 3D printing process.

3.2.9. XRD analysis

The XRD plots for both the PVA filament and 3D wafer are shown in **Figure 5.6**. The plot suggests a lack of high-intensity peaks showing no crystalline structure in either the PVA filament or 3D wafer. Interestingly, the intensity decreased in the 3D wafer compared to that in the PVA filament. This is due to the thermal shock to the filament during melting extrusion, followed by consolidation into a 3D printed wafer structure. Therefore, both materials are noncrystalline and amorphous in solid-state geometries.

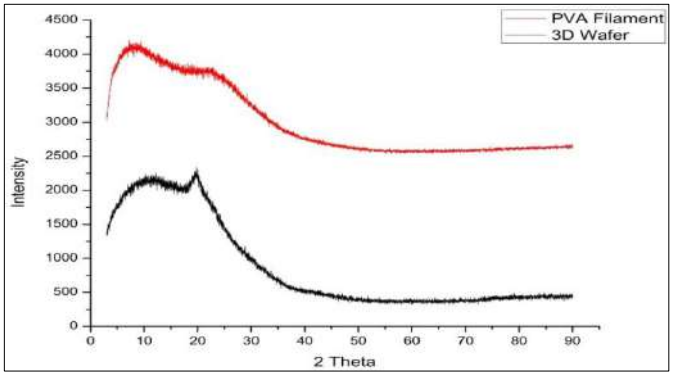

Figure 5. 6. XRD pattern for 3D wafer and PVA filament for the solid-state prediction of material' nature in terms of either crystalline or amorphous.

3.2.10. Determination of % Redispersibility of NLCs

The percent redispersibility of NLCs is an essential determinant of the lyophilized products. The study was performed in a context with a significant focus on KCPS-derived NLCs. Hence, the % redispersibility was also measured in terms of the derived KCPS and was found to be 104.67% ±1.68 % when lyophilisation and reconstitution were performed in MilliQ water in triplicate of the NLC sample.

3.2.11. *In-vitro* NLCs release study

An *in vitro* particle release study was performed on NLCs loaded into 3D wafers in artificial saliva as a dissolution medium. The particle concentration was estimated using DLS-based KCPS values. In this experiment, the release of particles from 3D wafers was estimated in artificial saliva at various time points using DLS in a similar way [12]. The final value of particle release was estimated by subtracting the derived KCPS values of the blank 3D wafer and the derived KCPS values of artificial saliva from the derived KCPS of NLC-loaded 3D wafers. The time taken for the progressive release of NLCs from the 3D wafer was plotted on the x-axis against the derived KCPS of particles on the y-axis, as shown in **Figure 5.7**. The particle size distribution plot measured by DLS from NLC-loaded 3D wafers at different time intervals (30 min, 60 min, 90 min, and 120 min) is displayed in **Figure 5.8**. The complete time-dependent release of NLCs from 3D wafers occurred within 120 min, and hence can be helpful in the delivery of nanoparticles inside the buccal cavity.

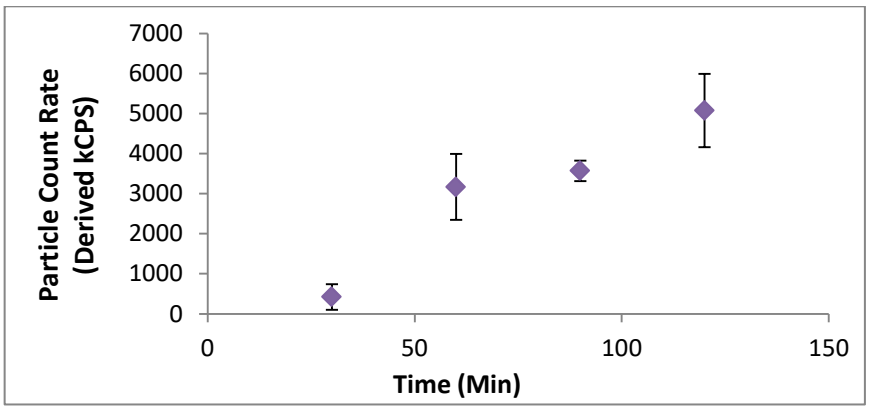

Figure 5. 7. Plot of *in-vitro* NLCs release from NLCs loaded 3D wafer as plotted in respect to percent cumulative particle release versus time in min.

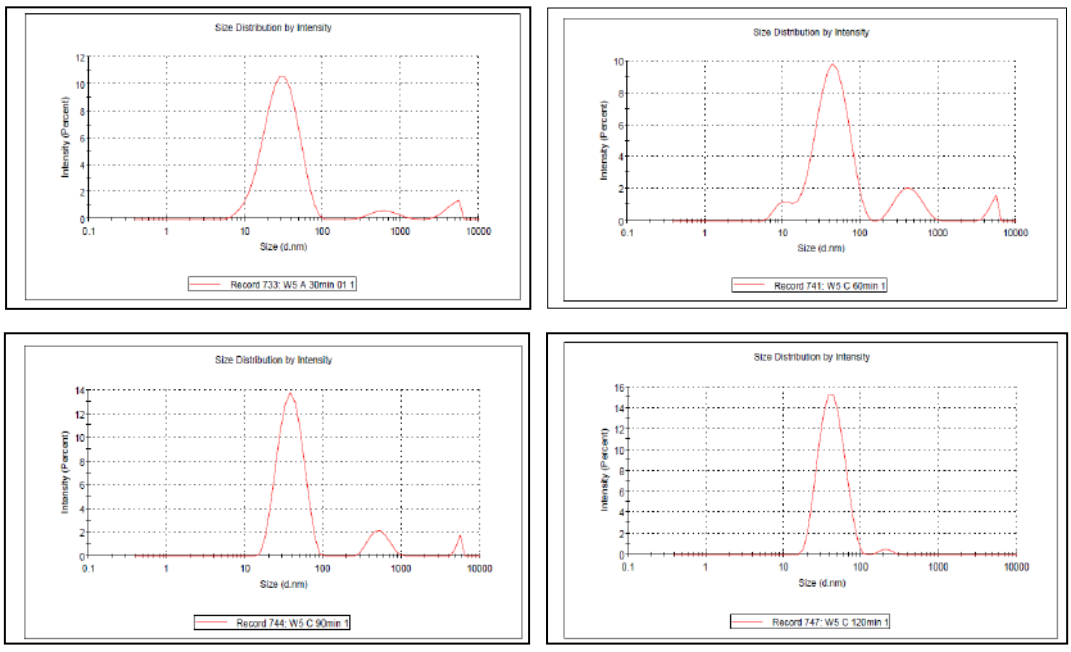

Figure 5. 8. Particle size distribution plot by DLS analysis of NLCs loaded 3D wafer at different time intervals i.e., 30 min, 60 min, 90 min, and 120 min, respectively.

4. Discussion

FDM-mediated 3D printing technology has reached a milestone in the field of drug delivery and pharmaceuticals. It provides flexibility in the fabrication of complex geometries and further integration [92b]. Hence, the implementation of 3D wafers to deliver NLCs provides a new dimension to the particle delivery perspective. It can deliver particles at the desired sites of action in a more localised manner and is further dissolvable owing to the biodegradable nature of native polymeric filaments. Thus, the overall study was projected to integrate NLCs with FDM-mediated 3D printed wafers to deliver the particles justifying their buccal delivery applications.

Initially, the 3D wafer was designed using CAD software and printed using fused deposition modelling (FDM)-mediated 3D printing technology. The PVA filament is a transparent, flexible, and smooth filament with an average diameter of 2.85 mm and is used for prototyping a 3D wafer. The variations in the printing process parameters of the 3D wafers did not show any significant differences in their physical dimensions, weight, and printability. This reflects the robustness of the prototype 3D wafer. The wafers showed a loading capacity of 50±2.5 mg of lyophilized NLCs, which reflects sufficient space to load the particles inside it without any leakage or spillage with proper tight fixation. This provides the delivery of NLCs in a lyophilized format, where reconstitution is not required. The squares can be seen from the microscopic evaluations simply reflecting the layer-by-layer printing nature of 3D wafers with a shiny surface. The presence of mini pores over the surfaces can provide space for saliva to erode the wafer and make the way available for the desired particle release. Similar results were obtained from scanning electron microscopy (SEM), where grid lines of structures with slight roughness and microstructural pores were also observed. This could play a crucial role in wafer dissolution. It predicts erosion followed by a diffusion-type release pattern owing to its surface.

In addition, SEM showed a cluster of nano-sized particles due to sucrose as a cryoprotectant with anomalousness and a slightly rough surface of particles. The DSC curve showed no drastic effect on the PVA before and after extrusion through the hot nozzle of the FDM-3D printer. The native PVA filament showed melting around 185-190°C followed by drastic degradation around 320°C; hence, we restricted the printing temperature to approximately 215-225°C to avoid degradation of the object, as observed previously [94]. There were no sharp, intense Bragg peaks observed in the XRD plot, except for a slight reduction in the intensity of the PVA filament compared to the 3D wafer [103]. A very recent report published by our research group for the fabrication of 3D printed compartmental delivery system for anti-tubercular drugs through print and fill strategy showed the utilisation of PVA polymer and its potential implication as a 3D printed housing device. The PVA polymers did not show any significant variations in their DSC and XRD patterns before and after 3D printing [102].

The concept of derived KCPS to determine the population of NLCs present in the nanodispersion is an innovative approach that has not been explored as such. Hence, we quantified the NLC population count rate from the prepared nanodispersions. The redispersibility of lyophilized NLCs reflects easy reconstitution with an almost similar concentration of NLCs. The critical application of this method was to estimate the NLC particle population count rate from 3D printed wafer matrix system. It was found to release complete NLCs within 120 min, as quantified from the derived KCPS concept. In a previous publication, the release of polymeric nano-capsules from 3D printed tablets was studied qualitatively, where nano-capsules released from the 3D printed tablets were determined through particle size distribution plots by DLS estimation [100b].

Nevertheless, the present work represents a quantification approach regarding the derived KCPS count rate for releasing NLCs from 3D printed PVA wafers. The mechanism of particle release may be predicted as initial wetting of the 3D wafer followed by diffusion of water inside it. This leads to the reconstitution of lyophilized NLCs, followed by the release of particles from the wafer into the artificial saliva as a release medium. Moreover, PVA is a water-soluble polymer, and through melt extrusion from the printing nozzle, it is converted into an amorphous form due to extrusion-mediated thermal shock, thereby improving the solubility of the printed matrix structure. Hence, particle release from 3D wafers in artificial saliva can be implemented in the treatment of oral cancer through localised buccal delivery of nanoparticles.

5. Summary

After the successful development of NLCs against oral cancer, there is a need for an advanced cutting-edge translational dosage form to deliver cargo at the local site of interest. PVA is a water-soluble polymer that can be easily 3D printed using its native filament. Initially, the wafer was designed using CAD software and 3D printed using FDM-mediated 3D printing technology using a PVA filament. Physico-technological evaluations were systematically performed for 3D wafers to measure the physical dimensions and surface morphology through optical microscopy, FESEM, DSC, and XRD analyses. Specified dimensions with a smooth surface texture and a loading capacity of approximately 50 mg of NLCs made the complete translational form of the 3D wafer. The in vitro release of NLCs wrapped inside the 3D printed wafers was observed within 120 min in the presence of artificial saliva, which was validated through derived kCPS data obtained from the DLS study. Hence, 3D wafers can be a suitable substitute for other localised drug delivery systems to deliver the moiety of interest inside the buccal cavity.

The present work has been published in the ***Journal of Materials Research*** **(IF: 3.091)** and has the translational potential to deliver nanoparticles at specific sites, such as the buccal cavity. This work was conducted in NIPER Guwahati along with a few characterisations at the Centre for Nanotechnology, IIT Guwahati.

1. Summary and Overall Conclusion

According to the latest 5-year survey report (2017) from the Indian Council for Medical Research (ICMR), the Ministry of Health & Family Welfare, New Delhi for head and neck cancer (HNC) burden in India, the northeastern region (NER) of India showed a higher prevalence of oral cancer, comprising 90% of HNC cases. In comparison, the five-year cumulative survival rates in the early stages of HNC were 73.6% and 40.5%, respectively, and in locally advanced stages which dropped to 44.5% and 16.9% in the rest of India and northeast India, respectively. The detection of oral cancer in later stages III or IV leads to a very low survival rate in patients with oral cancer. The major reason behind the prevalence of oral cancer in the northeast region comprises habits adapted by locals, such as excessive and continuous chewing of areca nuts, tobacco, and betel quid, which contains more than 300 carcinogens and pro-carcinogens, including nitrosamines. The overall scenario arises due to bad habits adopted by local people, lack of facilities in remote areas, and lack of social awareness about it and so many. These are the major reasons for the enlargement of oral cancer cases in this region. Hence, there is a need for robust, effective, and local delivery for the treatment of oral cancer.

In addition, NER is well known for its wealth in terms of tremendous biodiversity among medicinal plants and their therapeutic potential. People in the tribal region mostly depend on traditional knowledge and experiences of traditional healers to cure deadly diseases. This restricts people with long-term slow treatment due to the poor solubility and permeability of these herbal medicines, leading to low bioavailability, halting their development, and reducing utility from the delivery perspective. Advancements in nanotechnology, in combination with 3D printing technology, can be the best tool for the delivery of these phytoconstituents to treat life-threatening diseases.

To address this problem, we developed 3D printed wafers loaded with active plant constituents enriched with nanostructured lipid carriers (NLCs). This is a cutting-edge-based translational form of product developed for societal benefits which can overcome the barriers and limitations of drug delivery as well as disease.

In this regard, I have selected two drugs from edible sources of herbal origin in combination with quercetin and piperine, with previously well-proven anti-cancer potential at the cellular level. Both drugs lack physicochemical properties such as aqueous solubility, permeability, photosensitive nature, bitter taste, and gastrointestinal instability which subsequently affect their bioavailability and efficacy. To overcome these issues related to drugs, there is a need for a delivery system that can propagate its use in the treatment of the disease.

Nanostructured lipid carriers (NLCs) are second-generation lipid nanoparticles that contain a mixture of solid and liquid lipids with high drug encapsulation efficiency. Compritol® 888 ATO and squalene were used as lipids to encapsulate these hydrophobic drugs through a high shear homogenisation method. The optimised formulations included blank NLCs, P-NLCs, Q-NLCs, and PQ-NLCs. Further evaluation of the prepared NLCs was

performed using various sophisticated advanced analytical techniques for particle size analysis, microscopic imaging, and prediction of the particle nature and so far. The overall characterisation confirmed nano-sized monodispersed negatively charged spherical particles with an anomalous structure inside the matrix, which allowed the amorphous conversion of drugs during encapsulation. Approximately 40% of drug release was observed in NLCs within 12 h *in vitro*. In addition, *in vitro* cellular evaluation was performed in FaDu oral cancer cells. The developed NLCs were found to internalise inside cancer cells within 15 min and cause cell apoptosis. We examined the anti-tumor potential of IC50 P-NLCs, Q-NLCs, and PQ-NLCs for synergistic anti-tumor potential after treatment for 24 h in FaDu cells to induce apoptosis.

After the successful development of dual drug-loaded nanostructured lipid carriers against oral cancer, there is a need to cut the edge translational form of the dosage form to deliver at the local site. To date, various formulations have been developed to provide local delivery in oral cancer, including transdermal patches and topical gels. However, the incorporation of 3D printed wafers to deliver nanoparticles provides a new dimension to the delivery perspective. It improves patient compliance, personalised medicines, and delivers locally at sites of action with no side effects due to the biodegradable nature of polymers.

Natural PVA polymers are water-soluble and can be easily printed using filaments. The wafer was designed using computer-aided design (CAD) using SolidWorks software. 3D printed wafers were prepared from a biodegradable polymer such as polyvinyl acetate (PVA) using fused deposition modelling (FDM) technology. The physicochemical evaluation was performed for wafers, including the dimensions and surface morphology, using optical microscopy and SEM. Specified dimensions and a smooth surface with a loading capacity of 50 mg of NLCs made the wafer robust. The derived Kilo Counts per Second (KCPS) obtained from dynamic light scattering (DLS) corresponds to the number of particles, and hence was used to determine the concentration of nanoparticles released from the wafer. The in vitro release of embedded NLCs wrapped inside the 3D printed wafers was within 7 min in the presence of artificial saliva, which was validated by DLS. The matrix becomes wet and starts eroding through its surface, which allows saliva to enter the wafer, and then nanoparticles diffuse out from it. The wafer developed from mucoadhesive polymer tends to stick to the buccal cavity and hence can be useful for delivery of nanoparticles inside the buccal cavity as a localised delivery against oral cancer.

Overall, research has shown that the developed 3D printed wafers can significantly deliver active plant constituent-enriched NLCs inside the oral cavity in a short period. Direct local action can be achieved for oral cancer lesions and hence can mitigate the disease which is more prevalent in NER.

2. Future Prospective

Despite the increasing prevalence of oral squamous cell carcinoma worldwide, there is still no cost-effective therapy for halting the early progression of oral cancer. Medicinal plants and their active constituents have historically been a rich source of successful drugs and can be

delivered through various formulations, including nanoparticles and 3D printed prototypes. The translational aspects are associated with the developed nanostructured lipid carriers embedded into 3D printed mouth dissolving wafers as a formulation. Hence, some key points need to be addressed in the future prior to commercialisation. These are as follows:

- Process parameters have to be optimized to scale up the manufacturing for industrial production.
- Preclinical toxicity studies for NLC-loaded 3D wafers are required for commercialization.
- Need to take efforts for making the product commercialized

References

1. Da Poian, A.; BACHA, T.; Luz, M., Nutrient utilization in humans: metabolic pathways. **2010**.
2. Newman, D. J.; Cragg, G. M., Natural products as sources of new drugs from 1981 to 2014. *Journal of natural products* **2016,** *79* (3), 629-661.
3. Buenz, E. J.; Verpoorte, R.; Bauer, B. A., The ethnopharmacologic contribution to bioprospecting natural products. *Annual review of pharmacology and toxicology* **2018,** *58*, 509-530.
4. Du, G.-H., *Natural small molecule drugs from plants*. Springer: 2018.
5. Springob, K.; Kutchan, T. M., Introduction to the different classes of natural products. In *Plant-derived natural products*, Springer: 2009; pp 3-50.
6. Saklayen, M. G., The global epidemic of the metabolic syndrome. *Current hypertension reports* **2018,** *20* (2), 1-8.
7. Hazam, P. K.; Goyal, R.; Ramakrishnan, V., Peptide based antimicrobials: Design strategies and therapeutic potential. *Progress in biophysics and molecular biology* **2019,** *142*, 10-22.
8. Wojcik, M. H.; Schwartz, T. S.; Yamin, I.; Edward, H. L.; Genetti, C. A.; Towne, M. C.; Agrawal, P. B., Genetic disorders and mortality in infancy and early childhood: delayed diagnoses and missed opportunities. *Genetics in Medicine* **2018,** *20* (11), 1396-1404.
9. Espinosa, E.; Zamora, P.; Feliu, J.; Barón, M. G., Classification of anticancer drugs—a new system based on therapeutic targets. *Cancer treatment reviews* **2003,** *29* (6), 515-523.
10. (a) Demain, A.; Vaishnav, P., Natural products for cancer chemotherapy. Microb Biotechnol 4: 687–699. 2011; (b) Tewari, D.; Rawat, P.; Singh, P. K., Adverse drug reactions of anticancer drugs derived from natural sources. *Food and Chemical Toxicology* **2019,** *123*, 522-535.
11. Xie, J.; Yang, Z.; Zhou, C.; Zhu, J.; Lee, R. J.; Teng, L., Nanotechnology for the delivery of phytochemicals in cancer therapy. *Biotechnology advances* **2016,** *34* (4), 343-353.
12. Watkins, R.; Wu, L.; Zhang, C.; Davis, R. M.; Xu, B., Natural product-based nanomedicine: recent advances and issues. *International journal of nanomedicine* **2015,** *10*, 6055.
13. Enrico, C., Nanotechnology-based drug delivery of natural compounds and phytochemicals for the treatment of cancer and other diseases. In *Studies in natural products chemistry*, Elsevier: 2019; Vol. 62, pp 91-123.
14. Ghadi, R.; Dand, N., BCS class IV drugs: Highly notorious candidates for formulation development. *Journal of Controlled Release* **2017,** *248*, 71-95.
15. Arora, D.; Jaglan, S., Therapeutic applications of resveratrol nanoformulations. *Environmental chemistry letters* **2018,** *16* (1), 35-41.

16. Shrestha, H.; Bala, R.; Arora, S., Lipid-based drug delivery systems. *Journal of pharmaceutics* **2014,** *2014*.

17. Banerjee, S.; Roy, S., Polysaccharide installed lipid nanoparticles in targeted antituberculosis drug delivery applications. In *Polysaccharide Carriers for Drug Delivery*, Elsevier: 2019; pp 397-411.

18. Chaudhari, V. S.; Hazam, P. K.; Banerjee, S., Lipid Nanoarchitectonics for Natural Products Delivery in Cancer Therapy. In *Sustainable Agriculture Reviews 44*, Springer: 2020; pp 169-203.

19. Kazusaki, M.; Ueda, S.; Takeuchi, N.; Ohgami, Y., Validation of analytical procedures by high− performance liquid chromatography for pharmaceutical analysis. *Chromatography* **2012,** *33* (2), 65-73.

20. Nishimuro, H.; Ohnishi, H.; Sato, M.; Ohnishi-Kameyama, M.; Matsunaga, I.; Naito, S.; Ippoushi, K.; Oike, H.; Nagata, T.; Akasaka, H., Estimated daily intake and seasonal food sources of quercetin in Japan. *Nutrients* **2015,** *7* (4), 2345-2358.

21. David, A. V. A.; Arulmoli, R.; Parasuraman, S., Overviews of biological importance of quercetin: A bioactive flavonoid. *Pharmacognosy reviews* **2016,** *10* (20), 84.

22. Singh, A.; Duggal, S., Piperine-review of advances in pharmacology. *International journal of pharmaceutical sciences and Nanotechnology* **2009,** *2* (3), 615-620.

23. (a) Kumari, A.; Kumar, V.; Yadav, S. K., Plant extract synthesized PLA nanoparticles for controlled and sustained release of quercetin: a green approach. *PLoS one* **2012,** *7* (7), e41230; (b) Shao, B.; Cui, C.; Ji, H.; Tang, J.; Wang, Z.; Liu, H.; Qin, M.; Li, X.; Wu, L., Enhanced oral bioavailability of piperine by self-emulsifying drug delivery systems: in vitro, in vivo and in situ intestinal permeability studies. *Drug delivery* **2015,** *22* (6), 740-747.

24. (a) Dall'Acqua, S.; Miolo, G.; Innocenti, G.; Caffieri, S., The photodegradation of quercetin: relation to oxidation. *Molecules* **2012,** *17* (8), 8898-8907; (b) Quijia, C. R.; Chorilli, M., Characteristics, biological properties and analytical methods of piperine: a review. *Critical reviews in analytical chemistry* **2019**, 1-16.

25. Masri, M.; Booth, A.; DeEds, F., The metabolism and acid degradation of quercetin. *Archives of Biochemistry* **1959,** *85*, 284-286.

26. Banerjee, S.; Roy, S.; Bhaumik, K. N.; Pillai, J., Mechanisms of the effectiveness of lipid nanoparticle formulations loaded with anti-tubercular drugs combinations toward overcoming drug bioavailability in tuberculosis. *Journal of Drug Targeting* **2020,** *28* (1), 55-69.

27. Sanghavi, N.; Bhosale, S.; Malode, Y.; Sanghavi, N., RP-HPLC method development and validation of Quercetin isolated from the plant Tridax procumbens L. *Journal of Scientific and Innovative Research* **2014,** *3* (6), 594-597.

28. Aneja, G.; Dave, U.; Vadodaria, K., Simultaneous Estimation of Piperine, Quercetin and Curcumin in A Mixture Using UV-Visible Spectrophotometer and Method Validation. *IJTA* **2012,** *8*, 14-7.

29. Banerjee, S.; Roy, S.; Nath Bhaumik, K.; Kshetrapal, P.; Pillai, J., Comparative study of oral lipid nanoparticle formulations (LNFs) for chemical stabilization of antitubercular

drugs: physicochemical and cellular evaluation. *Artificial cells, nanomedicine, and biotechnology* **2018,** *46* (sup1), 540-558.

30. Guideline, I. H. T., Validation of analytical procedures: text and methodology. *Q2 (R1)* **2005,** *1* (20), 05.
31. Revision, U. S. P. C. C. o. In *The United States Pharmacopeia, the National Formulary*, United States Pharmacopeial Convention, Incorporated: 2007.
32. Chen, S.-F.; Nien, S.; Wu, C.-H.; Liu, C.-L.; Chang, Y.-C.; Lin, Y.-S., Reappraisal of the anticancer efficacy of quercetin in oral cancer cells. *Journal of the Chinese Medical Association* **2013,** *76* (3), 146-152.
33. Ma, Y. S.; Yao, C. N.; Liu, H. C.; Yu, F. S.; Lin, J. J.; Lu, K. W.; Liao, C. L.; Chueh, F. S.; Chung, J. G., Quercetin induced apoptosis of human oral cancer SAS cells through mitochondria and endoplasmic reticulum mediated signaling pathways. *Oncology letters* **2018,** *15* (6), 9663-9672.
34. Siddiqui, S.; Ahamad, M. S.; Jafri, A.; Afzal, M.; Arshad, M., Piperine triggers apoptosis of human oral squamous carcinoma through cell cycle arrest and mitochondrial oxidative stress. *Nutrition and cancer* **2017,** *69* (5), 791-799.
35. Khajuria, A.; Zutshi, U.; Bedi, K., Permeability characteristics of piperine on oral absorption-an active alkaloid from peppers and a bioavailability enhancer. *Indian journal of experimental biology* **1998,** *36*, 46-50.
36. Rather, R. A.; Bhagat, M., Cancer chemoprevention and piperine: Molecular mechanisms and therapeutic opportunities. *Frontiers in cell and developmental biology* **2018,** *6*, 10.
37. Cai, X.; Fang, Z.; Dou, J.; Yu, A.; Zhai, G., Bioavailability of quercetin: problems and promises. *Current medicinal chemistry* **2013,** *20* (20), 2572-2582.
38. WU, Z.-j.; XIA, X.-j.; HUANG, X.-s., Determination of equilibrium solubility and apparent oil/water partition coefficient of piperine. *Journal of Jinan University (Natural Science & Medicine Edition)* **2012,** (5), 7.
39. Banerjee, S.; Pillai, J., Solid lipid matrix mediated nanoarchitectonics for improved oral bioavailability of drugs. *Expert Opinion on Drug Metabolism & Toxicology* **2019,** *15* (6), 499-515.
40. Chaudhari, V. S.; Murty, U. S.; Banerjee, S., Lipidic nanomaterials to deliver natural compounds against cancer: a review. *Environmental Chemistry Letters* **2020**, 1-10.
41. Das, S.; Chaudhury, A., Recent advances in lipid nanoparticle formulations with solid matrix for oral drug delivery. *AAPS PharmSciTech* **2011,** *12* (1), 62-76.
42. Chen-yu, G.; Chun-fen, Y.; Qi-lu, L.; Qi, T.; Yan-wei, X.; Wei-na, L.; Guang-xi, Z., Development of a quercetin-loaded nanostructured lipid carrier formulation for topical delivery. *International journal of pharmaceutics* **2012,** *430* (1-2), 292-298.
43. Li, Q.; Cai, T.; Huang, Y.; Xia, X.; Cole, S. P.; Cai, Y., A review of the structure, preparation, and application of NLCs, PNPs, and PLNs. *Nanomaterials* **2017,** *7* (6), 122.
44. Mehnert, W.; Mäder, K., Solid lipid nanoparticles: production, characterization and applications. *Advanced drug delivery reviews* **2012,** *64*, 83-101.

45. Khosa, A.; Reddi, S.; Saha, R. N., Nanostructured lipid carriers for site-specific drug delivery. *Biomedicine & Pharmacotherapy* **2018,** *103*, 598-613.

46. (a) Natarajan, J.; Karri, V.; Anindita, D., Nanostructured lipid carrier (NLC): a promising drug delivery system. *Global Journal of Nanomedicine* **2017,** *1* (5), 001-006; (b) Khan, S.; Baboota, S.; Ali, J.; Khan, S.; Narang, R. S.; Narang, J. K., Nanostructured lipid carriers: An emerging platform for improving oral bioavailability of lipophilic drugs. *International journal of pharmaceutical investigation* **2015,** *5* (4), 182.

47. Das, S.; Ng, W. K.; Tan, R. B., Are nanostructured lipid carriers (NLCs) better than solid lipid nanoparticles (SLNs): development, characterizations and comparative evaluations of clotrimazole-loaded SLNs and NLCs? *European journal of pharmaceutical sciences* **2012,** *47* (1), 139-151.

48. Iqbal, M. A.; Md, S.; Sahni, J. K.; Baboota, S.; Dang, S.; Ali, J., Nanostructured lipid carriers system: recent advances in drug delivery. *Journal of drug targeting* **2012,** *20* (10), 813-830.

49. Graves, R. A.; Ledet, G. A.; Nation, C. A.; Pramar, Y. V.; Bostanian, L. A.; Mandal, T. K., Effect of squalane on mebendazole-loaded Compritol® nanoparticles. *Journal of Biomaterials Science, Polymer Edition* **2015,** *26* (13), 868-880.

50. Yoon, G.; Park, J. W.; Yoon, I.-S., Solid lipid nanoparticles (SLNs) and nanostructured lipid carriers (NLCs): recent advances in drug delivery. *Journal of Pharmaceutical Investigation* **2013,** *43* (5), 353-362.

51. Souza, L.; Silva, E.; Martins, A.; Mota, M.; Braga, R.; Lima, E.; Valadares, M.; Taveira, S.; Marreto, R., Development of topotecan loaded lipid nanoparticles for chemical stabilization and prolonged release. *European journal of pharmaceutics and biopharmaceutics* **2011,** *79* (1), 189-196.

52. Chaudhari, V. S.; Borkar, R. M.; Murty, U. S.; Banerjee, S., Analytical Method Development and Validation of Reverse-Phase High-Performance Liquid Chromatography (RP-HPLC) Method for Simultaneous Quantifications of Quercetin and Piperine in Dual-Drug Loaded Nanostructured Lipid Carriers. *Journal of Pharmaceutical and Biomedical Analysis* **2020**, 113325.

53. Moreno-Bautista, G.; Tam, K. C., Evaluation of dialysis membrane process for quantifying the in vitro drug-release from colloidal drug carriers. *Colloids and Surfaces A: Physicochemical and Engineering Aspects* **2011,** *389* (1-3), 299-303.

54. (a) Bose, S.; Michniak-Kohn, B., Preparation and characterization of lipid based nanosystems for topical delivery of quercetin. *European Journal of Pharmaceutical Sciences* **2013,** *48* (3), 442-452; (b) Liu, L.; Tang, Y.; Gao, C.; Li, Y.; Chen, S.; Xiong, T.; Li, J.; Du, M.; Gong, Z.; Chen, H., Characterization and biodistribution in vivo of quercetin-loaded cationic nanostructured lipid carriers. *Colloids and Surfaces B: Biointerfaces* **2014,** *115*, 125-131.

55. Wyatt, D., Taking poorly water soluble compounds through discovery. *Bulletin technique-Gattefossé report* **1999,** (92), 31-39.

56. Higuchi, T., Rate of release of medicaments from ointment bases containing drugs in suspension. *Journal of pharmaceutical sciences* **1961,** *50* (10), 874-875.

57. (a) Singhvi, G.; Singh, M., In-vitro drug release characterization models. *Int J Pharm Stud Res* **2011,** *2* (1), 77-84; (b) Ramteke, K.; Dighe, P.; Kharat, A.; Patil, S., Mathematical models of drug dissolution: a review. *Sch. Acad. J. Pharm* **2014,** *3* (5), 388-396.

58. Dobrovolskaia, M. A.; Clogston, J. D.; Neun, B. W.; Hall, J. B.; Patri, A. K.; McNeil, S. E., Method for analysis of nanoparticle hemolytic properties in vitro. *Nano letters* **2008,** *8* (8), 2180-2187.

59. Şengel-Türk, C. T.; Hasçiçek, C.; Dogan, A. L.; Esendagli, G.; Guc, D.; Gönül, N., Preparation and in vitro evaluation of meloxicam-loaded PLGA nanoparticles on HT-29 human colon adenocarcinoma cells. *Drug development and industrial pharmacy* **2012,** *38* (9), 1107-1116.

60. Smith, S. M.; Ribble, D.; Goldstein, N. B.; Norris, D. A.; Shellman, Y. G., A simple technique for quantifying apoptosis in 96-well plates. *Methods in cell biology* **2012,** *112*, 361-368.

61. Nordin, N.; Yeap, S. K.; Rahman, H. S.; Zamberi, N. R.; Abu, N.; Mohamad, N. E.; How, C. W.; Masarudin, M. J.; Abdullah, R.; Alitheen, N. B., In vitro cytotoxicity and anticancer effects of citral nanostructured lipid carrier on MDA MBA-231 human breast cancer cells. *Scientific reports* **2019,** *9* (1), 1-19.

62. Liu, J.; Hu, W.; Chen, H.; Ni, Q.; Xu, H.; Yang, X., Isotretinoin-loaded solid lipid nanoparticles with skin targeting for topical delivery. *International journal of pharmaceutics* **2007,** *328* (2), 191-195.

63. Haghiac, M.; Walle, T., Quercetin induces necrosis and apoptosis in SCC-9 oral cancer cells. *Nutrition and cancer* **2005,** *53* (2), 220-231.

64. Aditya, N. P.; Shim, M.; Lee, I.; Lee, Y.; Im, M. H.; Ko, S., Curcumin and genistein coloaded nanostructured lipid carriers: in vitro digestion and antiprostate cancer activity. *Journal of agricultural and food chemistry* **2013,** *61* (8), 1878-83.

65. Liu, Y.; Tseng, Y.-c.; Huang, L., Biodistribution studies of nanoparticles using fluorescence imaging: a qualitative or quantitative method? *Pharmaceutical research* **2012,** *29* (12), 3273-3277.

66. Dong, Z.; Iqbal, S.; Zhao, Z., Preparation of ergosterol-loaded nanostructured lipid carriers for enhancing oral bioavailability and antidiabetic nephropathy effects. *AAPS PharmSciTech* **2020,** *21* (2), 1-11.

67. Karn-Orachai, K.; Smith, S. M.; Phunpee, S.; Treethong, A.; Puttipipatkhachorn, S.; Pratontep, S.; Ruktanonchai, U. R., The effect of surfactant composition on the chemical and structural properties of nanostructured lipid carriers. *Journal of microencapsulation* **2014,** *31* (6), 609-618.

68. Bandi, S. P.; Kumbhar, Y. S.; Venuganti, V. V. K., Effect of particle size and surface charge of nanoparticles in penetration through intestinal mucus barrier. *Journal of Nanoparticle Research* **2020,** *22* (3), 1-11.

69. Li, S.-D.; Huang, L., Pharmacokinetics and biodistribution of nanoparticles. *Molecular pharmaceutics* **2008,** *5* (4), 496-504.

70. Abd-Elrahman, M.; Ahmed, S., Thermal degradation kinetics and geometrical stability of D-sucrose. *International Journal of Polymeric Materials* **2009,** *58* (6), 322-335.

71. Pereira, A. B.; da Silva, A. M.; Barroca, M. J.; Marques, M. P. M.; Braga, S. S., Physicochemical properties, antioxidant action and practical application in fresh cheese of the solid inclusion compound γ-cyclodextrin· quercetin, in comparison with β-cyclodextrin· quercetin. *Arabian Journal of Chemistry* **2020,** *13* (1), 205-215.

72. Jawad, R.; Elleman, C.; Martin, G. P.; Royall, P. G., Crystallisation of freeze-dried sucrose in model mixtures that represent the amorphous sugar matrices present in confectionery. *Food & function* **2018,** *9* (9), 4621-4634.

73. Lopes, R.; Eleutério, C.; Gonçalves, L.; Cruz, M.; Almeida, A., Lipid nanoparticles containing oryzalin for the treatment of leishmaniasis. *European Journal of Pharmaceutical Sciences* **2012,** *45* (4), 442-450.

74. Shah, N. V.; Seth, A. K.; Balaraman, R.; Aundhia, C. J.; Maheshwari, R. A.; Parmar, G. R., Nanostructured lipid carriers for oral bioavailability enhancement of raloxifene: Design and in vivo study. *Journal of advanced research* **2016,** *7* (3), 423-434.

75. Müller, R.; Radtke, M.; Wissing, S., Nanostructured lipid matrices for improved microencapsulation of drugs. *International journal of pharmaceutics* **2002,** *242* (1-2), 121-128.

76. Zhang, C.; Peng, F.; Liu, W.; Wan, J.; Wan, C.; Xu, H.; Lam, C. W.; Yang, X., Nanostructured lipid carriers as a novel oral delivery system for triptolide: induced changes in pharmacokinetics profile associated with reduced toxicity in male rats. *International journal of nanomedicine* **2014,** *9*, 1049.

77. Rinwa, P.; Kumar, A., Quercetin along with piperine prevents cognitive dysfunction, oxidative stress and neuro-inflammation associated with mouse model of chronic unpredictable stress. *Archives of pharmacal research* **2017,** *40* (10), 1166-1175.

78. Sandhir, R.; Mehrotra, A., Quercetin supplementation is effective in improving mitochondrial dysfunctions induced by 3-nitropropionic acid: implications in Huntington's disease. *Biochimica et Biophysica Acta (BBA)-Molecular Basis of Disease* **2013,** *1832* (3), 421-430.

79. Atal, C.; Dubey, R. K.; Singh, J., Biochemical basis of enhanced drug bioavailability by piperine: evidence that piperine is a potent inhibitor of drug metabolism. *Journal of Pharmacology and Experimental Therapeutics* **1985,** *232* (1), 258-262.

80. Chaudhari, V. S.; Murty, U. S.; Banerjee, S., Nanostructured lipid carriers as a strategy for encapsulation of active plant constituents: Formulation and in vitro physicochemical characterizations. *Chemistry and Physics of Lipids* **2021,** *235*, 105037.

81. (a) Liu, B.; Anderson, D.; Ferry, D. R.; Seymour, L. W.; de Takats, P. G.; Kerr, D. J., Determination of quercetin in human plasma using reversed-phase high-performance liquid chromatography. *Journal of Chromatography B: Biomedical Sciences and Applications* **1995,** *666* (1), 149-155; (b) Chaudhari, V. S.; Malakar, T. K.; Murty, U. S.; Banerjee, S., Extruded filaments derived 3D printed medicated skin patch to mitigate destructive pulmonary tuberculosis: Design to delivery. *Expert Opinion on Drug Delivery* **2020**, 1-13.

82. Erlund, I.; Alfthan, G.; Siren, H.; Ariniemi, K.; Aro, A., Validated method for the quantitation of quercetin from human plasma using high-performance liquid chromatography with electrochemical detection. *Journal of Chromatography B: Biomedical Sciences and Applications* **1999,** *727* (1-2), 179-189.

83. De Vries, J.; Hollman, P.; Meyboom, S.; Buysman, M.; Zock, P. L.; van Staveren, W. A.; Katan, M. B., Plasma concentrations and urinary excretion of the antioxidant flavonols quercetin and kaempferol as biomarkers for dietary intake. *The American journal of clinical nutrition* **1998,** *68* (1), 60-65.

84. (a) Wittig, J.; Herderich, M.; Graefe, E. U.; Veit, M., Identification of quercetin glucuronides in human plasma by high-performance liquid chromatography–tandem mass spectrometry. *Journal of Chromatography B: Biomedical Sciences and Applications* **2001,** *753* (2), 237-243; (b) Hong, Y.-J.; Mitchell, A. E., Metabolic profiling of flavonol metabolites in human urine by liquid chromatography and tandem mass spectrometry. *Journal of agricultural and food chemistry* **2004,** *52* (22), 6794-6801; (c) Mullen, W.; Boitier, A.; Stewart, A. J.; Crozier, A., Flavonoid metabolites in human plasma and urine after the consumption of red onions: analysis by liquid chromatography with photodiode array and full scan tandem mass spectrometric detection. *Journal of Chromatography A* **2004,** *1058* (1-2), 163-168.

85. Li, H.; Zhao, X.; Ma, Y.; Zhai, G.; Li, L.; Lou, H., Enhancement of gastrointestinal absorption of quercetin by solid lipid nanoparticles. *Journal of Controlled Release* **2009,** *133* (3), 238-244.

86. DK, V.; Verma, P.; Singh, S. K.; Viswanathan, S., LC-ESI-MS/MS analysis of quercetin in rat plasma after oral administration of biodegradable nanoparticles. *Biomedical chromatography: BMC* **2015,** *29* (11), 1731-1736.

87. Hua, S., Advances in Drug Formulation of the Sublingual and Buccal Routes for Gastrointestinal Drug Delivery. *Frontiers in Pharmacology* **2019,** *10*, 1328.

88. Allen, L.; Ansel, H. C., *Ansel's pharmaceutical dosage forms and drug delivery systems*. Lippincott Williams & Wilkins: 2013.

89. Dawes, C., Physiological factors affecting salivary flow rate, oral sugar clearance, and the sensation of dry mouth in man. *Journal of dental research* **1987,** *66* (2_suppl), 648-653.

90. Goyanes, A.; Det-Amornrat, U.; Wang, J.; Basit, A. W.; Gaisford, S., 3D scanning and 3D printing as innovative technologies for fabricating personalized topical drug delivery systems. *Journal of controlled release* **2016,** *234*, 41-48.

91. Ventola, C. L., Medical applications for 3D printing: current and projected uses. *Pharmacy and Therapeutics* **2014,** *39* (10), 704.

92. (a) Bhatt, U.; Malakar, T. K.; Murty, U. S.; Banerjee, S., 3D printing of immediate-release tablets containing olanzapine by filaments extrusion. *Drug Development and Industrial Pharmacy* **2021**, 1-10; (b) Norman, J.; Madurawe, R. D.; Moore, C. M.; Khan, M. A.; Khairuzzaman, A., A new chapter in pharmaceutical manufacturing: 3D-printed drug products. *Advanced drug delivery reviews* **2017,** *108*, 39-50.

93. Al-Taie, A.; Pan, J.; Polak, P.; Barer, M. R.; Han, X.; Abbott, A. P., Mechanical properties of 3-D printed polyvinyl alcohol matrix for detection of respiratory pathogens. *Journal of the Mechanical Behavior of Biomedical Materials* **2020,** *112*, 104066.

94. Goyanes, A.; Martinez, P. R.; Buanz, A.; Basit, A. W.; Gaisford, S., Effect of geometry on drug release from 3D printed tablets. *International journal of pharmaceutics* **2015,** *494* (2), 657-663.

95. Reddy, R. J.; Anjum, M.; Hussain, M. A., A comprehensive review on buccal drug delivery system. *Am J Advan Drug Deliv* **2013,** *1*, 300-312.

96. Chaudhari, V. S.; Murty, U. S.; Banerjee, S., Nanostructured Lipid Carriers as a strategy for encapsulation of active plant constituents: Formulation and in vitro physicochemical characterizations. *Chemistry and Physics of Lipids* **2021**, 105037.

97. Basahih, T. S.; Alamoudi, A. A.; El-Say, K. M.; Alhakamy, N. A.; Ahmed, O. A., Improved Transmucosal Delivery of Glimepiride via Unidirectional Release Buccal Film Loaded With Vitamin E TPGS-Based Nanocarrier. *Dose-Response* **2020,** *18* (3), 1559325820945164.

98. Raj, S. B.; Chandrasekhar, K. B.; Reddy, K. B., Formulation, in-vitro and in-vivo pharmacokinetic evaluation of simvastatin nanostructured lipid carrier loaded transdermal drug delivery system. *Future Journal of Pharmaceutical Sciences* **2019,** *5* (1), 1-14.

99. Sathe, P.; Saka, R.; Kommineni, N.; Raza, K.; Khan, W., Dithranol-loaded nanostructured lipid carrier-based gel ameliorate psoriasis in imiquimod-induced mice psoriatic plaque model. *Drug development and industrial pharmacy* **2019,** *45* (5), 826-838.

100. (a) Smeraldi, J.; Ganesh, R.; Safarik, J.; Rosso, D., Statistical evaluation of photon count rate data for nanoscale particle measurement in wastewaters. *Journal of Environmental Monitoring* **2012,** *14* (1), 79-84; (b) Beck, R.; Chaves, P.; Goyanes, A.; Vukosavljevic, B.; Buanz, A.; Windbergs, M.; Basit, A.; Gaisford, S., 3D printed tablets loaded with polymeric nanocapsules: An innovative approach to produce customized drug delivery systems. *International journal of pharmaceutics* **2017,** *528* (1-2), 268-279.

101. Miller, J. H.; Danielson, T.; Pithawalla, Y. B.; Brown, A. P.; Wilkinson, C.; Wagner, K.; Aldeek, F., Method development and validation of dissolution testing for nicotine release from smokeless tobacco products using flow-through cell apparatus and UPLC-PDA. *Journal of Chromatography B* **2020,** *1141*, 122012.

102. Malakar, T. K.; Chaudhari, V. S.; Dwivedy, S. K.; Murty, U. S.; Banerjee, S., 3D Printed Housing Devices for Segregated Compartmental Delivery of Oral Fixed-Dose Anti-Tubercular Drugs Adopting Print and Fill Strategy. *3D Printing and Additive Manufacturing* **2021**.

103. Goyanes, A.; Wang, J.; Buanz, A.; Martínez-Pacheco, R.; Telford, R.; Gaisford, S.; Basit, A. W., 3D printing of medicines: engineering novel oral devices with unique design and drug release characteristics. *Molecular pharmaceutics* **2015,** *12* (11), 4077-4084.

Annexure

Ph. D. Outcomes

Published Research Articles:

1. **Chaudhari VS**, Borkar RM, Murty USN, Banerjee S. Analytical method development and validation of reverse-phase high-performance liquid chromatography (RP-HPLC) method for simultaneous quantification of quercetin and piperine in dual-drug loaded nanostructured lipid carriers. *Journal of Pharmaceutical and Biomedical Analysis* 2020:186–113325. https://doi.org/10.1016/j.jpba.2020.113325 (Impact Factor **3.935**)
2. **Chaudhari VS**, Murty USN, Banerjee S. Nanostructured lipid carriers as a strategy for encapsulation of active plant constituents: Formulation and in vitro physicochemical characterisations. *Chemistry and Physics of Lipids* 2021: 235, 105037. https://doi.org/10.1016/j.chemphyslip.2020.105037 (Impact Factor **3.329**)
3. **Chaudhari VS,** Murty USN, Banerjee S. Fused deposition modelling (FDM)-mediated 3D printed mouth-dissolving wafers loaded with nanostructured lipid carriers (NLCs) for in vitro release. *Journal of Material Research*. 2021:1-10. https://doi.org/10.1557/s43578-021-00288-1. (Impact Factor **3.089**)
4. **Chaudhari VS**, Gavali B, Saha P, Murty USN, Naidu VGM, Banerjee S. Quercetin and piperine enriched nanostructured lipid carriers (NLCs) to improve apoptosis in oral squamous cell carcinoma (FaDu cells) with improved bio-distribution profile. *European Journal of Pharmacology*. 2021: 909, 174400. https://doi.org/10.1016/j.ejphar.2021.174400 (Impact Factor **4.432**)

Published Review Articles:

1. **Chaudhari VS**, Murty USN, Banerjee S. Lipidic nanomaterials to deliver natural compounds against cancer: a review. *Environmental Chemistry Letters*. 18(6), 1803-1812. 2020. https://doi.org/10.1007/s10311-020-01042-5 (Impact Factor: **9.027**)

Published Book Chapters:

1. **Chaudhari VS**, Hazam PK, Banerjee S. "Lipid nanoarchitectonics for natural product delivery in cancer therapy." SPRINGER-NATURE book titled Pharmaceutical Technology for Natural Products Delivery, Sustainable Agriculture Reviews, Vol-44, Chapter-5, 2020, 169-203. 2020. [ISBN: 9783030418410]

Design Patent (FER Issued):

1. **Vishal Sharad Chaudhari**, Tushar Kanti Malakar, USN Murty, and Subham Banerjee "3D Printed Mouth Dissolving Wafers" Application No. 342624-001. Cbr No. 202856, **FER replied**: 02 July, 2021 date of filing: 22 April 2021.

Presentation in Conferences:

1. **Best Oral presentation** at Dissolution Research Presentation India **(DRPI) – 2021**, "Combinatorial delivery of nanoencapsulated active constituents embedded in 3D

printed wafer for both drug and particle release applications"16th - 17th July, 2021. – **ZONAL Topper from East Zone** and **Finalist. Awarded with Certificate and INR 10,000/- cash prize**.

2. Oral presentation at **19th International e-Symposium conducted by Controlled Release Society Indian Local Chapter**, "Quercetin and Piperine Encapsulated Nanostructured Lipid Carriers to Attenuate Oral Cancer: Development, Characterization and in-vitro Cellular Evaluation" 25th to 27 February 2021.

3. **Best Poster presentation** at **Virtual Dissolution Discussion Group (DDG) India Meeting 2020**, "Development & in vitro release of nanostructured lipid carriers (NLCs) from FDM mediated 3D printed mouth-dissolving wafers" 15th and 16 October 2020. Agilent Technologies, USA**.**

4. Oral presentation at **4th International Conference on Nutraceuticals and Chronic Diseases – INCD 2019**, "Active Plant Constituents Enriched Nanostructured Lipid Carriers against Oral Cancer Mitigation in Northeast Region" 23rd to 25th September, 2019 held at IIT-Guwahati, Assam, India.